Purdue University
Purdue e-Pubs

Open Access Dissertations | Theses and Dissertations

12-2016

The development of preclinical strategies for facilitation of lead candidate selection

Christopher Dale Kulczar
Purdue University

Follow this and additional works at: https://docs.lib.purdue.edu/open_access_dissertations

 Part of the Pharmacy and Pharmaceutical Sciences Commons

Recommended Citation
Kulczar, Christopher Dale, "The development of preclinical strategies for facilitation of lead candidate selection" (2016). *Open Access Dissertations*. 961.
https://docs.lib.purdue.edu/open_access_dissertations/961

This document has been made available through Purdue e-Pubs, a service of the Purdue University Libraries. Please contact epubs@purdue.edu for additional information.

PURDUE UNIVERSITY
GRADUATE SCHOOL
Thesis/Dissertation Acceptance

This is to certify that the thesis/dissertation prepared

By Christopher Dale Kulczar

Entitled
The Development of Preclinical Strategies for Facilitation of Lead Candidate Selection

For the degree of Doctor of Philosophy

Is approved by the final examining committee:

Gregory Knipp
Chair

David Engers

Steven Byrn

Elizabeth Topp

To the best of my knowledge and as understood by the student in the Thesis/Dissertation Agreement, Publication Delay, and Certification Disclaimer (Graduate School Form 32), this thesis/dissertation adheres to the provisions of Purdue University's "Policy of Integrity in Research" and the use of copyright material.

Approved by Major Professor(s): Gregory Knipp

Approved by: Elizabeth Topp 8/16/2016
Head of the Departmental Graduate Program Date

THE DEVELOPMENT OF PRECLINICAL STRATEGIES FOR FACILITATION OF LEAD CANDIDATE SELECTION

A Dissertation

Submitted to the Faculty

of

Purdue University

by

Chris Kulczar

In Partial Fulfillment of the

Requirements for the Degree

of

Doctor of Philosophy

December 2016

Purdue University

West Lafayette, Indiana

This is dedicated in memory of my mother Lori Ann Kulczar who helped make me who I am, who is still a constant inspiration, and who I miss dearly and to my father Timothy Charles Kulczar who has always been there for me and who I look up to more and more every day.

ACKNOWLEDGEMENTS

I'd like to start by thanking my advisor, Dr. Gregory Knipp. Throughout my studies, both graduate and undergraduate, he has always been a constant support and motivation. Without his influence, I'm not sure I'd have been able to make it through to the end. The time I spent in his lab has made me better, both personally and scientifically. I'll be forever grateful for his patience and always being willing to lend his time whether that be to teach or just to listen.

I'd also like to thank all of the current and past members who I shared time with in the Knipp lab including Dr. Wyatt Roth, Mr. Aimable Ngendahimana, Ms. Monika Lavan, and Ms. Kelsey Lubin. I couldn't have asked for a better group of coworkers and friends to learn from, learn with, and teach over the past 5 years. You helped make long days, months, and years fly by. Along with the rest of the IPPH graduate students, they've been great to share my time with at Purdue.

Additionally, I'd like to thank my committee, Dr. Stephen Byrn, Dr. Elizabeth Topp, and Dr. David Engers, for their patience, support, and guidance. Specifically, I would like to express my gratitude to Dr. Byrn, Sister Zita Ekeocha, and the staff at KSP in Moshi, Tanzania for allowing me to help with the Sustainable Medicines in Africa Program. I always felt so welcomed. My trips to Moshi will be with me forever and were some of the most rewarding experiences of my life.

Finally, I would like to thank my friends and family who have always been there for me through thick and thin. I've been blessed to have such great people around me. We've shared so many memories together and I look forward to making many more. None of this would be possible without you.

TABLE OF CONTENTS

Page

Page

LIST OF TABLES

LIST OF FIGURES

Figure Page

Figure Page

Figure Page

Figure Page

LIST OF SCHEMES

ABSTRACT

Kulczar, Christopher D. Ph.D., Purdue University, December 2016. The Development of Preclinical Strategies for Facilitation of Lead Candidate Selection. Major Professor: Gregory T. Knipp.

Chapter 1 details a background of techniques used for modeling the blood-brain barrier (BBB). The BBB represents a diffusive barrier to both paracellular and transcellular movement of many compounds in and out of the brain. The main rate-limiting barriers of the BBB include exclusive tight junctions that prevent the movement of hydrophilic molecules through intercellular gaps, and efflux proteins in the membrane which pump many hydrophobic molecules back into the blood. In addition, the BBB contains metabolizing enzymes, including Cytochrome P450s. This barrier acts to protect the vulnerable tissues of the brain from harmful xenobiotics, but also can serve as a restrictive barrier for potential therapeutic compounds for the growing number of neurological diseases, including Alzheimer's disease, Parkinson's disease, stroke, depression, brain cancers, and many others. In fact, it is estimated that over 98% of pharmaceutical compounds are unable to cross into the brain. Due to this problem, many compounds must be screened in order to determine their BBB permeation and eventual druggability. While *in vivo* testing in pre-clinical animals and humans is ideal for testing, these methods aren't suitable for early screening because of their high cost, low throughput, and ethical considerations, especially in humans.

Therefore, a number of *in vitro* cell screens have been established to mimic the BBB for permeation testing. Principally, the best model should include primary human brain microvessel endothelial cells (BMECs), however, due to the growing interest in BBB permeation and lack of tissues, the supply is limited. As an alternative method, many groups have investigated the use of primary animal BMECs, usually of murine, porcine, or bovine source. These models prove effective at restricting paracellular movement; however, one must question the effects of animal isoforms on modeling uptake, efflux, and metabolism of transcellular markers. This proves important as *in vivo* most, if not all, therapeutic compounds will cross the BBB transellularly. Consequently, much work has been done to establish immortalized human BMECs. These immortalized cell lines alleviate the high cost and lack of supply found with primary human cells, but potentially may serve as a better model for transcellular permeation over animal cell lines. Currently, the most widely characterized immortalized human BMEC cell line is the human cerebral microvessel endothelial cell line (hCMEC/D3). These cells express tight junction proteins, efflux proteins, cyp450 enzymes, and are conducive to *in vitro* testing. However, while these cells express tight junctions, their function is less than ideal and leads to a leaky monolayer which may allow faster permeation through the paracellular route or paracellular permeation of compounds that move transcellularly *in vivo* leading to poor prediction of BBB permeability. One method of investigating the reason behind these leaky tight junctions was to take a closer look at the BBB itself.

Closer examination shows that while the endothelial cells of the BBB form the main permeation barrier, these cells are surrounded by supporting cells such as astrocytes

and pericytes. These cell lines are thought to promote proper differentiation of endothelial cells *in vivo,* therefore, some groups have moved to co- and triculture models. In these models, the supporting cells are plated on the basolateral side of a Transwell® support and/or on the bottom of the well plate. After a given time, endothelial cells are then plated on the apical side of the Transwell® and the cells are allowed to grow together in the same medium. Due to the nature of the filter support, this allows crosstalk of soluble factors between the endothelial cells and the supporting cells. In practice, this often leads to decreased paracellular permeability and increased expression of tight junction proteins. However, while having increased tightness, these models are still leaky in comparison to *in vivo* conditions and even primary BMECs.

It is hypothesized that one reason for the continued lack of tightness may be due the lack of direct contact between endothelial and supporting cells. While the Transwell® filter support allows movement of soluble factors between the compartments, the distance between cell layers is significantly higher than that found *in vivo*. This increased distance may allow for increased dilution and degradation of soluble factors, reducing their potency. In addition, the supporting cell lines are believed to secrete an extracellular matrix (ECM) which also helps to promote differentiation. By splitting the cell lines with the Transwell®, the endothelial cells are unable to interact with this secreted matrix. Therefore, Chapters 2 and 3 discuss the optimization and establishment of a direct contact coculture *in vitro* model in which both endothelial cells and astrocytes are plated on the apical side of the Transwell® allowing for more physiologically relevant signaling between the cells. Early results suggest decreased paracellular permeation in this

configuration compared to endothelial monocultures and indirect cocultures. In addition, this setup should allow for easier transition to high-throughput equipment.

Additional studies in Chapter 4 attempt to show the utility of a new mono-PEGylated Human Serum Albumin (HSA) as a potential enhancer of drug solubilization, permeation, and eventual cytotoxicty. Multi-gram batches of short (5 kDa) and long (20 kDa) PEG-HSA were synthesized with high efficiency (77%) and characterized in collaboration with Dr. Jonathan Mehtala and Dr. Alex Wei in the Department of Chemistry. Furthermore, effects of PEG-HSA on permeation of paclitaxel through peripheral and BBB *in vitro* cell models as well as changes in cytotoxicity against MCF-7 cells was investigated.

Finally, Chapter 5 includes an investigation into the characterization, formulation, and *in vitro/in vivo* testing of a potent V-ATPase inhibitor known as Saliphenylhalamide. The V-ATPase is an endogenous protein that is responsible for acidifying intercellular compartments and has been targeted in the past with *in vitro* success for treatment of cancer and osteoporosis among other diseases. However, here we investigate its use as an anti-viral therapeutic as acidification of endosomes by the V-ATPase is thought to be a critical step in replication of alpha viruses. Initial characterization showed poor water solubility and acid liability. Therefore, two solubility enabling formulations were created and tested for *in vitro* permeability and *in vivo* murine pharmacokinetics.

CHAPTER 1. MODELING THE BLOOD-BRAIN BARRIER

1.1 The Blood-Brain Barrier

The blood-brain barrier (BBB) is an active barrier, which selectively controls molecular and cellular movement between peripheral blood flow and the brain.[1] While preventing the movement of harmful xenobiotics from entering the brain, it also allows for selective uptake of endogenous substrates needed for optimal neuronal activity.[2] Integrity of the BBB is necessary for proper neuronal function and disruption of the barrier is very often associated with CNS-related diseases such as Alzheimer's, Parkinson's, epilepsy, schizophrenia, as well as many others.[3] While proper maintenance and upkeep of the BBB is important for healthy living, the BBB also presents a major obstruction to delivery of pharmaceutical compounds to treat neurological and neurodegenerative disorders.[4]

The BBB's effectiveness in excluding xenobiotics is often attributed to the brain microvessel endothelial cells (BMECs) that form the capillaries of the brain.[5] These endothelial cells are significantly restrictive to both paracellular permeation of hydrophilic molecules, through the formation of exclusive tight junctions, and transcellular diffusion of hydrophobic molecules, through the presence of luminal efflux proteins and intracellular metabolizing enzymes.[6] However, while they represent the rate-limiting permeation step, histological analysis shows the presence of other cells at the

BBB, including astrocytes, pericytes, neurons, and microglia. Further investigation into these cells has shown their importance in BBB development and upkeep. Due to the cohesive nature of these cells, the group was termed the neurovascular unit.[7]

1.2 The Neurovascular Unit

A cross-section of the BBB shows the coordination of the neurovascular unit and can be seen in Figure 1.1. As noted, the initial and rate-limiting barrier in blood-to-brain permeation is the endothelial cells. These cells, however, are wrapped in supporting cells which are thought to be the differentiating factor between BMECs and endothelial cells of the periphery.[8] This was confirmed through *in vivo* animal experiments showing that growing brain grafts in the periphery lead to decreased paracellular tightness, while grafting peripheral tissues into the brain induced tightening of the endothelium.[9] Here we look further into the roles of both the endothelial cells as well as some of the supporting cells of the neurovascular unit.

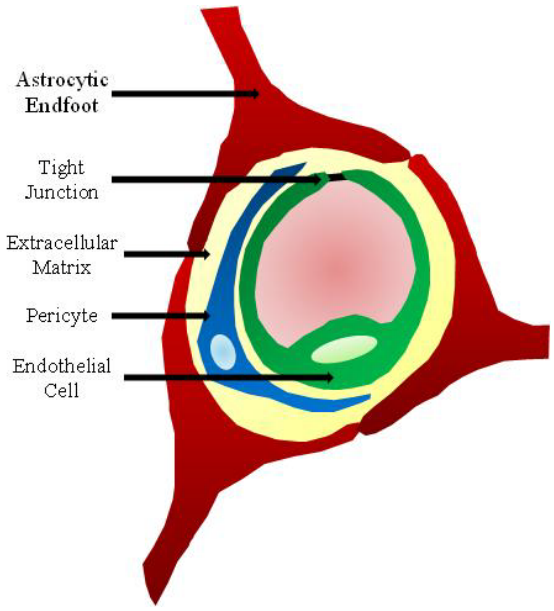

Figure 1.1. The Cellular Associations of Neurovascular Unit. Modified From Abbott NJ, et al. 2010.[10]

Endothelial Cells

The endothelial cells that form the capillaries of the BBB are different from those in the periphery in a number of ways. The first, as mentioned above, is a reduced paracellular permeability due to the presence of specialized tight junctions.[11] In addition, the endothelium of the BBB is continuous and lacks fenestrations which further limits paracellular permeability.[12] Permeability of even large hydrophobic molecules is restricted in comparison to the periphery due to reduction in both transcytosis and pinocytosis.[13] The BMECs also contain a high number of energy-producing mitochondria in comparison to the periphery which allows for increased metabolism and transport.[14] Finally, endothelial cells contain a higher density of nutrient, i.e. glucose and amino acid, and efflux transporters, i.e. p-glycoprotein, which allows for increased

selectivity of transcellular permeability.[15] While these characteristics distinguish the BBB from the periphery, the manifestation of these properties is determined by interactions of the supporting cells of the neurovascular unit as discussed below.

Astrocytes

As mentioned above, the properties of BMECs are not intrinsic to the cells, but brought on through induction in the CNS environment.[16] This induction is in part thought to be due to BMEC-astrocyte intercellular signaling. This hypothesis was confirmed through early *in vitro* studies which showed BBB-like differentiation in astrocyte-conditioned media.[17] This media is partially spent media in which astrocytes are temporarily grown in and contains soluble factors secreted by the astrocytes. This suggests that paracrine signaling by the astrocytes is likely to be important. However, further studies showed that additional BBB induction, i.e. decreased paracellular permeability and increased tight junction protein expression, was seen when astrocytes and BMECs were grown together separated by a filter support.[18,19] This possibly suggests cross-talk between the astrocytes and BMECs is necessary for physiologically-relevant BMEC differentiation.

A number of studies have been conducted to delineate the agents which lead to astrocyte-induced BBB differentiation and maintenance. Some of these signaling pathways can be seen in Figure 1.2.

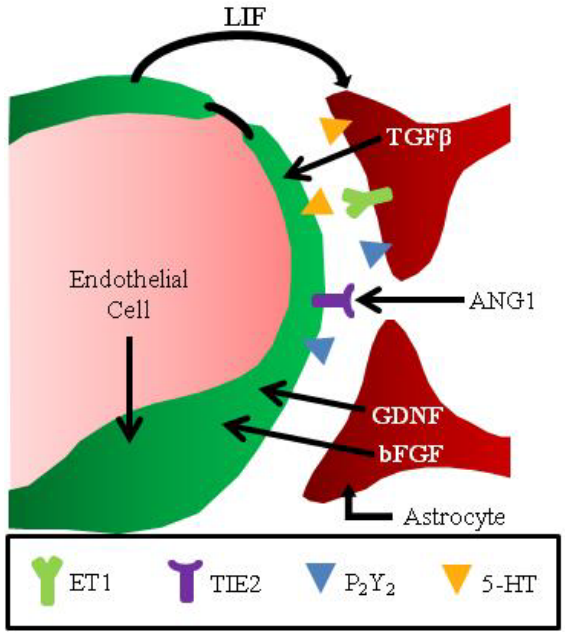

Figure 1.2. BMEC-Astrocyte Cell-Cell Signaling. LIF- Leukemia Inhibitory Factor, TGFβ-Transforming Growth Factor-β, bFGF- Basic Fibroblast Growth Factor, ANG1- Angiopoetin 1, GDNF- Glial-Derived Neurotrophic Factor, ET- Endothelin 1, TIE2- Endothelium Specific Receptor Tyrosine Kinase 2, P2Y2- Purinergic Receptor, and 5-HT- Serotonin . Modified From Abbott NJ, 2006.[20]

As can be seen in the figure, signaling occurs in both directions with astrocytes inducing BMECs through soluble factors such as basic fibroblast growth factor (bFGF) and vice versa with factors such as leukemia inhibitory factor (LIF) which is released by the endothelial cells to promote astrocyte differentiation. While the importance and function of these factors is under some debate, addition and removal of these markers in *in vitro* cell models leads to significant changes in physiological relevance.[18,20,21]

It should also be noted that astrocytes are glial cells with a star-shaped morphology. This star shape is formed by the outgrowth of a number of processes which end at a portion of the cell known as the astrocyte end foot. These end feet wrap

endothelial cells, covering almost the entirety of the capillaries basolateral surface area creating a large surface area in close contact.[22] This may suggest that close interactions between the astrocytes and BMECs is important, and is the basis for the chapters 2 and 3.

Pericytes

Early investigations of the BBB suggested that while other cell types were found in the neurovascular unit, the main cell line responsible for BBB induction was the astrocytes.[23] However, recent *in vitro* studies suggest that the pericytes may also play a role as BMECs grown in coculture with pericytes sometimes show increased TEER values which are indicative of BBB induction.[24] Interestingly, pericyte coverage is not uniform throughout the BBB and varies from approximately 30-100% depending on the location in the brain. This may suggest varying roles throughout the brain.[25]

Unfortunately, little is known about pericyte and endothelial cell interactions, though their close interaction suggests that pericytes may be important for the BBB phenotype. Interestingly, pericytes are found throughout the vasculature and are thought to be important for structural stability and microcontrol of capillary blood flow.[26] They also appear to play a role in regulation of BBB angiogenesis. In addition, recent investigation shows that the pericytes may produce much of the extracellular matrix responsible for supporting cell-cell interactions in the BBB as pericytes are known to secrete collagen, laminin, fibronectin, and glycosaminoglycans.[27]

Extracellular Matrix

As it is not a cell-line and therefore not involved in active signaling, the extracellular matrix (ECM), also known as the basement membrane or basal lamina, is often thought of as a passive player in BBB differentiation. However, the ECM serves as important site for adhesion of the cells of the neurovascular unit, keeping them in close contact.[28] It also may be important for promotion of cell polarity.[29] The ECM of the BBB varies in thickness and is thinner than that of the periphery ranging from 20-200 nm.[30] It consists of entwined protein sheets comprised of mainly collagen (mostly Type IV which is indicative of the BBB), laminins, nidogens, heparin sulfate proteoglycans (i.e. agrin).[31] Interestingly, each of these proteins is mostly excreted by different cell lines, which suggests that interaction between different cells in the neurovascular unit may be important.[32]

Support for the importance of the ECM at the BBB can be seen in a number of disease states. For instance, tumors of the brain are often absent of the astrocyte-produced agrin.[20] This is thought to play a part in the increased leakiness found in the vasculature feeding these tumors. In addition, genetic mutations in Type IV collagen leads to brain hemorrhage in animal models.[33] While this suggests that the ECM is important, the exact functions are still unknown. One method of studying these interactions is through *in vitro* cell culture, however, the ECM used in these cultures is often much simpler than the complex matrix found *in vivo*. This makes it difficult to draw conclusions, and also may represent a deficiency in *in vitro* BBB cell models.

1.3 Permeability Barriers of the Blood-Brain Barrier

As stressed above, the main feature of the BBB is its ability to act as a highly selective barrier to permeation into the brain. This helps to protect the vulnerable neurons, while allowing permeation of nutrients needed for proper brain function.[6] While nutrient uptake transporters are physiologically important and may be taken advantage of for drug delivery, this section will focus on barriers. These barriers include, tight junctions which are responsible for preventing paracellular permeation of hydrophilic molecules, efflux transporters which pump hydrophobic molecules back into the blood preventing transcellular permeability, and drug metabolizing enzymes (DMEs) which act to break down and inactivate potentially harmful xenobiotics that manage to enter the cell cytoplasm.[34] Potential routes of permeation are shown in Figure 1.3 below.

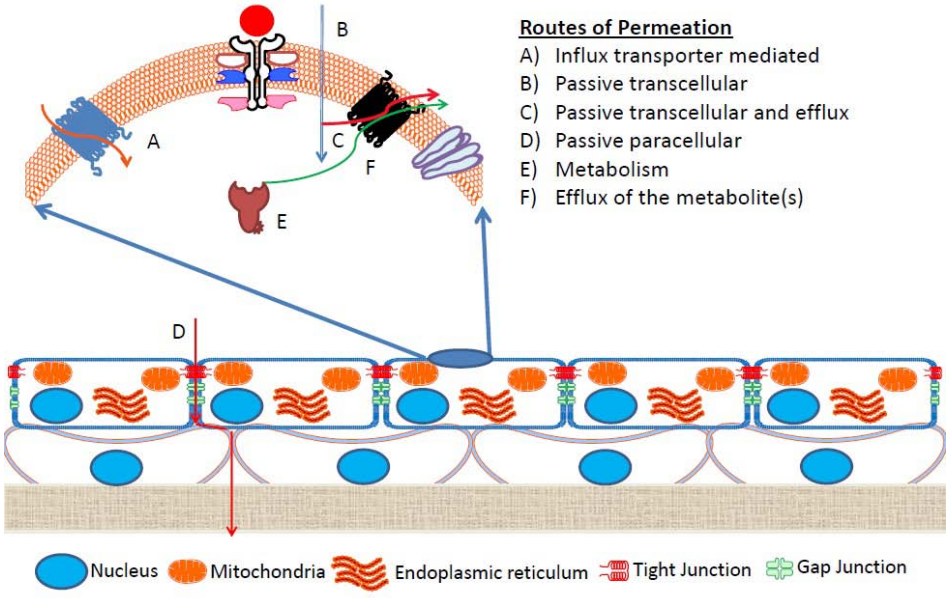

Figure 1.3. Routes of Permeation Across the Blood-Brain Barrier. Modified from Knipp GT, Unpublished.

Tight Junctions

Tight junctions are protein assemblies which form complex intramembranous strands.[11] Complementary strands on neighboring cells interact through protein-protein interactions of integral membrane proteins, closing the gap between the cells.[35] While found in other areas of the body including the kidney and intestine, the tight junctions of the BBB are the most exclusive and most abundant.[5] In the brain, these tight junctions are known to exclude even small elemental ions such as Na^+ and Cl^-. This restriction of ions leads to high *in vivo* transendothelial electrical resistance (TEER) of 1,500-2,000 Ω*cm.[2,20] This high electrical resistance is indicative of the BBB phenotype, and is often used as a marker for distinguishing BBB induction. The main function of the tight junctions is to prevent the movement of hydrophilic molecules by the paracellular route through cell-cell junctions.[36] In addition, the tight junctions also promote cell polarity by preventing the diffusion of transmembrane proteins expressed on the apical and basolateral surfaces of the cell.[37]

The tight junctions are highly regulated and organized being composed of a complex interaction of both integral membrane proteins, i.e. occludin, claudins, and junctional adhesion molecules (JAMs), and intercellular accessory proteins , i.e. zona occludins (ZO) and cingulin, which can be seen in Figure 1.4.[11] As mentioned above, the integral membrane proteins act as extracellular sites for cell-cell interactions, however, these proteins must be connected to the cytoskeleton by the cytoplasmic accessory proteins to allow for the contraction responsible for closing cell-cell gaps.[28]

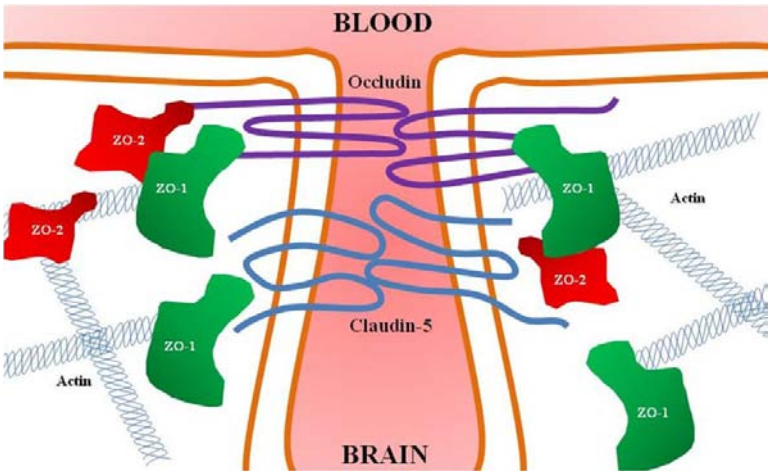

Figure 1.4. Molecular Organization of the Tight Junctions. Modified From Neuwelt, et al. 2008[38]

Within the tight junction, different proteins are believed to have different roles. Claudins are believed to be the main protein responsible for sealing the tight junction through homo- or heterotypic binding.[39] While well over 20 claudins are known, claudin-1, claudin-3, and particularly claudin-5 are thought to be responsible for the increased tightness found in the brain.[11,39] Occludin proteins were once thought to be the main permeation barrier, however, knockout studies have shown only small changes in paracellular permeability *in vivo*, which are not indicative of a phenotype devoid of tight junctions.[40] Instead, it is now thought that changes in occludin phosphorylation state may be important for regulating small changes in tight junction permeability.[11] While not playing a physical role in actual permeability restriction, the intracellular accessory proteins are important for tight junction localization, formation, and function. In fact, loss of ZO-1 and ZO-2 leads to loss of claudin recruitment and failure to form tight junctions.[40]

Drug Efflux

While the tight junctions prevent paracellular permeation at the cell junction, the BBB is also impermeable to many hydrophobic molecules which must often transverse the barrier through passive transcellular permeation.[3] In large part, this impermeability is due the dense presence of energy dependent ATP Binding Cassette (ABC) transporters known as efflux transporters shown in Figure 1.5. These transporters use ATP to pump molecules out of the cell against their concentration gradients.[41] The transporters are comparatively unspecific in comparison to their uptake counterparts, and act to pump a variety of different compounds. In addition, they have a large overlap of substrates leading to reduced permeation of many compounds even if one efflux transporter is absent or knocked down.[42] It is likely that these transporters evolved to prevent harmful toxins and xenobiotics from reaching the brain, however, these proteins now present a significant barrier to drug delivery.[43]

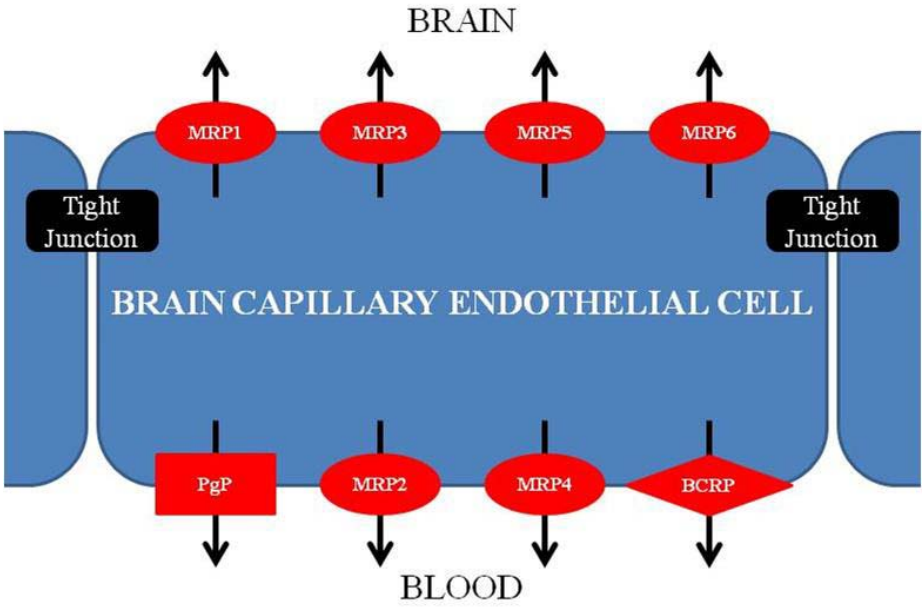

Figure 1.5. Efflux Proteins at the Blood-Brain Barrier. Modified From Löscher. 2005.[41]

Looking at Figure 1.5, it is interesting to see that while a number of the most commonly cited efflux proteins such as P-glycoprotein (P-gp), breast cancer resistance protein (BCRP), and some multidrug resistance proteins (MRPs) are found on the luminal membrane of the endothelial cells, additional transporters are found on the abluminal surface facing the brain.[41] This is likely to pump endogenous neurotrophic factors against their concentrations and kept within the brain.[44] While these abluminal transporters may serve as a potential area for drug delivery exploitation, through both increased permeation across the endothelial barrier and reduced clearance from the brain, little investigation in this area appears in the literature. Instead, most research is focused on overcoming luminal efflux.

In general, the more hydrophobic the molecule the more readily it permeates the BBB as can be seen in Figure 1.6. However, as mentioned above, the efflux proteins of

the BBB are notoriously promiscuous and in addition, many of these transporters are upregulated in various disease states.[45] As indicated in the figure, while BBB permeability increases with the partition coefficient, so does the likelihood of being a substrate for efflux transporters.[46] This further complicates drug development making early prediction through *in silico* and *in vitro* modeling imperative.

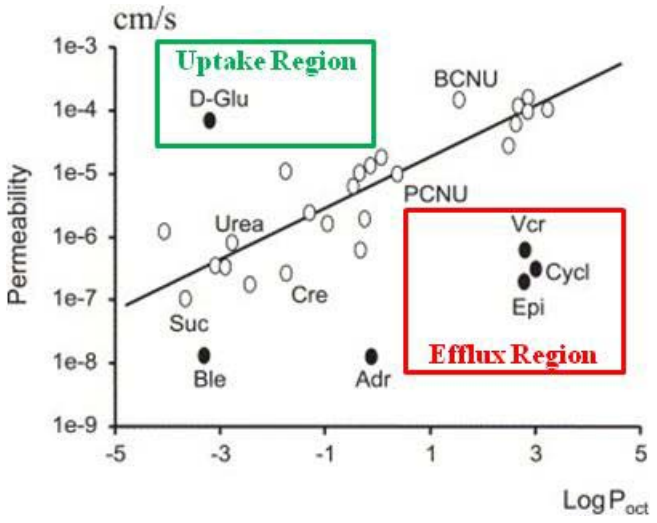

Figure 1.6. Blood-Brain Barrier Permeability vs. Partition Coefficient. Dark Colored Ovals Reflect Efflux and Uptake Markers. Modified From Begley, D. 2004.[46]

Drug Metabolizing Enzymes

Drug metabolizing enzymes are a class of enzymes known to modify pharmaceutical compounds in a number of ways often leading to increased clearance and reduced potency. Drug metabolism is broken up into two categories known as Phase I and II. Phase I metabolism (including oxidation, reduction, or hydrolysis) acts to introduce reactive/polar constituents into their substrates which often leads to increased

elimination.[47] Phase II metabolism, on the other hand, utilizes molecular conjugation (i.e. methylation, acetylation, glucuronidation, etc) as opposed to molecular modification.[48] Oftentimes, these routes of metabolism are used in conjunction with a site for Phase II conjugation being first formed through Phase I molecular modification.[47]

As can be seen in Figure 1.7, even if pharmaceutical compounds are able to permeate into the cell, a number of DMEs are present to potentially degrade them. Interestingly, expression of DMEs at the BBB is significantly different at the microvessel than in the cortex which may be due in part to the differences in endogenous metabolomic needs.[49] In addition, while CYP3A4 is generally first thought of due to its high expression in the periphery, some suggest little expression is seen in the brain. Instead, high amounts of CYP1B1 are found compared to the periphery.[34] It should also be noted, that in addition to BMECs, astrocytes are also thought to produce CYPs, though *in vivo* expression patterns aren't well understood.

		Expression	
	Gene	Brain Cortex	Microvessels
ABC Transporters	ABCB1	+	+
	ABCG2	+	+
	ABCC1	+	+
	ABCC2	ND	ND
	ABCC3	ND	ND
	ABCC4	+	+
	ABCC5	+	+
	ABCC6	+	+
	ABCC11	+	+
	ABCC12	+	+
Cytochrome P450	CYP1A1	+	+
	CYP1A2	ND	ND
	CYP1B1	+	+
	CYP2A6	ND	ND
	CYP2A7	ND	ND
	CYP2A13	ND	ND
	CYP2B6	+	+
	CYP2C8	+	+
	CYP2C9	ND	ND
	CYP2C18	ND	ND
	CYP2C19	ND	ND
	CYP2D6	+	+
	CYP2E1	+	+
	CYP3A4	ND	ND
	CYP3A5	ND	ND
	CYP3A7	ND	ND
Transcription Factors	PXR	ND	ND
	CAR	NQ	NQ
	AhR	+	+

Figure 1.7. In Vivo mRNA Expression of Human Drug Metabolizing Enzymes at the BBB. ND-Not Detected, NQ-Non-Quantifiable. Results are from 7 patients. Modified From Dauchy, et. al. 2008.[49]

1.4 In Vitro Models of the Blood Brain Barrier

Ideally, one would use *in vivo* animal models to predict disposition into the brain due the complexity of the BBB. A number of techniques are available including intravenous injection, injection into the carotid artery, perfusion studies, and intracerebral

microdialysis.[50,51] While these techniques are highly invasive and only possible in diseased patients and animal models, sampling of human cerebral spinal fluid (CSF) is possible for compounds which have reached clinical trials. However, the correlation between disposition into the brain and CSF is debatable.[52] Nonetheless, all of these studies are rather expensive and unrealistic especially for drug discovery and lead selection. Therefore, *in silico* and *in vitro* models have been established to, at minimum, help rank order druggable candidates in discovery.

The simplest *in vitro* BBB models consist of cerebral microvessels in monoculture. In these models, BMECs are plated onto microporous inserts, i.e. Transwell® filter supports.[53] While human BMECs would be ideal, models often utilize primary cells of various animal origins including bovine, porcine, murine, rat, and monkey due to the high demand and low availability of human tissues.[34] While these cells are often cheaper and easier to acquire, it is important to recognize potential species differences, which affect all routes of permeation. For instance, many animal endothelial cells express over two-fold increases in claudin-5 as compared to human BMECs.[54] In addition, many species express varying levels of efflux transporters, often with much higher P-glycoprotein expression and lower levels of BCRP and MRPs.[55] Finally, expression differences in DMEs are speculated to be highly variable between species.[56] These changes can culminate in significant changes in BBB permeability prediction as shown in a recent study comparing rodent and human BBB models which predicted, on average, two-fold higher permeability in rodent models for a small catalog of compounds.[57]

In order to alleviate some of these issues, a number of groups have begun work in immortalization of human BMECs. Immortalization of these cells allows for a more consistent phenotype over a longer number of passages, drastically increasing supply. A few immortalized human BMEC cell lines are currently available including human cerebral microvessel endothelial cells (hCMEC/D3s), human brain microvessel endothelial cells (hBMEC), TY10 cells, BB19 cells, as well as a number of proprietary cell lines.[58] However, all of these cell lines suffer from one significant detriment in an inability to prevent paracellular permeation, a hallmark of the BBB.[58] Immortalized cell lines often suffer from low TEER which rarely reaches 150 Ohm*cm^2, much lower than reported *in vivo* values (though it should be noted that these *in vivo* values are reported from animal specimens).[34,59] In an attempt to increase TEER, some progress has been made through media optimization, different immortalization techniques, and primary cell culture selection; however, the largest increases have been seen through coculture with supporting cells of the neurovascular unit.[8,16-18,24,53,57,60-65]

Since it is believed that interactions between BMECs and supporting cells of the neurovascular unit are at least in part responsible for the BBB endothelial cell phenotype, it is somewhat unsurprising that lack of this interaction leads to poor *in vitro* relevance. As discussed above, while first studied to examine the role of supporting cells at the BBB, coculture with these cells has lead to increased tight junction complexity and function as well as upregulation of a number of transporters.[16,20,21] For this reason, many studies now utilize co- and triculture in *in vitro* BBB permeability prediction. A number

of setups have been reported including culture with astrocytes, pericytes, and/or neurons. Some of these models are shown in Figure 1.8.

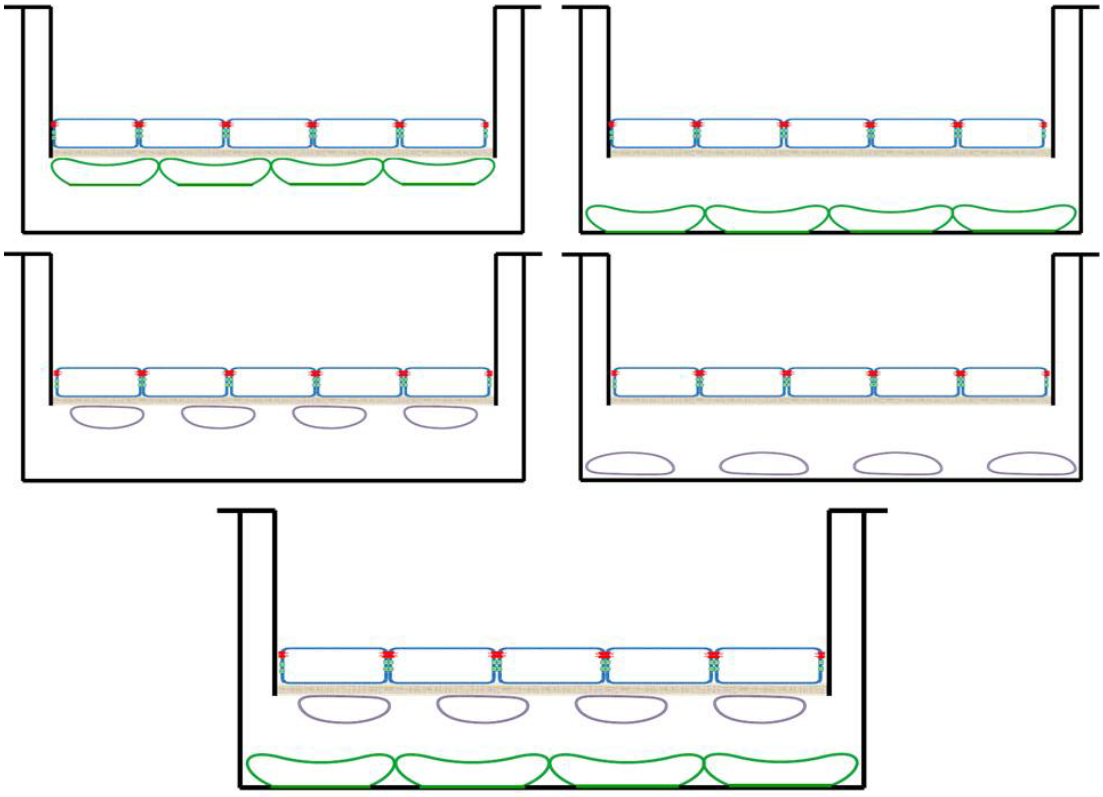

Figure 1.8. In Vitro Transwell Co- and Triculture Models. Cells are represented as Blue-Endothelial Cells, Purple-Pericytes, and Green-Astrocytes.

While results have been somewhat inconsistent, all of these models have been shown to lead to varying degrees of increased TEER. However, while TEER has increased, only small changes in marker paracellular permeability were seen and still represent a drastically less restrictive model in comparison to *in vivo* conditions.[34] An additional downside to these models is in increased complexity in cell culture which may hinder their utility in high-throughput screens. This is especially true of the models

which utilize culturing cells on the underside of the Transwell® support. In order to culture in this fashion, the filter is first flipped and cells are allowed to adhere and proliferate for a designated amount of time.[62] This process is likely to be a very difficult accomplishment by automated high-throughput cell culture technologies.

Due to the continued lack of adequate tight junctions in the Transwell® model, a few new models have been developed. One of these models was coined the dynamic *in vitro* model.[66] Here a hollow porous fiber is used instead of a flat filter. Endothelial cells are seeded onto the inside of this fiber and in some cases supporting cells are seeded onto the outside. After adhesion, media is pumped through the model which allows for continual shear on the cells similar to that found *in vivo*.[67] Interestingly, while further investigation is needed, hCMEC/D3 TEER approaches 1000 Ω*cm^2 suggesting that shear may play a crucial role in BMEC differentiation.[68] Additionally, new microfluidic models have been established which also utilize shear as a mechanism of differentiation.[69] In these models, a semi-porous filter is placed between two microfluidic channels. The setup of these models is very similar to the Transwell® models, with the exception that media is then pumped across these channels to mimic shear. Due to the small size of these models, they also require a much lower number of cells, which may allow them to be conducive to studies with primary human cells.[69] Although it is an interesting model, at this time TEER values in these microfluidic models are still comparable to Transwell® models.

1.5 References

1. Abbott NJ Blood-brain barrier structure and function and the challenges for CNS drug delivery. J Inherit Metab Dis 36(3):437-449.
2. Cecchelli R, Berezowski V, Lundquist S, Culot M, Renftel M, Dehouck MP, Fenart L 2007. Modelling of the blood-brain barrier in drug discovery and development. Nat Rev Drug Discov 6(8):650-661.
3. Ballabh P, Braun A, Nedergaard M 2004. The blood-brain barrier: an overview: structure, regulation, and clinical implications. Neurobiol Dis 16(1):1-13.
4. Chen Y, Liu L Modern methods for delivery of drugs across the blood-brain barrier. Adv Drug Deliv Rev 64(7):640-665.
5. Liebner S, Kniesel U, Kalbacher H, Wolburg H 2000. Correlation of tight junction morphology with the expression of tight junction proteins in blood-brain barrier endothelial cells. Eur J Cell Biol 79(10):707-717.
6. Poller B, Gutmann H, Krahenbuhl S, Weksler B, Romero I, Couraud PO, Tuffin G, Drewe J, Huwyler J 2008. The human brain endothelial cell line hCMEC/D3 as a human blood-brain barrier model for drug transport studies. J Neurochem 107(5):1358-1368.
7. Abbott NJ 2005. Dynamics of CNS barriers: evolution, differentiation, and modulation. Cell Mol Neurobiol 25(1):5-23.

8. Cecchelli R, Dehouck B, Descamps L, Fenart L, Buee-Scherrer VV, Duhem C, Lundquist S, Rentfel M, Torpier G, Dehouck MP 1999. In vitro model for evaluating drug transport across the blood-brain barrier. Adv Drug Deliv Rev 36(2-3):165-178.

9. Stewart PA, Wiley MJ 1981. Developing nervous tissue induces formation of blood-brain barrier characteristics in invading endothelial cells: a study using quail--chick transplantation chimeras. Dev Biol 84(1):183-192.

10. Abbott NJ, Patabendige AA, Dolman DE, Yusof SR, Begley DJ Structure and function of the blood-brain barrier. Neurobiol Dis 37(1):13-25.

11. Wolburg H, Lippoldt A 2002. Tight junctions of the blood-brain barrier: development, composition and regulation. Vascul Pharmacol 38(6):323-337.

12. Weiss N, Miller F, Cazaubon S, Couraud PO 2009. The blood-brain barrier in brain homeostasis and neurological diseases. Biochim Biophys Acta 1788(4):842-857.

13. Pardridge WM Drug transport across the blood-brain barrier. J Cereb Blood Flow Metab 32(11):1959-1972.

14. Oldendorf WH, Cornford ME, Brown WJ 1977. The large apparent work capability of the blood-brain barrier: a study of the mitochondrial content of capillary endothelial cells in brain and other tissues of the rat. Ann Neurol 1(5):409-417.

15. Golden PL, Pollack GM 2003. Blood-brain barrier efflux transport. J Pharm Sci 92(9):1739-1753.

16. Arthur FE, Shivers RR, Bowman PD 1987. Astrocyte-mediated induction of tight junctions in brain capillary endothelium: an efficient in vitro model. Brain Res 433(1):155-159.

17. Yamagata K, Tagami M, Nara Y, Mitani M, Kubota A, Fujino H, Numano F, Kato T, Yamori Y 1997. Astrocyte-conditioned medium induces blood-brain barrier properties in endothelial cells. Clin Exp Pharmacol Physiol 24(9-10):710-713.

18. Garcia CM, Darland DC, Massingham LJ, D'Amore PA 2004. Endothelial cell-astrocyte interactions and TGF beta are required for induction of blood-neural barrier properties. Brain Res Dev Brain Res 152(1):25-38.

19. Holash JA, Noden DM, Stewart PA 1993. Re-evaluating the role of astrocytes in blood-brain barrier induction. Dev Dyn 197(1):14-25.

20. Abbott NJ, Ronnback L, Hansson E 2006. Astrocyte-endothelial interactions at the blood-brain barrier. Nat Rev Neurosci 7(1):41-53.

21. Berezowski V, Landry C, Dehouck MP, Cecchelli R, Fenart L 2004. Contribution of glial cells and pericytes to the mRNA profiles of P-glycoprotein and multidrug resistance-associated proteins in an in vitro model of the blood-brain barrier. Brain Res 1018(1):1-9.

22. Li G, Simon MJ, Cancel LM, Shi ZD, Ji X, Tarbell JM, Morrison B, 3rd, Fu BM Permeability of endothelial and astrocyte cocultures: in vitro blood-brain barrier models for drug delivery studies. Ann Biomed Eng 38(8):2499-2511.

23. Al Ahmad A, Taboada CB, Gassmann M, Ogunshola OO Astrocytes and pericytes differentially modulate blood-brain barrier characteristics during development and hypoxic insult. J Cereb Blood Flow Metab 31(2):693-705.

24. Nakagawa S, Deli MA, Nakao S, Honda M, Hayashi K, Nakaoke R, Kataoka Y, Niwa M 2007. Pericytes from brain microvessels strengthen the barrier integrity in primary cultures of rat brain endothelial cells. Cell Mol Neurobiol 27(6):687-694.

25. Mathiisen TM, Lehre KP, Danbolt NC, Ottersen OP The perivascular astroglial sheath provides a complete covering of the brain microvessels: an electron microscopic 3D reconstruction. Glia 58(9):1094-1103.

26. Liu S, Agalliu D, Yu C, Fisher M The role of pericytes in blood-brain barrier function and stroke. Curr Pharm Des 18(25):3653-3662.

27. Hirschi KK, D'Amore PA 1996. Pericytes in the microvasculature. Cardiovasc Res 32(4):687-698.

28. Engelhardt B 2003. Development of the blood-brain barrier. Cell Tissue Res 314(1):119-129.

29. Engelhardt B beta1-integrin/matrix interactions support blood-brain barrier integrity. J Cereb Blood Flow Metab 31(10):1969-1971.

30. Engelhardt B, Sorokin L 2009. The blood-brain and the blood-cerebrospinal fluid barriers: function and dysfunction. Semin Immunopathol 31(4):497-511.

31. Hohenester E, Yurchenco PD Laminins in basement membrane assembly. Cell Adh Migr 7(1):56-63.

32. Baeten KM, Akassoglou K Extracellular matrix and matrix receptors in blood-brain barrier formation and stroke. Dev Neurobiol 71(11):1018-1039.

33. Plaisier E, Ronco P 1993. COL4A1-Related Disorders.

34. Wilhelm I, Krizbai IA In vitro models of the blood-brain barrier for the study of drug delivery to the brain. Mol Pharm 11(7):1949-1963.

35. Wolburg H, Neuhaus J, Kniesel U, Krauss B, Schmid EM, Ocalan M, Farrell C, Risau W 1994. Modulation of tight junction structure in blood-brain barrier endothelial cells. Effects of tissue culture, second messengers and cocultured astrocytes. J Cell Sci 107 (Pt 5):1347-1357.

36. Luissint AC, Artus C, Glacial F, Ganeshamoorthy K, Couraud PO Tight junctions at the blood brain barrier: physiological architecture and disease-associated dysregulation. Fluids Barriers CNS 9(1):23.

37. Shin K, Fogg VC, Margolis B 2006. Tight junctions and cell polarity. Annu Rev Cell Dev Biol 22:207-235.

38. Neuwelt E, Abbott NJ, Abrey L, Banks WA, Blakley B, Davis T, Engelhardt B, Grammas P, Nedergaard M, Nutt J, Pardridge W, Rosenberg GA, Smith Q, Drewes LR 2008. Strategies to advance translational research into brain barriers. Lancet Neurol 7(1):84-96.

39. Schrade A, Sade H, Couraud PO, Romero IA, Weksler BB, Niewoehner J Expression and localization of claudins-3 and -12 in transformed human brain endothelium. Fluids Barriers CNS 9:6.

40. Marchiando AM, Graham WV, Turner JR Epithelial barriers in homeostasis and disease. Annu Rev Pathol 5:119-144.

41. Loscher W, Potschka H 2005. Blood-brain barrier active efflux transporters: ATP-binding cassette gene family. NeuroRx 2(1):86-98.

42. Wong K, Ma J, Rothnie A, Biggin PC, Kerr ID Towards understanding promiscuity in multidrug efflux pumps. Trends Biochem Sci 39(1):8-16.

43. Terasaki T, Ohtsuki S 2005. Brain-to-blood transporters for endogenous substrates and xenobiotics at the blood-brain barrier: an overview of biology and methodology. NeuroRx 2(1):63-72.

44. Roberts LM, Black DS, Raman C, Woodford K, Zhou M, Haggerty JE, Yan AT, Cwirla SE, Grindstaff KK 2008. Subcellular localization of transporters along the rat blood-brain barrier and blood-cerebral-spinal fluid barrier by in vivo biotinylation. Neuroscience 155(2):423-438.

45. Hoffmann K, Loscher W 2007. Upregulation of brain expression of P-glycoprotein in MRP2-deficient TR(-) rats resembles seizure-induced up-regulation of this drug efflux transporter in normal rats. Epilepsia 48(4):631-645.

46. Begley DJ 2004. Delivery of therapeutic agents to the central nervous system: the problems and the possibilities. Pharmacol Ther 104(1):29-45.

47. Iyanagi T 2007. Molecular mechanism of phase I and phase II drug-metabolizing enzymes: implications for detoxification. Int Rev Cytol 260:35-112.

48. Jancova P, Anzenbacher P, Anzenbacherova E Phase II drug metabolizing enzymes. Biomed Pap Med Fac Univ Palacky Olomouc Czech Repub 154(2):103-116.

49. Dauchy S, Dutheil F, Weaver RJ, Chassoux F, Daumas-Duport C, Couraud PO, Scherrmann JM, De Waziers I, Decleves X 2008. ABC transporters, cytochromes P450 and their main transcription factors: expression at the human blood-brain barrier. J Neurochem 107(6):1518-1528.

50. Boje KM 2001. In vivo measurement of blood-brain barrier permeability. Curr Protoc Neurosci Chapter 7:Unit 7 19.

51. Hansen DK, Scott DO, Otis KW, Lunte SM 2002. Comparison of in vitro BBMEC permeability and in vivo CNS uptake by microdialysis sampling. J Pharm Biomed Anal 27(6):945-958.

52. Ylitalo P, Salmela P, Elo HA 1983. Correlation between brain tissue and cerebrospinal fluid concentrations of selected compounds in rats with intact and injured blood-brain barrier. Exp Neurol 81(3):517-527.

53. Weksler B, Romero IA, Couraud PO The hCMEC/D3 cell line as a model of the human blood brain barrier. Fluids Barriers CNS 10(1):16.

54. Hoshi Y, Uchida Y, Tachikawa M, Inoue T, Ohtsuki S, Terasaki T Quantitative atlas of blood-brain barrier transporters, receptors, and tight junction proteins in rats and common marmoset. J Pharm Sci 102(9):3343-3355.

55. Deo AK, Theil FP, Nicolas JM Confounding parameters in preclinical assessment of blood-brain barrier permeation: an overview with emphasis on species differences and effect of disease states. Mol Pharm 10(5):1581-1595.

56. Shawahna R, Decleves X, Scherrmann JM Hurdles with using in vitro models to predict human blood-brain barrier drug permeability: a special focus on transporters and metabolizing enzymes. Curr Drug Metab 14(1):120-136.

57. Lacombe O, Videau O, Chevillon D, Guyot AC, Contreras C, Blondel S, Nicolas L, Ghettas A, Benech H, Thevenot E, Pruvost A, Bolze S, Krzaczkowski L, Prevost C, Mabondzo A In vitro primary human and animal cell-based blood-brain barrier models as a screening tool in drug discovery. Mol Pharm 8(3):651-663.

58. Eigenmann DE, Xue G, Kim KS, Moses AV, Hamburger M, Oufir M Comparative study of four immortalized human brain capillary endothelial cell lines, hCMEC/D3, hBMEC, TY10, and BB19, and optimization of culture conditions, for an in vitro blood-brain barrier model for drug permeability studies. Fluids Barriers CNS 10(1):33.

59. Butt AM, Jones HC, Abbott NJ 1990. Electrical resistance across the blood-brain barrier in anaesthetized rats: a developmental study. J Physiol 429:47-62.

60. Di L, Kerns EH, Fan K, McConnell OJ, Carter GT 2003. High throughput artificial membrane permeability assay for blood-brain barrier. Eur J Med Chem 38(3):223-232.

61. Gaillard PJ, Voorwinden LH, Nielsen JL, Ivanov A, Atsumi R, Engman H, Ringbom C, de Boer AG, Breimer DD 2001. Establishment and functional characterization of an in vitro model of the blood-brain barrier, comprising a co-culture of brain capillary endothelial cells and astrocytes. Eur J Pharm Sci 12(3):215-222.

62. Hatherell K, Couraud PO, Romero IA, Weksler B, Pilkington GJ Development of a three-dimensional, all-human in vitro model of the blood-brain barrier using mono-, co-, and tri-cultivation Transwell models. J Neurosci Methods 199(2):223-229.

63. Helms HC, Waagepetersen HS, Nielsen CU, Brodin B Paracellular tightness and claudin-5 expression is increased in the BCEC/astrocyte blood-brain barrier model by increasing media buffer capacity during growth. AAPS J 12(4):759

64. Lippmann ES, Al-Ahmad A, Palecek SP, Shusta EV Modeling the blood-brain barrier using stem cell sources. Fluids Barriers CNS 10(1):2.

65. Schiera G, Bono E, Raffa MP, Gallo A, Pitarresi GL, Di Liegro I, Savettieri G 2003. Synergistic effects of neurons and astrocytes on the differentiation of brain capillary endothelial cells in culture. J Cell Mol Med 7(2):165-170.

66. Cucullo L, Marchi N, Hossain M, Janigro D A dynamic in vitro BBB model for the study of immune cell trafficking into the central nervous system. J Cereb Blood Flow Metab 31(2):767-777.

67. Naik P, Cucullo L In vitro blood-brain barrier models: current and perspective technologies. J Pharm Sci 101(4):1337-1354.

68. Cucullo L, Couraud PO, Weksler B, Romero IA, Hossain M, Rapp E, Janigro D 2008. Immortalized human brain endothelial cells and flow-based vascular modeling: a marriage of convenience for rational neurovascular studies. J Cereb Blood Flow Metab 28(2):312-328.

69. Booth R, Kim H Characterization of a microfluidic in vitro model of the blood-brain barrier (muBBB). Lab Chip 12(10):1784-1792.

CHAPTER 2. INNOVATION AND OPTIMIZATION OF A DIRECT CONTACT BLOOD-BRAIN BARRIER *IN* VITRO MODEL

2.1 Innovation of a Direct Contact Coculture In Vitro Model

Cell Selection

Cell selection first began with selection of an endothelial cell line. While it is believed that primary human BMEC's may represent the most physiologically relevant cell line for the model, at this time they are cost prohibitive due to their low supply and high demand. Therefore, an immortalized human BMEC line was selected.[1] Because of its history in our lab and popularity in the field, the human cerebral microvessel endothelial cell line (hCMEC/D3) was selected as the endothelial cell line for initial studies.

The hCMEC/D3 cell line was developed and graciously donated by Dr. Pierre Couraud of the Universite Rene Descartes. The primary cell line was isolated from excised tissue of an adult female with epilepsy and then immortalized through lentiviral transduction of hTERT and SV40 large T-antigen.[2] These proteins act in conjunction to prevent reduction in telomere length which acts to extend the useful number of passages for a cell line. The hCMEC/D3s are known to grow for at least 35 passages without exhibiting dedifferentiation or senescence, which represents a large increase in useful

lifespan over primary cells which often last less than 5 passages.[3] In addition, hCMEC/D3 cells are contact-inhibited meaning that upon cell-cell contact the cells move from a proliferative state to a differentiated state. This makes them a good candidate for monolayer formation in *in vitro* studies.[2,3]

In addition, the cell line also expresses most BBB-specific markers which are important in cell screening of pharmaceutical compounds across the BBB.[3] hCMEC/D3s express tight junction proteins such as ZO-1, JAM-A, occludin, as well as claudins, including claudin-5 which is thought to be the most important for BBB tightness.[4] They are also known to express a number of efflux proteins including P-glycoprotein, MRP1, and BCRP.[5] Finally, previous work in our lab has shown expression of a number of ABC and SLC transporters.[6] However, while all of these proteins are expressed, their expression in hCMEC/D3s varies widely when compared to primary human BMECs.[7] In addition, at least when grown in monoculture, localization at cell-cell contacts of some tight junction proteins is not seen which may indicate the reason for increased paracellular permeation across hCMEC/D3 monolayers.

Due to the current lack of an established immortalized human astrocyte cell line, primary human astrocytes were purchased from ScienCell. While a lack of supply and high cost are disadvantages to using the primary human astrocytes, the use of a human cell line was deemed necessary leaving few options at this time. In addition, it's speculated that lot-to-lot differences in astrocytes would have reduced effects when compared to endothelial cells due to their mostly supportive role in barrier formation.

This is confirmed in part by insignificant differences between multiple cell lots currently used in the lab.

Direct Contact Model

In order to initially test the hypothesis that direct-contact coculture of hCMEC/D3 and human astrocytes leads to a more physiologically relevant model, a preliminary study was run to measure the differences in [C14]-Mannitol permeability between hCMEC/D3 cells alone in monoculture and in coculture with human astrocytes. Initial studies were conducted on collagen coated Transwell® filter supports. In order to maintain physiological relevance, the human astrocytes were plated first at 40,000 cells/cm^2 in astrocyte medium. Astrocytes were allowed to proliferate to confluence which took approximately two days. A confluent layer of astrocytes was used to allow maximum contact between human astrocytes and hCMEC/D3s as well as to allow the hCMEC/D3s to have an increased chance of forming their own confluent monolayer on a more even surface. In addition, this time allows the astrocytes to produce their ECM which is thought to enhance BBB differentiation. After human astrocytes reached confluence, hCMEC/D3 cells were plated in supplemented EBM-2 at a density of 100,000 cells/cm^2. This density, up to two-fold higher than normally used, was selected as 100% attachment to the astrocyte monolayer wasn't expected. The hCMECs were then allowed 7 days to proliferate and differentiate in contact with the human astrocytes before [C14]-Mannitol permeability was measured. The hCMEC/D3 monocultures were grown in a similar

fashion, onto collagen-coated Transwells® at a density of 100,000 cells/cm^2 and allowed to grow for 7 days before studies. The results of the initial study are shown below.

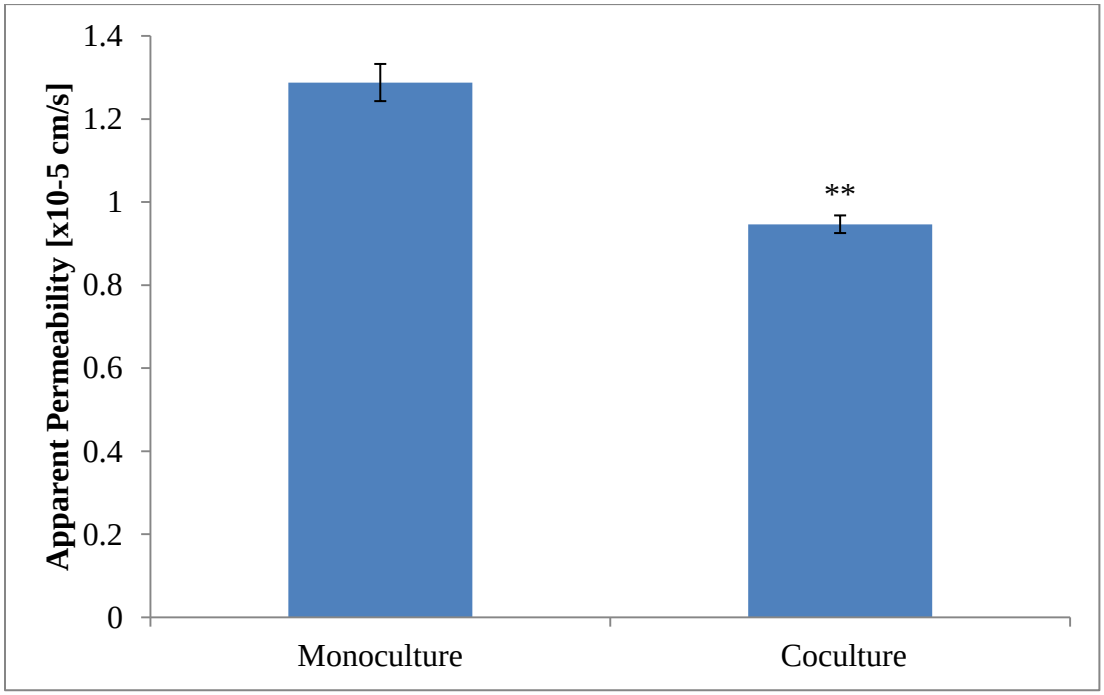

*Figure 2.1. Effect of Direct Astrocyte Coculture on hCMEC/D3 [C14]-Mannitol Permeability. Data is means ± 1 standard deviation of N=3 studies. **:p<0.05*

As can be seen, a significant reduction in [C14]-Mannitol, a paracellular marker, was measured when growing hCMEC/D3 cells in coculture with human astrocytes versus monoculture. Given that one of the significant limitations of hCMEC/D3 monolayers lies in their inability to prevent paracellular permeation, this preliminary study suggests that

direct-contact coculture may serve as a more physiologically-relevant model for *in vitro* BBB permeability prediction.

2.2 Optimization

While initial studies were promising, additional optimization was conducted. Optimization of *in vitro* models is often extensive as many factors play a role in protein expression and cell function. While not an exhaustive optimization, the following studies elucidate parameters that may have the most influence. Since the greatest drawback to the hCMEC/D3 cell line is its high paracellular permeability, optimization was focused on reducing permeability of the paracellular markers [C-14]-Mannitol and [C14]-Sucrose.

Seeding Density

Seeding density represents the number of cells per area plated on the Transwell® permeable support and is given in the units of cells/cm^2. Seeding density serves as an important parameter, especially for contact inhibited cell lines like the hCMEC/D3s. Overseeding at a high density can lead to overgrowth, monolayer doming, and multi-layer formation which reduce the formation of tight junctions. On the other hand, underseeding contact-inhibited cells can lead to colony-like growth due to high amounts of localized cell-cell contact before confluence is reached. A broad range of densities for both hCMEC/D3s (50-100,000 cells/cm^2) and human astrocytes (10-40,000 cells/cm^2) were tested. Results are shown below:

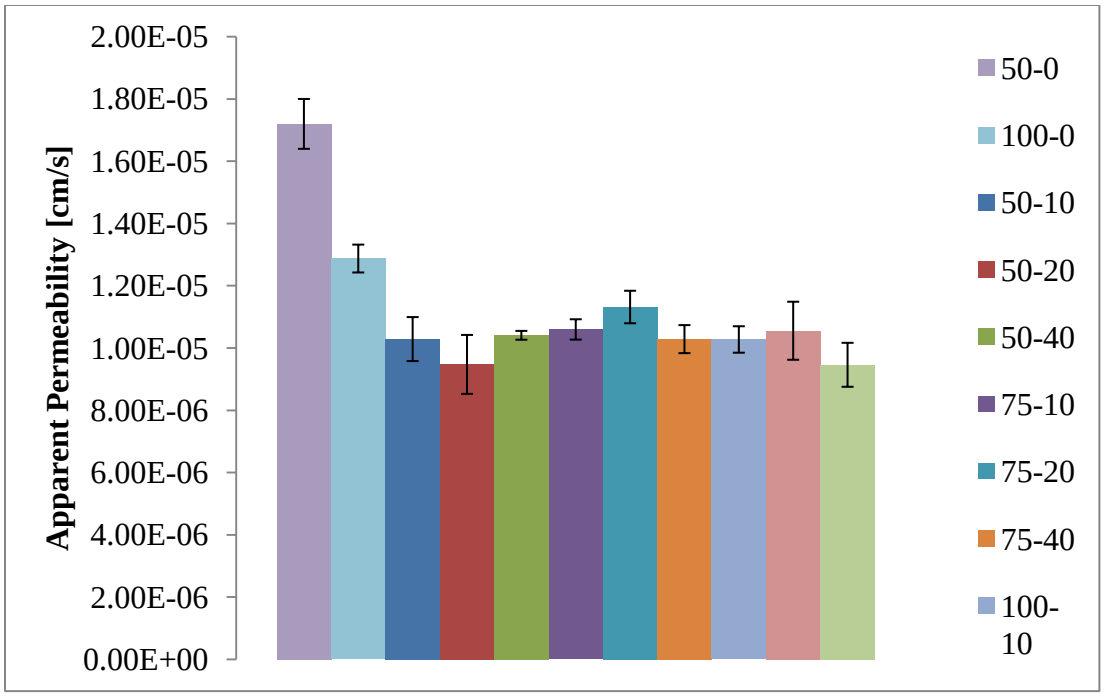

Figure 2.2. Effect of Human Astrocyte and hCMEC/D3 Cell Densities on [C14]-Mannitol Permeability. Key is represented as hCMEC/D3 density x1000 followed by human astrocyte density x1000). Data is means ± 1 standard deviation of N=3 studies.

As can be seen, initial studies suggest that at least in monoculture, higher hCMEC/D3 cell densities lead to lower permeability. It should be noted that 250,000 cells/cm^2 was also run, however, the cell monolayers began to roll making them unable to be used for permeability testing. Interestingly, however, at least in the large range of densities measured, neither the hCMEC/D3 or human astrocyte density seems to play a significant role under current culturing conditions. In addition, no trends were seen that would suggest that the ratio of hCMEC/D3 to human astrocytes is significant in our model.

Seeding Time

In this case, seeding time represents the number of days the cells are allowed to grow post-hCMEC/D3 seeding. Seeding time is often useful in determining both the optimal and acceptable range of days to conduct permeation studies. If studies are done too quickly, the cells do not have adequate time to reach confluence, differentiate, and express tight junction proteins, efflux transporters, etc. However, if the cells are grown for too long, the cells begin to go through apoptosis and monolayer integrity is lost. Also, these additional culture days represent an increase in both cost and time which hinder the utility of a model. Previous work in our lab suggests that the best day for culturing hCMEC/D3 monocultures is approximately 14 days. For this reason we chose to center around this time and measure permeation every other day from day 5 to day 19.

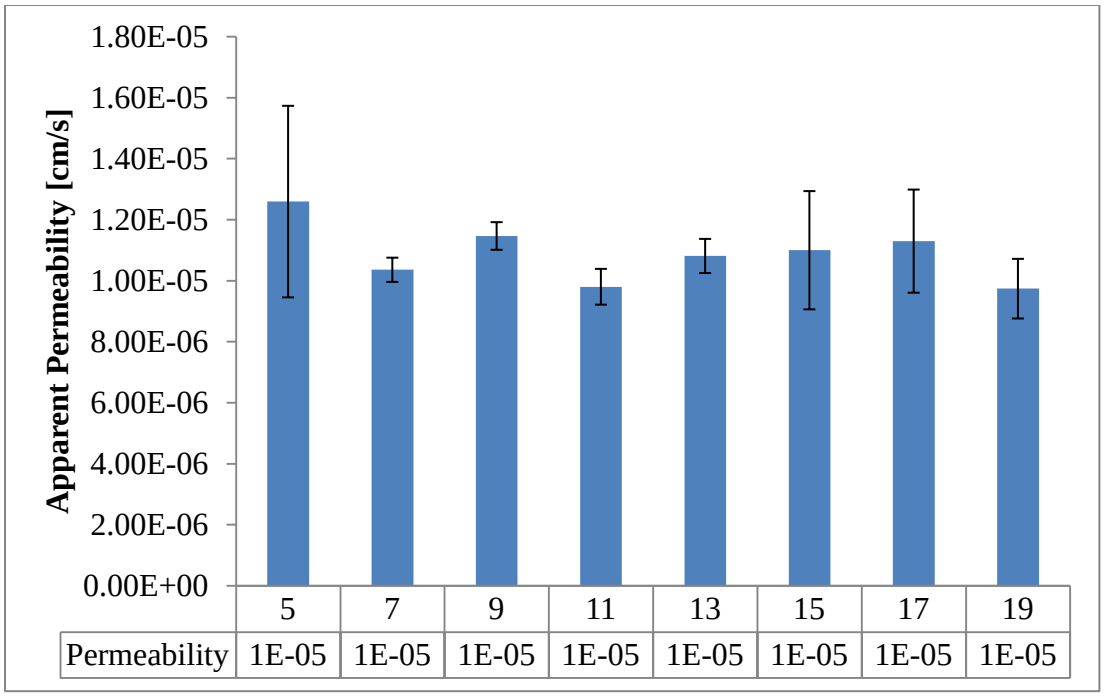

Figure 2.3. Effect of Seeding Time on [C14]-Mannitol Permeability. Data is means ± 1 standard deviation of N=3 studies.

Interestingly, over the time course of the studies run from day 5-19, seeding time seemed to show little significance on [C14]-Mannitol permeability. The highest permeability was on day 5, which suggests that full confluence and differentiation still isn't reached at this time. However, neither significant differences nor trends were seen from day 7 to day 19. This suggests that the hCMEC/D3 monolayers reach full confluence and tight junction differentiation by day 7 and are viable at least until day 19. While for our purposes day 7 appears to be the best day for studies in terms of cost, time, and money, it should be noted that only paracellular permeability has been measured at this time. Additional culture time may be required for full differentiation and

physiologically relevant protein expression and function. Further studies need to be conducted to elucidate these changes in protein expression over time, however, these studies are currently cost-prohibitive.

Seeding Order

In order to determine if a confluent astrocyte monolayer was necessary for hCMEC/D3 monolayer formation, both hCMEC/D3 cells and human astrocytes were plated concurrently. In these studies, hCMEC/D3s and human astrocytes were plated together at 100,000 and 40,000 cells/cm^2 together on collagen coated Transwells® and compared to studies conducted as described in section 2.1.2. Results of the study are shown below.

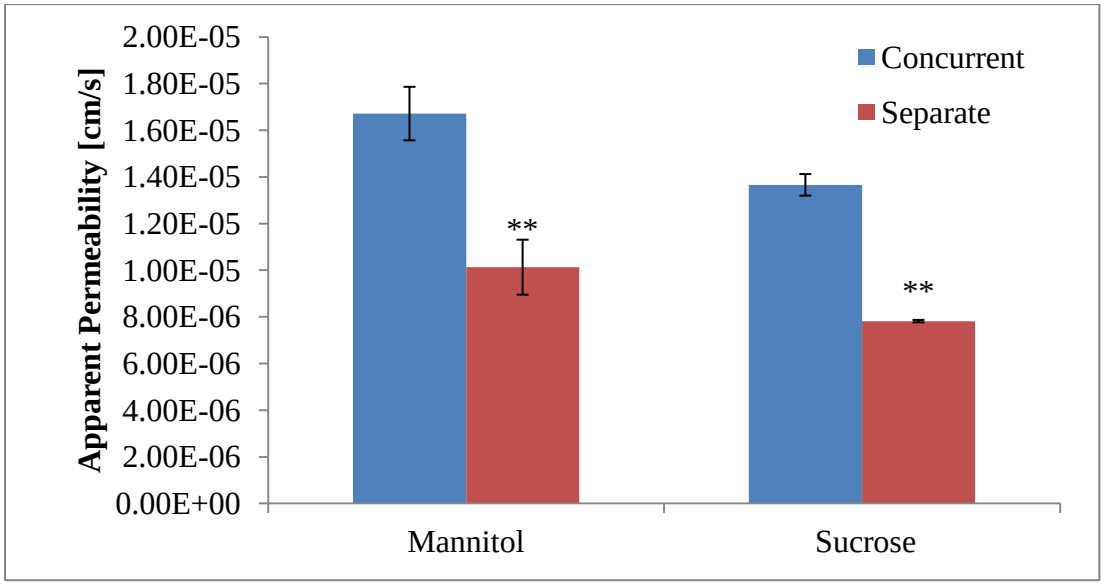

*Figure 2.4. Effect of Concurrent Plating on [C14]-Mannitol and [C14]-Sucrose Permeability. Data is means ± 1 standard deviation of N=3 studies. **:p<0.05*

As expected, it is apparent from this study that concurrent plating of human astrocytes and hCMEC/D3's significantly disrupts the ability of the hCMEC/D3s to form a monolayer and establish cellular tight junctions. This is likely due to a purely physical or steric interaction with the human astrocytes blocking the ability of neighboring hCMEC/D3 cells to establish cell-cell contact. While concurrent plating doesn't appear to be ideal, additional studies could be conducted to establish the optimal of time to seed hCMEC/D3 cells after human astrocyte plating.

Basement Membrane Selection

The basement membrane protein(s) used in a cell culture system are often used as a means to keep a cell monolayer flat for *in vitro* studies. Frequently, endothelial cells will roll into a capillary-like formation upon differentiation due to the poor adhesion between endothelial cells and cell culture plastics. This prevents their use in Transwell® based permeability studies due to the lack of a monolayer and a defined direction of membrane polarization. To counteract this, a basement membrane protein is first seeded down onto the Transwell® and given time to adhere to the plastic. After which, the cell line is placed onto of this ECM layer which acts as a "glue" between the cell line and the plastic.

However, while the basement membrane protein is often chosen solely on its ability to stabilize a cell monolayer, it is known that the ECM is important for cell proliferation and differentiation.[8] Therefore, four different membrane proteins were

tested including Type I rat tail collagen, poly-L-lysine, fibronectin, and MaxGel to measure their influence on tight junction formation. It should be noted that *in vivo* some of the basement membrane proteins tested are found at low or zero levels. Consequently, MaxGel, a proprietary ECM made by Sigma-Aldrich, was also selected as a more relevant matrix. MaxGel contains a mixture of basement membrane proteins including collagens, laminin, fibronectin, tenascin, elastin, proteoglycans, and glycoaminoglycans. Due to the complex nature and closer composition to that found *in vivo*, MaxGel is often used to help promote proliferation and differentiation in BBB cell lines.

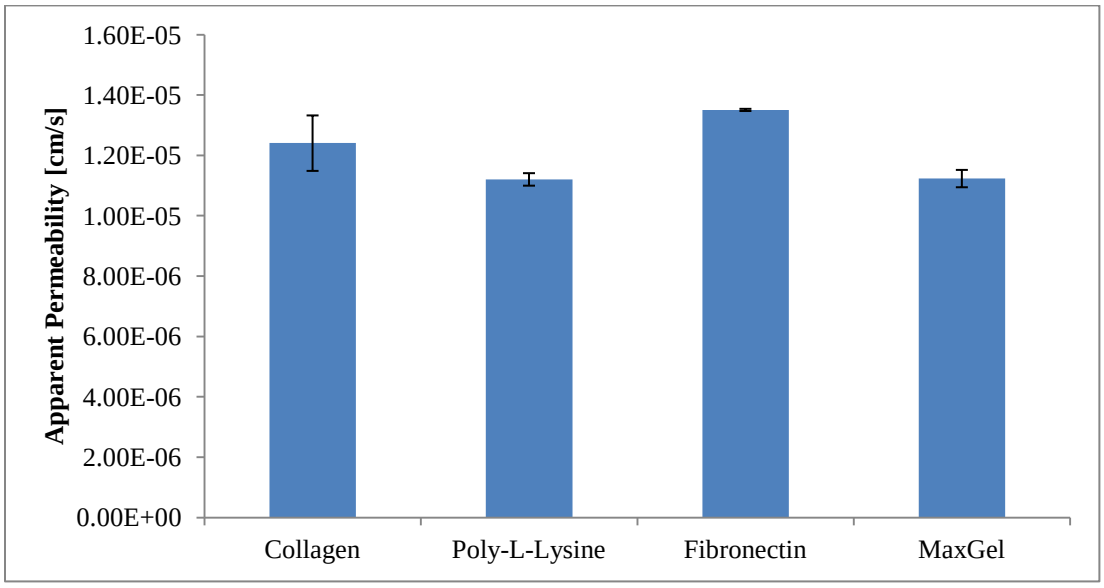

Figure 2.5. Effect of Basement Membrane Protein Selection on [C14]-Mannitol Permeability. Data is means ± 1 standard deviation of N=3 studies.

While fibronectin was found to give a significantly higher permeability for [C14]-Mannitol, the other three basement membrane proteins tested showed no significant

differences. However, seeding onto poly-L-lysine and Maxgel led to quantitatively slower paracellular permeability. Due the high cost of MaxGel, and the difficulty in working with it, poly-L-lysine was selected as the best choice for future studies. One may question why such small changes were seen upon using different basement membrane proteins, particularly in the case of MaxGel. It is hypothesized that this is due to the nature of the direct coculture model. In this case, human astrocytes are plated onto the basement membrane protein and then allowed to produce their own ECM in which the hCMEC/D3 cells can adhere. As the hCMEC/D3 cells are the rate-limiting barrier in paracellular permeation across the coculture model, a large change would only be expected if the modification in basement membrane proteins caused an alteration in astrocyte secretion of a matrix protein involved in BMEC differentiation.

Media Selection

Due to the nature of the direct contact coculture model containing two cell lines, it is possible that differentiation and proliferation may occur better in one media over another. The hCMEC/D3 cell line is grown in an endothelial basal medium (EBM-2) base from Lonza Inc., while the human astrocytes are grown in a proprietary human astrocyte medium (AM) sold with the primary cells by ScienCell. In practice, both cell lines grow in both mediums, but in monoculture grow best in their perspective mediums. For this reason, all coculture studies began with plating, proliferation, and differentiation of astrocytes in astrocyte media for the first two days prior to hCMEC/D3 plating. Following hCMEC/D3 plating, the cells were then either kept in astrocyte media for the

remaining seven days or switched over to EBM-2 for the remaining seven days. In addition, due to the nature of the Transwell®, it is also possible to add separate mediums in the apical and basolateral compartment. This allowed for the investigation of EBM-2 on the apical side in contact with the hCMEC/D3 cells and astrocyte medium in the basolateral side in closer contact to the human astrocytes.

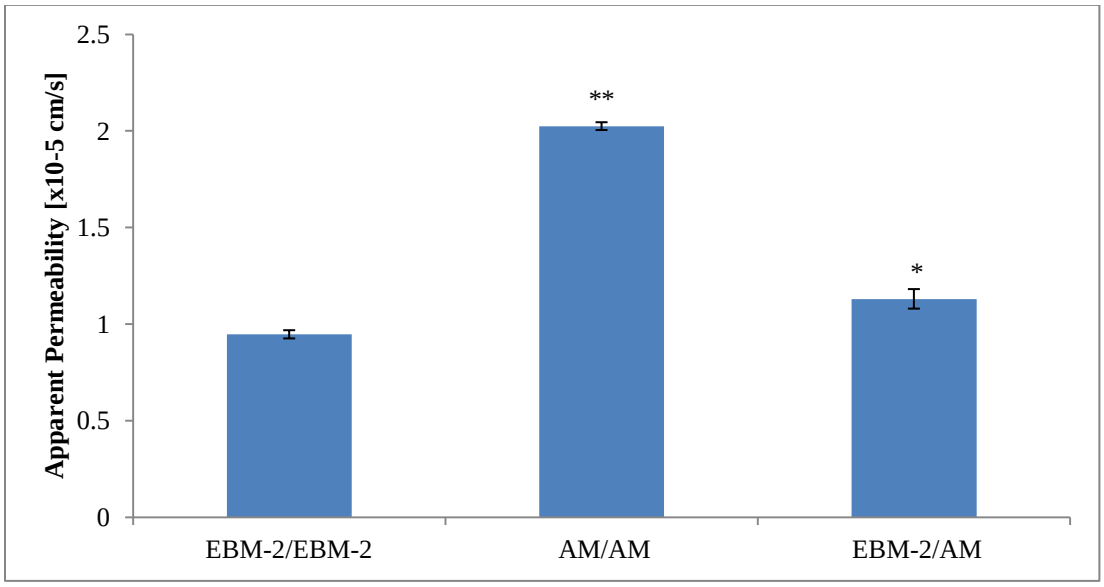

*Figure 2.6. Effect of Base Medium on [C14]-Mannitol Permeability Across the Direct Contact Coculture Model. Data is means ± 1 standard deviation of N=3 studies. *: p<0.05 **:p<0.01*

Figure 2.6 shows that the coculture model grown with EBM-2 in both compartments leads to the lowest paracellular permeation of [C14]-Mannitol. The combination of EBM-2 in the apical compartment and astrocyte medium in the

basolateral compartment was significantly less restrictive than EBM-2 in both compartments, however, both were much tighter than the coculture grown in just astrocyte medium. This isn't unexpected as the hCMEC/D3 cell line is the rate limiting barrier in the model and grows best in EBM-2. In addition, the majority of the proliferation and differentiation of the human astrocytes is likely completed by the time the media is switched to EBM-2. Further investigation would need to be completed to elucidate the mechanism behind the differences between hCMEC/D3 differentiation in EBM-2 vs. astrocyte medium, however, due to the proprietary formulas of each medium investigation would be difficult.

Media Optimization

While EBM-2 in both the apical and basolateral compartments of the coculture model was found to elicit the tightest paracellular barrier, further media modifications may lead to further tightening. Previous unpublished work in our lab has shown that for hCMEC/D3 monolayers, addition of different soluble factors, including growth factors, metal ions, antioxidants, lipids, and buffers, leads to significant tightening. As the direct mechanisms behind hCMEC/D3 monolayer tightening upon coculture with astrocytes are unknown, further investigation was done to elucidate the effects of media modification on the direct contact coculture model.

Serum-Free Media

Serum is often used in cell culture as it contains a number of factors important for cell growth and proliferation.[9] Its use is often needed not only for initial growth, but also to prevent senescence or apoptosis even after differentiation of some cell lines. However, studies using primary porcine BMECs have found that removal of serum during cell culture led to a two-fold increase in transendothelial electrical resistance (TEER) which is often indicative of a restriction in paracellular flux.[10] In addition, cells exhibited increased localization of ZO-1, occluding, and claudin-5 to cell-cell junctions and a flatter morphology.[11] In order to test these conditions, the direct contact coculture system was grown in serum for the first two days of culture to allow for proliferation and confluence. After two days, serum-free media was added and compared to cell cultures grown with serum for the extent of the study. To measure changes in paracellular permeability, [C14]-mannitol and [C14]-sucrose were used.

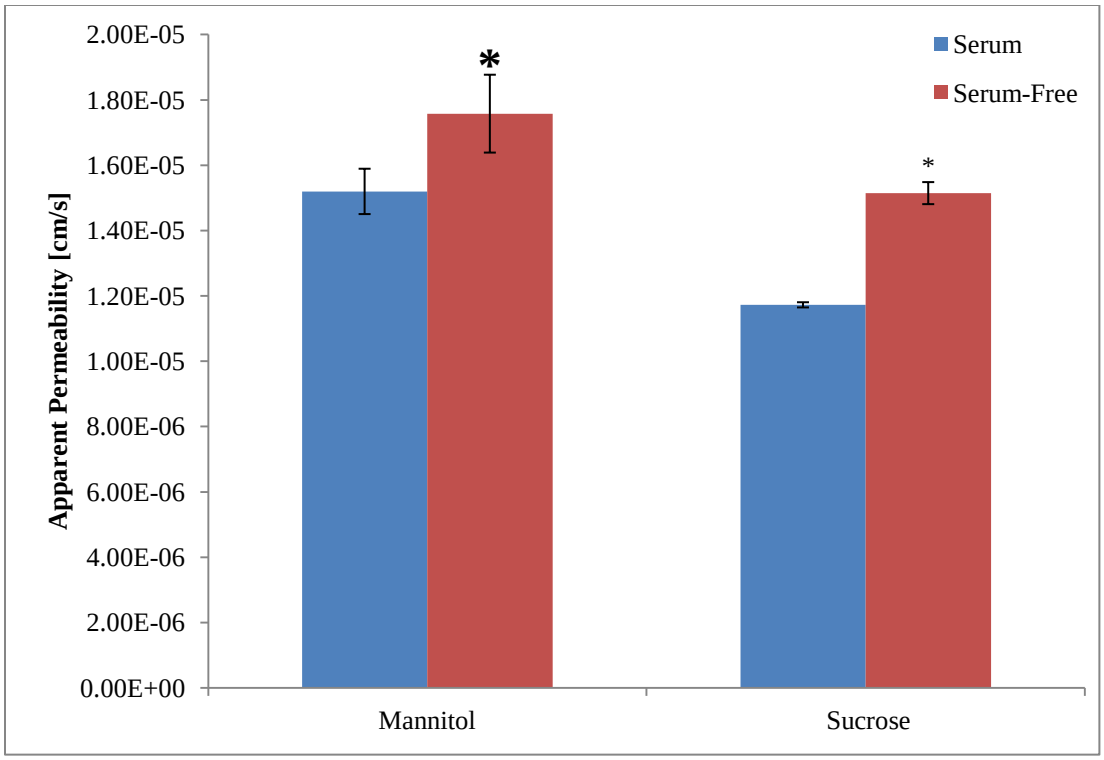

*Figure 2.7. Effect of Serum-Free Differentiation Conditions on [C14]-Mannitol Permeability Across the Direct Contact Coculture Model. Data is means ± 1 standard deviation of N=3 studies. *: $p<0.05$*

Figure 2.7, indicates that in both cases, media containing serum for the extent of the study provided a tighter monolayer. This may indicate that extended time without the presence of serum caused hCMEC/D3 dedifferentiation and loss of some tight junction structure or function. It should be noted that the cells used in the studies above utilized primary porcine BMECs which may be less susceptible to dedifferentiation in serum-free conditions than the immortalized hCMEC/D3s. Additional studies could be conducted to

measure the effects removing serum later in culture and of reduced-serum conditions as opposed to serum-free conditions.

Hydrocortisone

Hydrocortisone is an endogenous anti-inflammatory glucocorticoid hormone which acts through inhibition of pro-inflammatory factors such as tumor-necrosis-factor alpha (TNF-alpha). *In vitro* studies have shown that TNF-alpha signaling is responsible for tight junction breakdown and increased paracellular permeability.[12] While TNF-alpha mRNA is not found in hCMEC/D3 lysates, it is possible that it may be produced by the human astrocytes or found in the fetal bovine serum added to cell culture medium. To counteract the possible effects of TNF-alpha from cell culture media, previous studies were completed to examine the effects of adding 50 nM hydrocortisone to cell culture media which resulted in substantial decreases in paracellular permeability and increases in claudin-1, claudin-5, occludin, and VE-cadherin.[12] Furthermore, previous unpublished work in the Couraud lab suggests that an increased amount of hydrocortisone (1.4 μM) provides additional monolayer tightening. However, due to the increased complexity with the coculture, similar studies were conducted with 1.4 μM or 100 nM hydrocortisone added at the start of hCMEC/D3 culture, or after two days of proliferation. These two days were given to allow the hCMEC/D3 cells to first proliferate and differentiate.

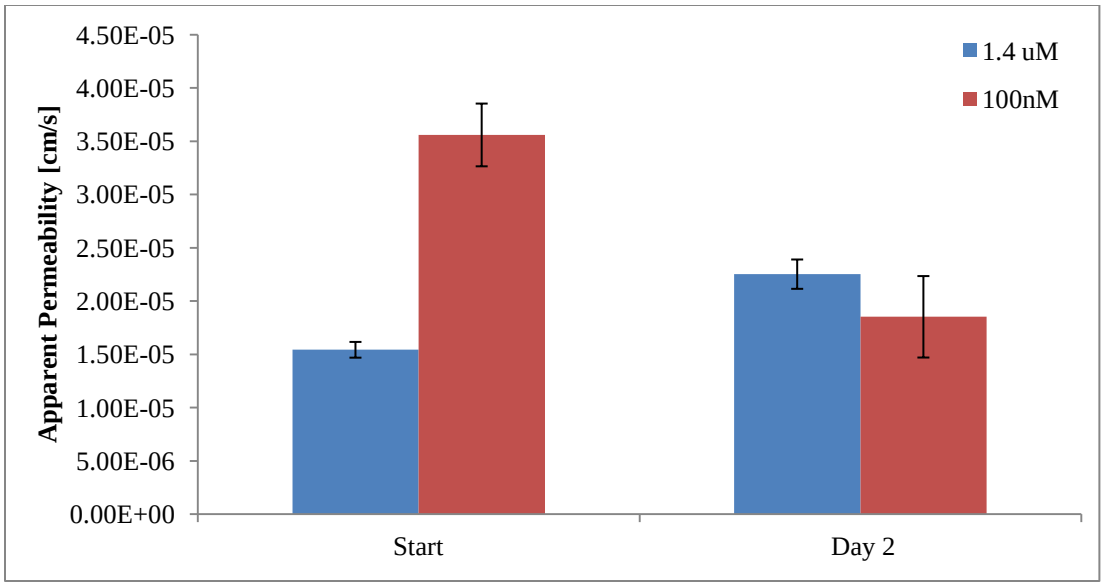

*Figure 2.8. Effect of Hydrocortisone Concentration and Time of Addition on [C14]-Mannitol Permeability. Here, 1.4 μM at the Start Represents Control Conditions. Data is means ± 1 standard deviation of N=3 studies. *: p<0.05*

Results in Figure 2.8 suggest that a larger hydrocortisone from the beginning of cell culture represent the lowest [C-14]-Mannitol permeability. Interestingly, for lower hydrocortisone levels, a substantial decrease in permeability was seen when supplementing media after two days. Additional studies may be conducted to analyze effects of later hydrocortisone addition to see if this trend continues.

HEPES Concentration

While sodium bicarbonate is the most common buffer used in cell culture, a number of organic buffers are also used.[13] Sodium bicarbonate is often used due to its low cost and ability to buffer around physiological pH in 37^{o}C, 95% relative humidity, and 5% CO_2 conditions used in cell culture incubators. However, due to the chemical nature of the sodium bicarbonate, if excess CO_2 is not provided, it is released into the atmosphere leading to high alkalinity up to pH 8.5. This could be problematic for hCMEC/D3 cell culture as these cells are known to be susceptible to even relatively small pH changes.[14] In an attempt to counteract this, an organic buffer, HEPES, 4-(2-hydroxyethyl)-1-piperazineethanesulfonic acid, was selected to buffer EBM-2 medium. HEPES has a pH of approximately 7.4 at 37^{o}C making it a good choice for physiologically-relevant BMEC growth. Yet, HEPES is not without its own drawbacks. In *in vitro* cultures of some cell lines, HEPES is known to reduce the uptake of amino acids by glial cells.[15] As the human astrocytes are a glial cell line, it is possible that HEPES may be detrimental to the coculture model. In order to analyze possible toxicities with the coculture, a broad range of HEPES concentrations from (10-50 mM) were tested on both hCMEC/D3 monolayers and the direct contact coculture.

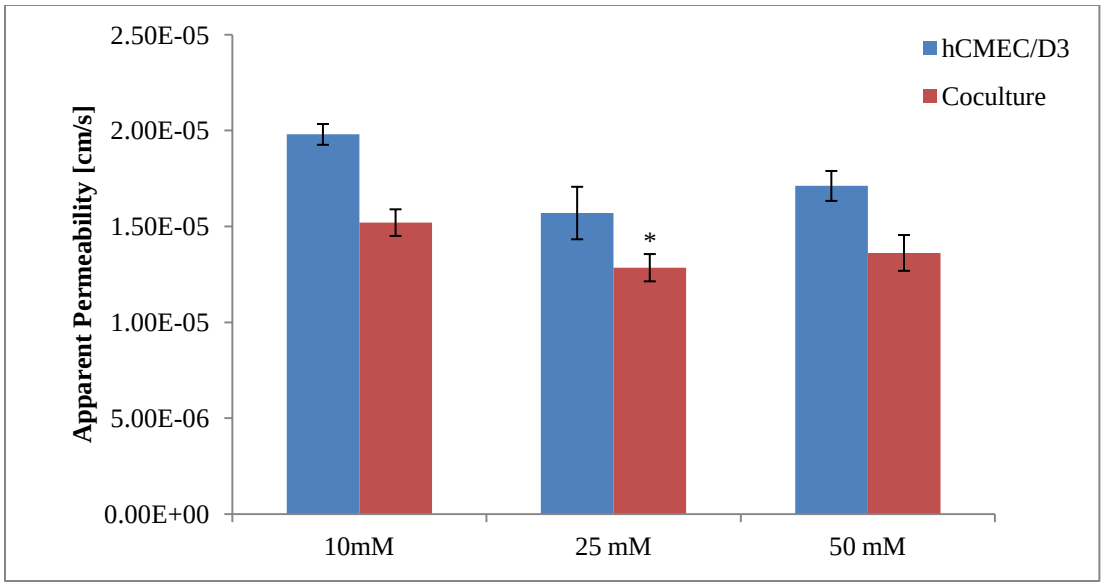

*Figure 2.9. Effect of HEPES Buffer Concentration on [C14]-Mannitol Permeability. Data is means ± 1 standard deviation of N=3 studies. *: p<0.05. Note: All Coculture Permeabilities are Significantly Lower (p<0.05) than hCMEC/D3 Permeabilities at the same HEPES Concentration. Significance in the Figure is Represented as a Significant Decrease over Control (10mM) HEPES Concentration for Coculture Data.*

Interestingly, while the coculture was found to still be significantly less permeable than hCMEC/D3 monolayers at all HEPES concentrations, higher HEPES concentrations led to quantitatively lower [C14]-Mannitol permeability. However, it does appear that some toxicities may be evident at 50 mM HEPES due to a non-significant increase over 25mM. As manufacturer-reported toxicities are usually found between 40 and 50 mM, our findings correlate with literature. While HEPES appears to provide non-toxic conditions at least up to 25 mM, further investigation is needed to determine the

mechanistic pathway leading to the significant tightening found when increasing HEPES buffer from 10 mM to 25 mM. This may be due to the increase in buffer capacity, or small change in pH caused by increasing buffer concentration.[16] However, some literature suggests that HEPES may play a role in increasing ATP concentrations *in vitro.*[15] This increased ATP may possibly lead to a cascade of events leading to increased tight junction protein expression or localization.

Lithium Chloride

Studies in animal primary endothelial cells suggest that activation of the Wnt/β-catenin pathway leads to increased expression of claudin and other tight junction proteins by BMECs.[17] While both expression and localization are necessary in tight junction formation, an increased expression of claudins, especially claudin-5, which is thought to be one of the main BBB phenotypic proteins, may lead to an increase in tight junction formation and decreased paracellular flux. A number of proprietary molecules are available to upregulate the Wnt/β-catenin pathway, however, lithium chloride (LiCl), a relatively cheap and obtainable compound is also known to stimulate this pathway through inhibition of β-catenin phosphorylation and eventual degradation.[18] In fact, previous work on hCMEC/D3 monolayers has shown that 10 mM LiCl supplementation led to 2-3 fold increases in claudin-3 and -5 expression and approximately 20% reduction in Lucifer Yellow, a fluorescent paracellular marker, permeation.[17] In order to test this hypothesis, 10 mM LiCl was added to EBM-2 at the start of hCMEC/D3 culture or two-days after. These two days were given to allow the hCMEC/D3 cells to proliferate and

become confluent as LiCl is also known to promote differentiation. Premature differentiation before reaching confluence may lead to incomplete monolayer formation as little proliferation occurs after differentiation. Results of the study are shown below.

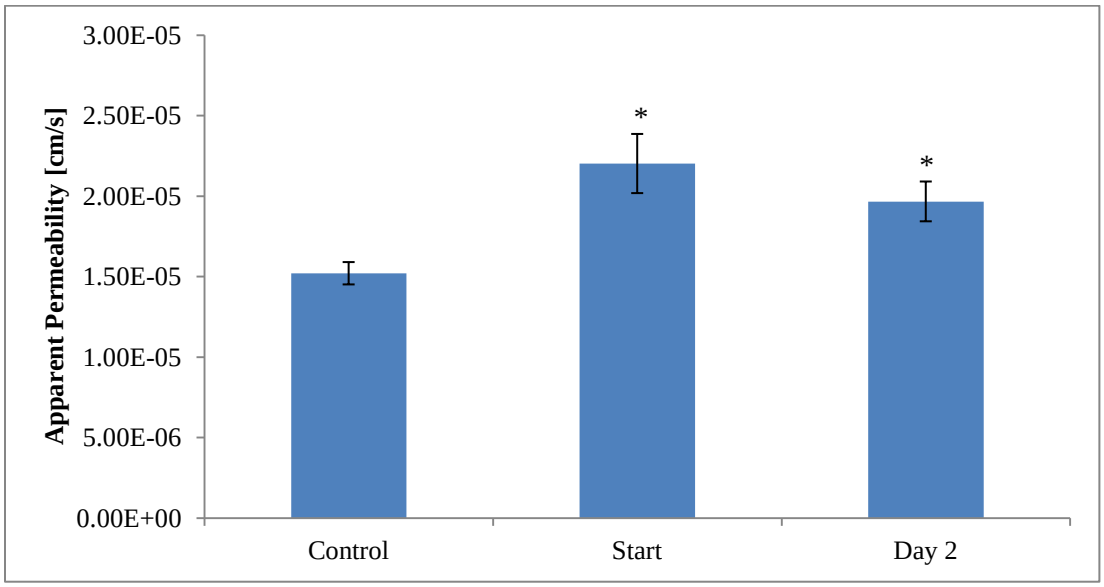

*Figure 2.10. Effect of 10mM Lithium Chloride on [C14]-Mannitol Permeability. Control Conditions are Grown Without Lithium Chloride. Data is means ± 1 standard deviation of N=3 studies. *: p<0.05*

While literature suggests increased tight junction protein expression and reduced paracellular flux in hCMEC/D3 monocultures, similar results were not seen in coculture under the conditions tested. In fact, significantly increased paracellular permeability was seen for cultures containing LiCl. However, as noted above, LiCl is known to promote differentiation. It is possible that two days was not enough time for full hCMEC/D3

confluence to be reached in coculture. This idea is upheld by a quantitative, though non-significant, decrease in permeability when adding LiCl on day 2 as well as Figure 2.3 which shows increased permeability of cocultures until day 5.

Calcium

Some investigation in our lab has led to the finding that the EBM-2 media, manufactured by Lonza, contains a minimal amount of calcium (Stephen Carl Thesis, 2009). While the mechanism is not well understood, extracellular calcium concentration is known to play a role in tight junction function. This was shown through addition of EGTA and other calcium chelators which lead to the opening of tight junctions and large increases in paracellular permeability.[19] That being said, previous unpublished studies in our lab have shown that adding excess calcium to EBM-2 media led to insignificant changes in [C14]-Mannitol permeability across hCMEC/D3 monolayers. However, to ensure low calcium levels aren't responsible for high paracellular permeability in the coculture model, 1mM calcium was added in excess and [C-14]-Mannitol and [C14]-Sucrose permeability was measured.

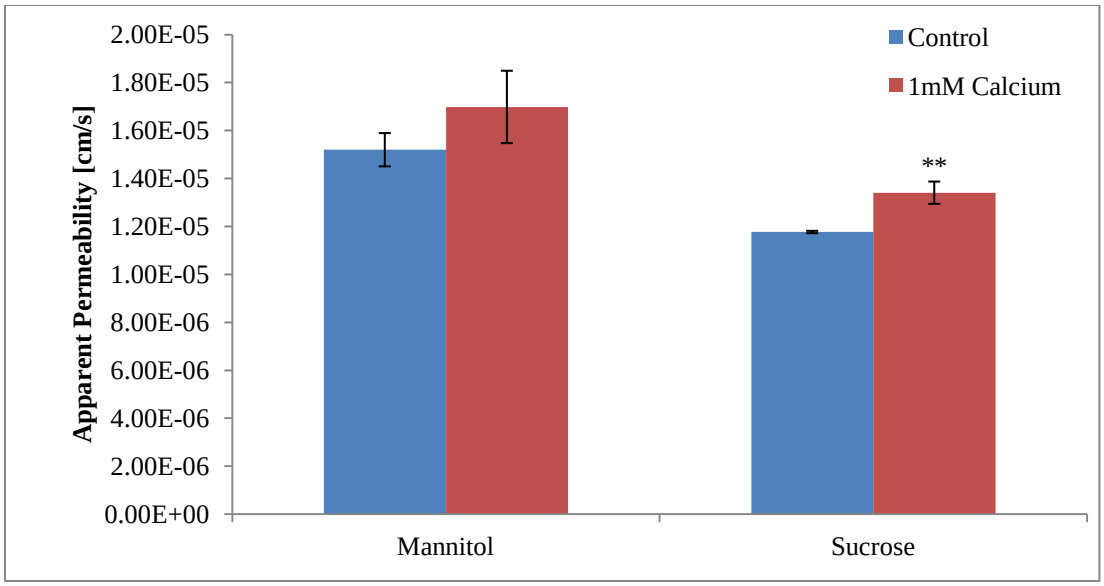

*Figure 2.11. Apparent Permeability of [C14]-Mannitol and [C14]-Sucrose in Normal EBM-2 (Control) and EBM-2 with 1 mM Excess Calcium Ion. Data is means ± 1 standard deviation of N=3 studies.**: p<0.01*

Similar to previous hCMEC/D3 monoculture studies in our lab, Figure 2.11 shows insignificant changes in coculture [C14]-Mannitol permeability. In fact, for both [C14]-Mannitol and [C14]-Sucrose excess calcium led to increased paracellular permeability. Interestingly, significant changes were seen for [C14]-Sucrose, however, it should be noted that this significance is in most part due to unusually small deviations. While this study suggests that excess calcium may actually impair tight junction function in our model, it should be noted that only a single excess calcium concentration was measured and varying this excess concentration may result in differing results.

Functional Drug Efflux

The optimization studies above, as well as previous media optimization by our lab and other labs using the hCMEC/D3 cell line have mostly focused reduction in paracellular permeability. While the exclusion of small hydrophilic molecules from moving through paracellular tight junctions is one of the BBB's main barriers to drug delivery, efflux of hydrophobic molecules, preventing transcellular permeation, also represents a significant barrier. Therefore, it is important to also measure changes in functional hCMEC/D3 efflux when cocultured in direct contact with human astrocytes. In order to assess functional efflux, two types of studies are common. The first is the measurement of the directional permeability in both the apical-to-basolateral (AB) and basolateral-to-apical (BA) directions. Due to the unidirectional efflux back into the apical compartment, an efflux substrate should have increased permeation in the basolateral-to-apical direction and reduced permeation in the apical-to-basolateral direction. Therefore an AB/BA ratio greater than 2.5 or 3 is often believed to represent the presence of drug efflux transporters. Additionally, efflux activity can be estimated through uptake experiments. In this case, cells are seeded onto culture well plates instead of Transwell® supports and the rate of cell uptake is measured over a defined time. In this case decreases in the rate of uptake suggest increased efflux activity. These studies are especially useful when trying to optimize conditions due to the low cost of well-plates in comparison to Transwell® supports.

In order to examine efflux of the direct contact coculture model in comparison to hCMEC/D3 monocultures the bidirectional permeability of 1μM [C14]-Verapamil was

measured and can be seen in Figure 2.12. No change was seen in either direction when comparing the mono- and cocultures. In addition, there were no significant differences in AB or BA directional permeability in either model suggesting no functional efflux. This is interesting as numerous previous reports, including those in our own lab, have shown the functional presence of p-glycoprotein including bidirectional studies, uptake studies, and localization by microscopy.[4,6,20-22] However, upon further investigation, it was found that Verapamil is both a P-gp substrate as well as an inhibitor (though we are approximately 10-fold below reported K_i values) which may confound results.

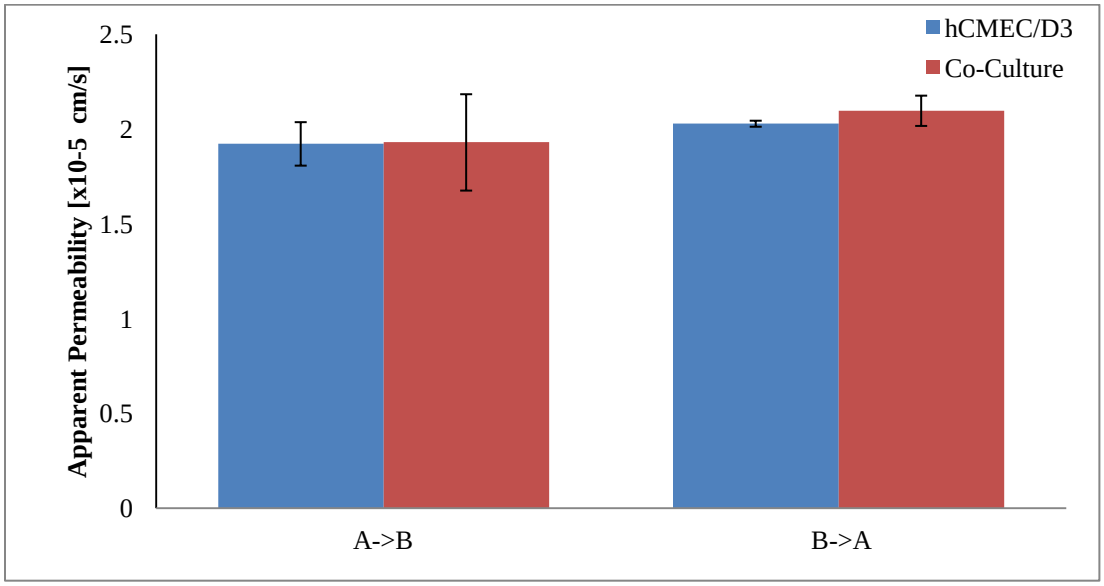

Figure 2.12. Apparent Permeability of [C14]-Verapamil in Apical-to-Basolateral and Basolateral-to-Apical Directions for hCMEC/D3 and Coculture Models. Data is means ± 1 standard deviation of N=3 studies.

As Verapamil was found to potentially be a conflicting substrate, further investigation was done using [C14]-Paclitaxel. Additionally focus was moved to first quantifying function efflux in the direct coculture system due to costs associated with the studies. Paclitaxel studies were run at 10 μM concentration in a similar fashion; however, in this case bidirectional permeability was also measured in the presence of a p-glycoprotein inhibitor, 5 μM Cyclosporine A (CsA). Again, no significant differences were seen between AB and BA permeability coefficients in Figure 2.13. CsA did lead to a small increase in AB permeation, which may signify some inhibition, however, this is complicated by a concurrent increase in BA permeability.

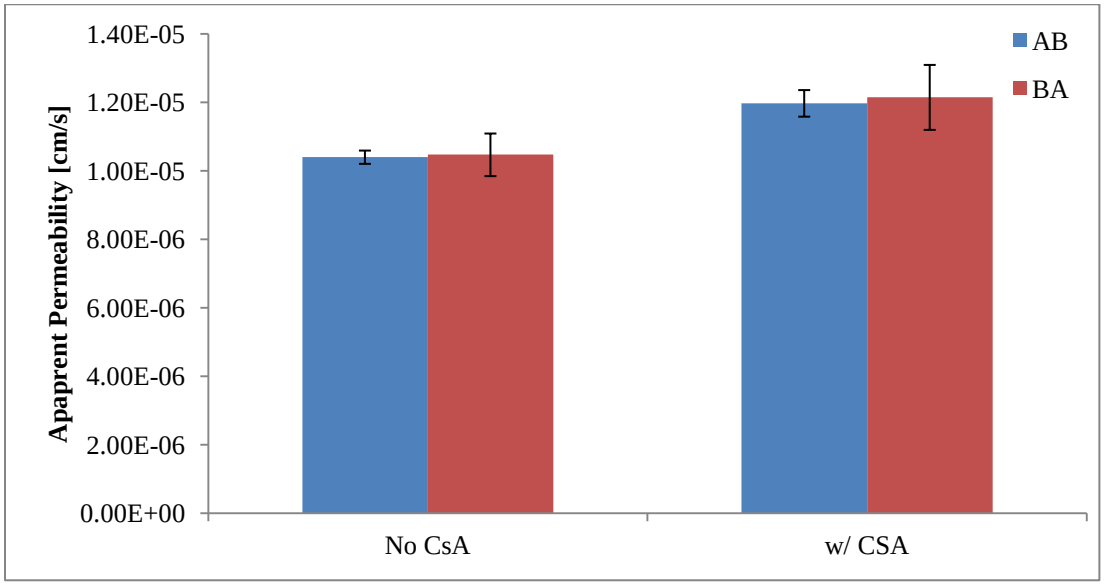

Figure 2.13. Apparent Permeability of [C14]-Paclitaxel in Apical-to-Basolateral and Basolateral-to-Apical Directions for Coculture Models with and without Cyclosporin A Inhibition. Data is means ± 1 standard deviation of N=3 studies.

This data seems to support, the conclusions found with Verapamil, however, to be confident a final study was done measuring the bidirectional permeability of 5 μM Rhodamine-123 (R123) with inhibition by 20 μM Verapamil. As noted above, while Verapamil is a p-glycoprotein substrate, it also acts as an inhibitor at concentrations above ~10 μM.[23] Results in Figure 2.14 are slightly more encouraging as R123 showed nearly significant (p=.058) increases in BA permeability over BA. In addition, these differences disappeared in the presence of an inhibitor with a reduction in BA permeability and an increase in AB. That being said, the BA/AB ratio is still well under 2 which suggests that even if functional efflux is present it is at a low level.

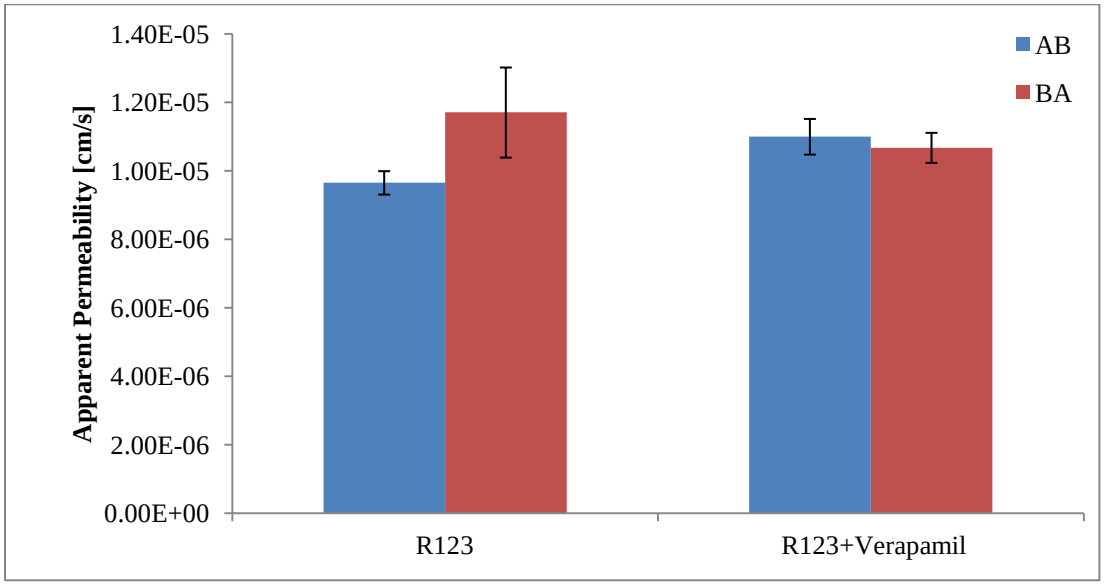

Figure 2.14. Apparent Permeability of Rhodamine-123 in Apical-to-Basolateral and Basolateral-to-Apical Directions for Coculture Models with and without Verapamil Inhibition. Data is means ± 1 standard deviation of N=3 studies.

These studies all appear to contradict the results found by others who have shown active efflux expression and function in the hCMEC/D3 model. At least in the case of our lab's hCMEC/D3 cells, functional expression of efflux proteins has been reduced or lost completely. One speculation of why this may be is the high passage number used in these studies. Studies were conducted around passage 45, and recent research suggests that P-gp expression may be reduced after passage 40.[22] However, even at the reduced levels shown at higher passage numbers, the expression found was still relatively high. In order to test this hypothesis, cells of lower passage number have been purchased and will be tested in the future. Another possibility is a lack of polarized efflux expression in our model. In this scenario, efflux would occur in both directions and any changes in AB and BA permeability would be equivalent. One method to test this hypothesis would be cellular uptake as even unpolarized expression will limit uptake into the cell. However, it is possible that uptake by astrocytes in the coculture model could make delineation of hCMEC/D3 uptake difficult. Finally, through discussion with others working with the cell line, this problem does not seem to be solely ours. While not discussed in the literature, it appears that this cell line has the tendency to gain and lose efflux expression in culture which may limit its utility.

2.3 References

1. Wilhelm I, Krizbai IA In vitro models of the blood-brain barrier for the study of drug delivery to the brain. Mol Pharm 11(7):1949-1963.
2. Weksler B, Romero IA, Couraud PO The hCMEC/D3 cell line as a model of the human blood brain barrier. Fluids Barriers CNS 10(1):16.
3. Weksler BB, Subileau EA, Perriere N, Charneau P, Holloway K, Leveque M, Tricoire-Leignel H, Nicotra A, Bourdoulous S, Turowski P, Male DK, Roux F, Greenwood J, Romero IA, Couraud PO 2005. Blood-brain barrier-specific properties of a human adult brain endothelial cell line. FASEB J 19(13):1872-1874.
4. Poller B, Gutmann H, Krahenbuhl S, Weksler B, Romero I, Couraud PO, Tuffin G, Drewe J, Huwyler J 2008. The human brain endothelial cell line hCMEC/D3 as a human blood-brain barrier model for drug transport studies. J Neurochem 107(5):1358-1368.
5. Dauchy S, Dutheil F, Weaver RJ, Chassoux F, Daumas-Duport C, Couraud PO, Scherrmann JM, De Waziers I, Decleves X 2008. ABC transporters, cytochromes P450 and their main transcription factors: expression at the human blood-brain barrier. J Neurochem 107(6):1518-1528.
6. Carl SM, Lindley DJ, Couraud PO, Weksler BB, Romero I, Mowery SA, Knipp GT ABC and SLC transporter expression and pot substrate characterization across the human CMEC/D3 blood-brain barrier cell line. Mol Pharm 7(4):1057-1068.

7. Urich E, Lazic SE, Molnos J, Wells I, Freskgard PO Transcriptional profiling of human brain endothelial cells reveals key properties crucial for predictive in vitro blood-brain barrier models. PLoS One 7(5):e38149.

8. Engelhardt B beta1-integrin/matrix interactions support blood-brain barrier integrity. J Cereb Blood Flow Metab 31(10):1969-1971.

9. Brunner D, Frank J, Appl H, Schoffl H, Pfaller W, Gstraunthaler G Serum-free cell culture: the serum-free media interactive online database. ALTEX 27(1):53-62.

10. Patabendige A, Skinner RA, Abbott NJ Establishment of a simplified in vitro porcine blood-brain barrier model with high transendothelial electrical resistance. Brain Res 1521:1-15.

11. Nitz T, Eisenblatter T, Psathaki K, Galla HJ 2003. Serum-derived factors weaken the barrier properties of cultured porcine brain capillary endothelial cells in vitro. Brain Res 981(1-2):30-40.

12. Forster C, Burek M, Romero IA, Weksler B, Couraud PO, Drenckhahn D 2008. Differential effects of hydrocortisone and TNFalpha on tight junction proteins in an in vitro model of the human blood-brain barrier. J Physiol 586(7):1937-1949.

13. Eagle H 1971. Buffer combinations for mammalian cell culture. Science 174(4008):500-503.

14. Zougbede S, Miller F, Ravassard P, Rebollo A, Ciceron L, Couraud PO, Mazier D, Moreno A Metabolic acidosis induced by Plasmodium falciparum intraerythrocytic stages alters blood-brain barrier integrity. J Cereb Blood Flow Metab 31(2):514-526.

15. Luo S, Pal D, Shah SJ, Kwatra D, Paturi KD, Mitra AK Effect of HEPES buffer on the uptake and transport of P-glycoprotein substrates and large neutral amino acids. Mol Pharm 7(2):412-420.

16. Helms HC, Waagepetersen HS, Nielsen CU, Brodin B Paracellular tightness and claudin-5 expression is increased in the BCEC/astrocyte blood-brain barrier model by increasing media buffer capacity during growth. AAPS J 12(4):759-770.

17. Paolinelli R, Corada M, Ferrarini L, Devraj K, Artus C, Czupalla CJ, Rudini N, Maddaluno L, Papa E, Engelhardt B, Couraud PO, Liebner S, Dejana E Wnt activation of immortalized brain endothelial cells as a tool for generating a standardized model of the blood brain barrier in vitro. PLoS One 8(8):e70233.

18. van Noort M, Meeldijk J, van der Zee R, Destree O, Clevers H 2002. Wnt signaling controls the phosphorylation status of beta-catenin. J Biol Chem 277(20):17901-17905.

19. Stelwagen K, Farr VC, Davis SR, Prosser CG 1995. EGTA-induced disruption of epithelial cell tight junctions in the lactating caprine mammary gland. Am J Physiol 269(4 Pt 2):R848-855.

20. Ohtsuki S, Ikeda C, Uchida Y, Sakamoto Y, Miller F, Glacial F, Decleves X, Scherrmann JM, Couraud PO, Kubo Y, Tachikawa M, Terasaki T Quantitative targeted absolute proteomic analysis of transporters, receptors and junction proteins for validation of human cerebral microvascular endothelial cell line hCMEC/D3 as a human blood-brain barrier model. Mol Pharm 10(1):289-296.

21. Dickens D, Yusof SR, Abbott NJ, Weksler B, Romero IA, Couraud PO, Alfirevic A, Pirmohamed M, Owen A A multi-system approach assessing the interaction of anticonvulsants with P-gp. PLoS One 8(5):e64854.

22. Tai LM, Reddy PS, Lopez-Ramirez MA, Davies HA, Male DK, Loughlin AJ, Romero IA 2009. Polarized P-glycoprotein expression by the immortalised human brain endothelial cell line, hCMEC/D3, restricts apical-to-basolateral permeability to rhodamine 123. Brain Res 1292:14-24.

23. Rautio J, Humphreys JE, Webster LO, Balakrishnan A, Keogh JP, Kunta JR, Serabjit-Singh CJ, Polli JW 2006. In vitro p-glycoprotein inhibition assays for assessment of clinical drug interaction potential of new drug candidates: a recommendation for probe substrates. Drug Metab Dispos 34(5):786-792.

CHAPTER 3. DEVELOPMENT OF A PHYSIOLOGICALLY RELEVANT BLOOD-BRAIN BARRIER COCULTURE MODEL

Modified From: Kulczar C, Lubin KE, Ngendahimana A, Lefebvre S, Miller DW, Knipp GT. Development of a Direct Contact Astrocyte-hCMEC/D3 Blood-Brain Barrier Coculture Model. (*In Submission*)

3.1. Introduction

The blood-brain barrier (BBB) is a highly restrictive barrier between the systemic circulation and the brain parenchyma.[1-5] The BBB functions to exclude harmful xenobiotics while permitting the entry of nutrients and removal of waste allowing for a neuronal environment optimal for development and function.[6-8] One of the key elements of the BBB is a continuous endothelium with the presence of exceedingly restrictive tight junctions between brain microvessel endothelial cells. These tight junctions prevent the paracellular movement of hydrophilic molecules and ions to a greater extent than anywhere else in the body.[9,10] This tightness is believed to be due, in part, to an increased expression of claudin-3, 5, and 12 in brain microvessel endothelial cells compared to microvessel endothelial cells in the periphery.[11] In addition to tight junctions, BBB endothelial cells also express a number of drug metabolizing enzymes, such as cytochrome P450 enzymes (CYP450), and efflux transporters, such as P-glycoprotein (P-

gp) and breast cancer resistance protein (BCRP), which act to efflux xenobiotics moving transcellularly.[12-14]

Further investigation of the BBB reveals supporting cells, such as astrocytes and pericytes, form a symbiotic, synergistic relationship with BMECs that significantly enhances the barrier properties.[3,15,16] Due to their close-knit interactions leading to BBB formation, the collection of endothelial cells, astrocytes, and pericytes was coined the neurovascular unit. Each of the cells play a role in creation of the barrier, and while tight junctions between the endothelial cells are responsible for the barrier function itself, the astrocytes and pericytes are thought to be necessary for co-differentiation with the endothelial cells.[17] Among other things, astrocytes are believed to be responsible for regulating development of tight junctions, the movement of water and glucose across the BBB, metabolism, and the localization of transporters.[2] In addition, astrocytes highly express CYP450 enzymes and may serve an important neuroprotective role by metabolizing and removing many xenobiotics, including pharmaceutical compounds.[18] Pericytes on the other hand, are thought to be important for production of soluble growth factors as well as production and maintenance of an extracellular matrix rich in collagen, fibronectin, proteoglycans, and laminin that is important for integrity of the BBB and may be important for proper BBB differentiation.[19-21]

Due to the increasing importance of translatable knowledge of the BBB and permeation across the barrier, a number of different *in vitro* models have been established.[8,17,22-32] Many of these models utilize primary human or animal BMECs.[33] While primary human BMECs may provide the most ideal and relevant model, the

availability of such tissues is minimal, reducing their utility for high throughput screening.[6] Due to the lack of human tissues, many attempts have been made to use animal tissues as a surrogate. These cells are often of murine, bovine, or porcine origin. Primary cells of animal origin have been shown to provide relatively high transendothelial electrical resistance (TEER) indicative of the presence of developed tight junctions.[25,29,31,34] However, one must question the physiological relevance of these models for drug screening, especially based on species differences including non-paracellular routes of permeation indicative of the vast majority of BBB permeable compounds. Therefore, new models have been established making use of immortalized human tissues which provide the relevance of a human cell line without the disadvantage of short supply.

One of the most often used immortalized human BMEC cell lines is the human cerebral microvessel endothelial (hCMEC/D3) cell line. The hCMEC/D3 cell line was established through hTERT and SV40 large T antigen immortalization of endothelial cells isolated from microvessels of a human temporal lobe.[35] hCMEC/D3 cultures form monolayers on collagen-coated surfaces and are contact inhibited lending themselves to high throughput Transwell® permeation studies. Analysis of the cell line and has shown similarities in morphology and protein expression between hCMEC/D3s and primary human BMECs. However, hCMEC/D3s do not appear to form tight junctions consistent with those found *in vivo*, reaching TEER values of only 30-50 $\Omega*cm^2$ compared to TEER values of over 1000 $\Omega*cm^2$ *in vivo* in the frog.[8,32,35-37] These leaky tight junctions may allow paracellular movement of compounds that permeate by the transcellular route *in*

vivo, leading to irrelevant permeability values. While optimization of culture conditions, *e.g.* media, density, cell source, etc., has led to modest increases in monoculture TEER, these values are still well below those seen *in vivo*.[6,38]

Due to the leakiness of these monocultures, many groups have examined methods for reducing the paracellular permeability of these models. One approach is to use astrocyte conditioned media.[39] In these studies, soluble factors released by the astrocytes were able to interact with BMECs to create a more *in vivo*-like environment that lead to enhanced differentiation and reduced paracellular permeability. However, for hCMEC/D3 cultures, non-significant changes were seen in TEER when using astrocyte conditioned media.[27,35] Instead, the most significant reductions in paracellular permeability were seen when astrocytes were grown on the basolateral side of the filter or on the plastic well surface in the same Transwell® as the hCMEC/D3s (Figure 3.1A).[8,32] While a reduction in paracellular permeability of marker compounds and increases in TEER were seen for both of these conditions, greater changes were observed in cells grown on the basolateral side of the Transwell®.[6] These models are likely more physiologically relevant due to the symbiotic signaling and differentiation that is able to occur when both cell types are grown in the same culture. In addition, the increased tightness seen when growing astrocytes on the basolateral side of the Transwell® may reflect a closer proximity of astrocytic-released factors to endothelial cells thus producing a greater response through reduced dilution.[28] Moreover, it is thought that the model in which cells are grown on the bottom of the Transwell® permeable support may lead to tighter junctions due to the ability of the astrocytic endfeet to migrate through the pores of the filter and interact with

the BMECs through direct contact. However, it should be noted, that migration through Transwell® supports, especially through 0.4μm pores which best support endothelial cell culture, is infrequent.[34,40]

It is apparent from the studies mentioned above and analysis of the neurovascular unit, that the interplay between BMECs and astrocytes may serve an important role in differentiation of BMECs into providing a BBB phenotype. In addition, these studies have shown the proximity of astrocytes and BMEC may be crucial.[2,28,40] However, the methods described in previous coculture models entails separating BMECs and astrocytes by a filter support. While the Transwell® support is often depicted to be thin in cartoon representations, the support is approximately 10μm thick and may represent a significant barrier to cell-cell interactions. It is hypothesized that removing this obstruction and allowing direct cell-cell contact may allow further symbiotic signaling and differentiation to occur, which in turn may lead to further reduction in paracellular permeability and a more *in vivo* relevant model. An illustration of the model is shown in Figure 3.1B. To our knowledge, this is the first study that provides evidence that direct contact may provide additional benefit to the coculture tightness and physiological relevance.

A.

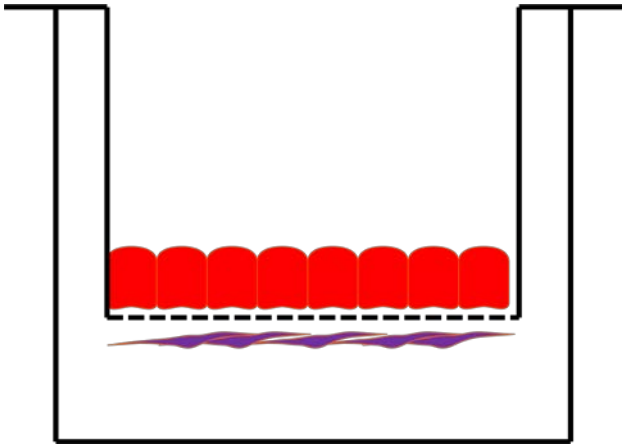

B.

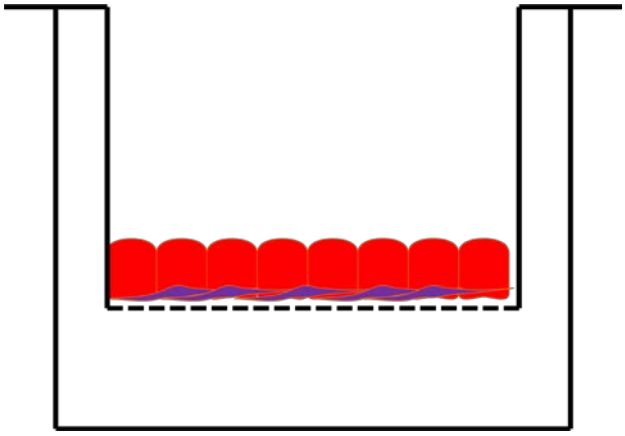

Figure 3.1. Past (indirect) vs. current direct contact coculture models. A, previous direct contact coculture model with BMEC and astrocytes separated by Transwell® permeable filter support. B, current direct contact coculture model, with BMEC and astrocytes in direct cell-cell contact. BMEC and astrocytes depicted in red and purple respectively.

3.2 Materials and Methods

Materials

Trypsin, Phosphate Buffered Saline (PBS), Penicillin/Streptomycin, Type I Rat Tail Collagen, Poly-L-Lysine, HEPES (4-(2-hydroxyethyl)-1-piperazineethanesulfonic acid) Buffer, Fibronectin, Maxgel™, Hank's Balanced Salt Solution (HBSS), Hydrocortisone, human Basic Fibroblast Growth Factor (bFGF), Ascorbic Acid, and Fetal Bovine Serum (FBS) were acquired from Sigma-Aldrich Company (St. Louis, MO). EBM-2 growth media was manufactured by Lonza Group (Walkersville, MD). Lipid Concentrate was obtained from BD Biosciences (Sparks, MD). 0.4 μm Transwell® 12 well plates and T75 flasks were made by Corning Lifesciences (Corning, NY). Radiolabeled compounds were purchased from Moravek Biochemicals Inc. (Brea, CA). The hCMEC/D3 cell line was graciously provided by Dr. Pierre Couraud of the Université Rene Descartes (Paris, France), while human astrocytes, Human Astrocyte Media, and Astrocyte Growth Factor were acquired from ScienCell Research Laboratories (Carlsbad, CA).

Methods

Cell Culture

The hCMEC/D3 cells were cultured in EBM-2 supplemented with FBS, Penicillin/Streptomycin, bFGF, Hydrocortisone, Ascorbic Acid, Lipid Concentrate, and HEPES buffer. Cells were maintained in a 5% environment at 37°C. HCMEC/D3 cells were passaged when confluence reached approximately 80%, at which time trypsinized cells were placed in a pre-collagenated (Type I) flask. Media was changed every other

day. Human astrocytes were cultured under similar conditions in Human Astrocyte Media supplemented with FBS, Astrocyte Growth Factor, and Penicillin/Streptomycin. Cells were passaged approximately every 5 days into flasks pre-coated with Poly-L-Lysine.

Monoculture Studies

In hCMEC/D3 monocultures, cells were seeded at a density of 1 $x10^5$ cells/cm^2 on Corning Costar 12-well 0.4 μm polyester Transwells® pretreated with 65 μL of 1 mg/mL Type I rat tail collagen and allowed to grow for 7 days. For human astrocyte monoculture, 4 $x10^4$ cells were seeded onto Transwells® coated with 2 μg/cm^2 poly-L-lysine and grown for 9 days prior to permeability studies.

Indirect Coculture Studies

Indirect coculture Transwells® were first pretreated with 65 μL of 1 mg/mL Type I rat tail collagen in ethanol in the apical chamber and left to evaporate for 4 hours. Following evaporation, the Transwells® were flipped and 2 μg/cm^2 poly-L-lysine was added to the basolateral side of the Transwells® and left overnight. Human astrocytes were plated on the basolateral side of the flipped Transwells® at a density of 4 $x10^4$ cells/cm^2 and left to attach for 4 hours. Transwells® were then placed into the normal orientation and grown for 48 hours. After this time, hCMEC/D3 cells were plated in the apical compartment at a density of 1 $x10^5$ cells/cm^2. The coculture was left to proliferate/differentiate in EBM-2 for an additional 7 days with media changes every other day before the permeability studies were conducted.

Direct Coculture Studies

For direct coculture studies, Transwell® inserts were coated with 2 μg/cm^2 poly-L-lysine and left overnight. Human astrocytes were then plated at a density of 4 x10^4 cells/cm^2. Astrocytes were allowed to proliferate/differentiate for 48 hours in astrocyte media. After 48 hours, media was removed and hCMEC/D3s were plated in EBM-2 at a density of 1 x10^5 cells/cm^2. The coculture was grown in EBM-2 with media changes every other day for an additional 7 days before studies were conducted.

Permeability Studies

Permeability studies were performed at 37^{o}C on a rocker plate in triplicate using [C14]-labeled markers ([C14]-Urea, [C14]-Mannitol, [C14]-Sucrose, [C14]-Inulin, [C14]-PEG-4000, and [C14]-Propranolol) at a concentration of 0.25 μCi/mL in HBSS. In all studies, human astrocytes ranged from passages 6-12 while hCMEC/D3 cells ranged from passage 36-48. Before all permeability studies, cells were washed twice with PBS before equilibrating in HBSS for 20 minutes shortly before the study. 100μL samples were taken at 15, 30, 45, 60, and 90 minute time points. 4mL of scintillation cocktail was added for analysis by scintillation counting. Permeability coefficients (cm/s) were obtained through the following equation:

$$P_{apparent} = \frac{\frac{dM}{dt}}{C_0 * SA * 60}$$

where $\frac{dM}{dt}$ is the rate of radionucleotide transfer across the cell layer, C_0 is the initial donor concentration, SA is the surface area of the Transwell® filter support, and 60 represents a correction factor from minutes to seconds.

Statistics

Permeability studies were compared using a two-tailed unpaired student's t-test with n=3. Studies with p-values less than 0.05 were considered to have significant differences.

3.3 Results

In order to delineate changes in BBB phenotype upon coculture with human astrocytes, permeability was measured with a number of marker compounds. However, the model was first optimized for minimal paracellular permeability. Extensive optimization of hCMEC/D3 and astrocyte seeding density, basement matrix, media, and seeding time were performed prior to the following studies (data not shown). The current method proved to be superior to other growth conditions investigated.

Direct Contact Coculture

As noted above, the hCMEC/D3 cell line, while tighter than other immortalized human BMEC cells, possess tight junctions that lack ideal physiological relevance. To investigate changes in tight junction pore radius, five marker compounds of varying

hydrodynamic radii were used to determine changes in paracellular permeability. As expected, increases in hydrodynamic radii lead to decreased apparent permeability coefficients for paracellular markers. However, the extent of changes in permeability varied between mono- and coculture, likely due to the effects predicted by the Renkin molecular sieving function as the pore radii approaches the size of the sieved molecule.[31,36,41,42] Although, it should be noted that in the presence of astrocytes the assumptions made by the Renkin function including the presence of a single pore, varied and increased tortuosity and porosity exists, thus the effects of permeation across the astrocytes cannot be easily corrected to obtain a pore radius.

As shown in Figure 3.2, significant changes between the mono- and coculture were seen for [^{14}C]-urea (2.96 ± 0.11 x10^{-5} cm/s and 2.43 ± 0.15 x10^{-5} cm/s; p=0.030), [^{14}C]-mannitol (1.98 ± 0.05 x10^{-5} cm/s and 1.52 ± 0.07 x10^{-5} cm/s; p=0.0004), [^{14}C]-sucrose (1.52 ± 0.13 x10^{-5} cm/s and 1.17 ± 0.008 x10^{-5} cm/s; p=0.005), and [^{14}C]-inulin (8.46 ± 0.02 x10^{-6} cm/s and 7.55 ± 0.3 x10^{-6} cm/s; p=0.034) respectively. Insignificant (p>0.05) changes were seen for [^{14}C]-PEG-4000 (3.93 ± 0.36 x10^{-6} and 3.57 ± 0.10 x10^{-6} cm/s; p=0.227) respectively.

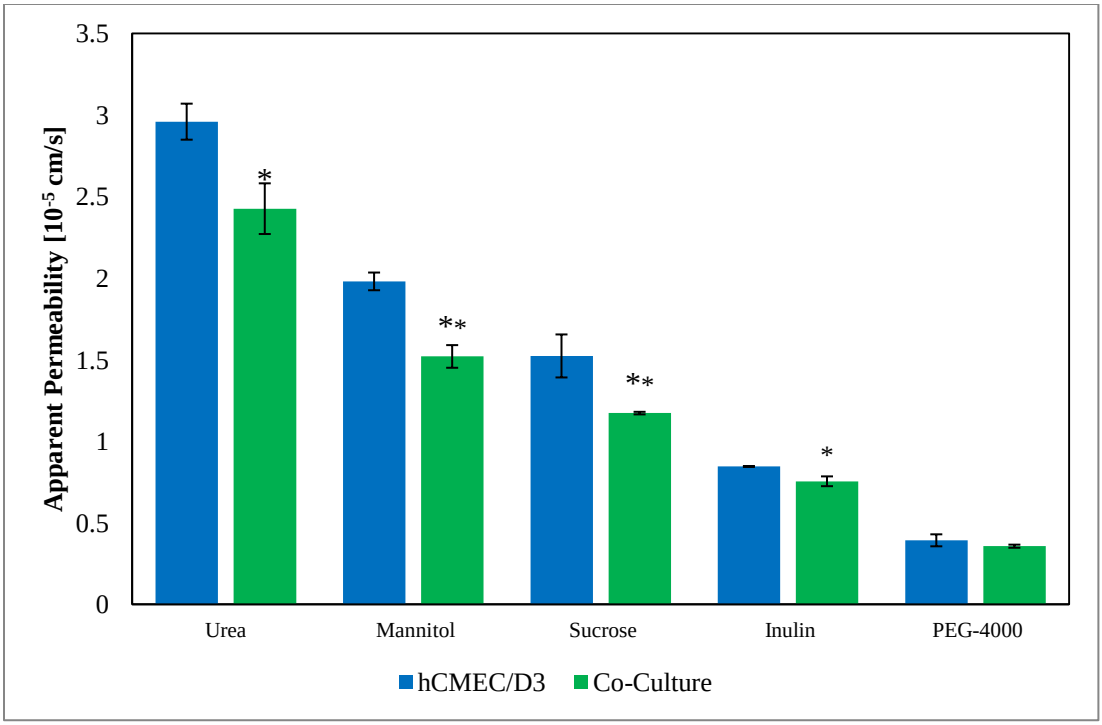

Figure 3.2. Apparent permeability for 5 paracellular [^{14}C]-labeled markers of various hydrodynamic radii. Studies were run in triplicate and subjected to student's T-Test. Significant changes are noted with an asterisk (*) for $p<0.05$ and (**) for $p<0.01$. Error bars represent 1 standard deviation (n=3).

Indirect Contact Coculture

It is well established that changes in culture conditions and cell source can cause significant changes in protein expression of drug metabolizing enzymes, efflux proteins, etc,, which are the focus of ongoing studies.[43,44] In addition, modifications in media have been shown to have considerable effects on BMEC differentiation and tight junction formation.[32,45,46] To establish an internal lab control, an indirect coculture model was also run to investigate differences in paracellular permeability when culturing human

astrocytes in direct contact with hCMEC/D3 cells. Figure 3.3 shows that direct contact leads to significant reduction in permeation compared to indirect contact of both [^{14}C]-mannitol (1.52 ± 0.07 x10^{-5} cm/s and 1.89 ± 0.15 x10^{-5} cm/s; p=0.038), and [^{14}C]-sucrose (1.17 ± 0.008 x10^{-5} cm/s and 1.53 ± 0.12 x10^{-5} cm/s; p=0.035) respectively.

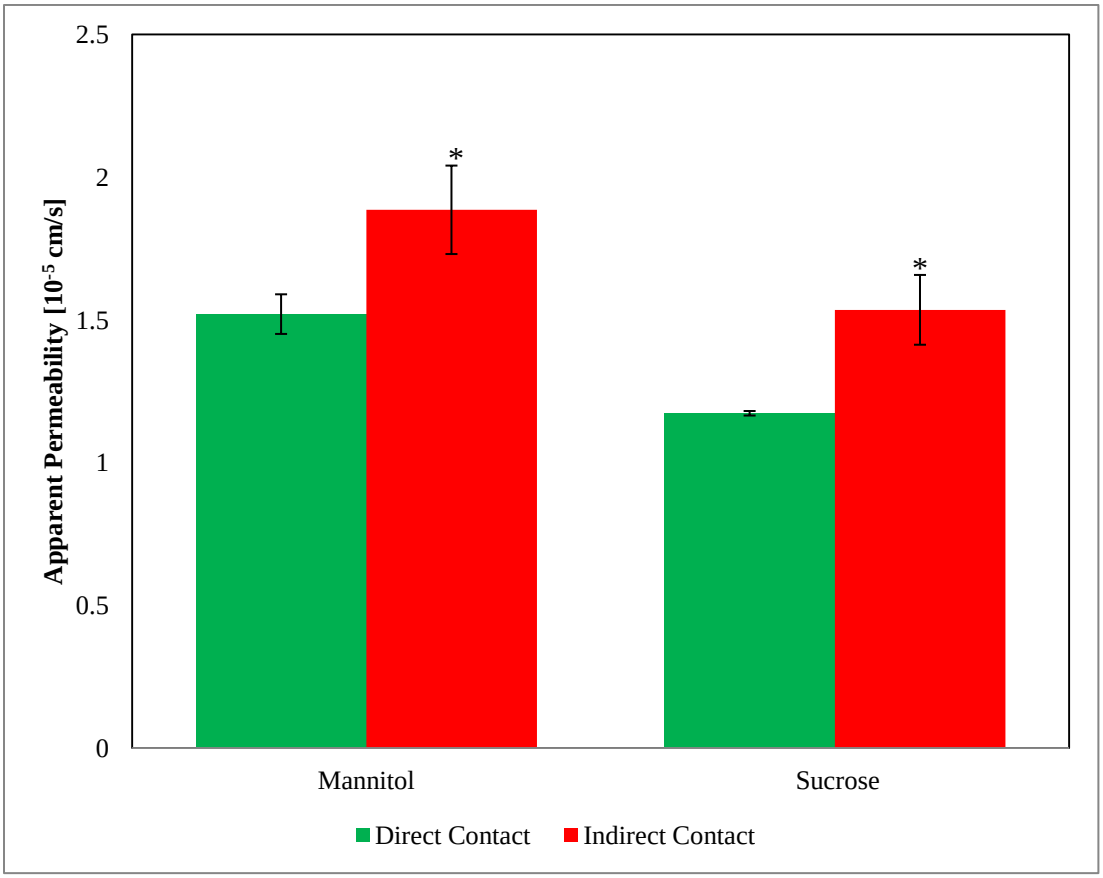

Figure 3.3. Apparent permeability of [^{14}C]-Mannitol and [^{14}C]-Sucrose across direct and indirect contact cocultures. Studies were run in triplicate and subjected to student's T-Test. Significant changes are noted with an asterisk (*) for p<0.05 and (**) for p<0.01. Error bars represent 1 standard deviation (n=3).

Passive Transcellular Permeability

To investigate the effects on transcellular permeation when culturing human astrocytes and hCMEC/D3 cells in direct contact, [^{14}C]-propranolol apparent permeability was measured. Due to its high lipophilicity, the majority of propranolol is uncharged at physiological and a presumed minimal paracellular permeation it was selected as a marker for transcellular permeation. Figure 3.4 shows that insignificant changes in [^{14}C]-Propranolol apparent permeability were seen between hCMEC/D3 and direct contact coculture (1.91 ± 0.19 x10^{-5} cm/s and 1.61 ± 0.04 x10^{-5} cm/s; p=0.103). This may indicate transcellular permeation through hCMEC/D3 cells followed by passive transport across the human astrocyte layer which don't possess tight junctions. However, these values are nearly 3-fold lower than astrocytes grown in monoculture (4.58 ± 0.41 x10^{-5} cm/s). This makes it difficult to assess the effect of astrocytes on transcellular permeation of [^{14}C]-propranolol across the hCMEC/D3 monolayer.

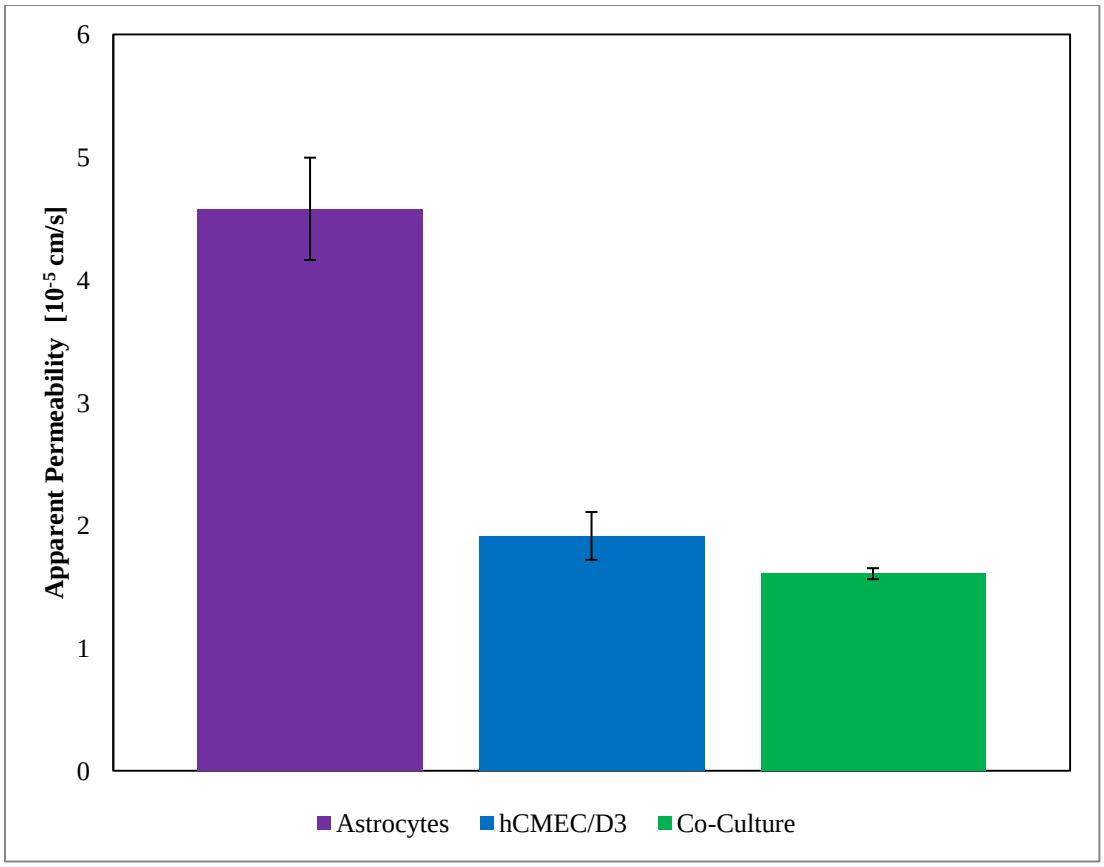

Figure 3.4. Apparent permeability of [^{14}C]-Propranolol, a passive transcellular permeability marker. Non-significant changes ($p<0.05$) were seen between monoculture and coculture. Error bars represent 1 standard deviation ($n=3$).

3.4 Discussion

Previous research has demonstrated that the hCMEC/D3 cell line forms a barrier that is a functionally and physiologically relevant model for human BMECs. This is predicated on the fact that hCMEC/D3 cells possess a similar morphology and protein expression as found in primary human BMECs.[35,47] In addition, the cell line is

immortalized, of human origin, can be grown in monolayers, and is contact inhibited, properties which all lend themselves for use in *in vitro* permeability screening.[32] However, hCMEC/D3 monolayers lack the tightness found *in vivo* which may lead to increased paracellular permeation of drug molecules that in turn may obfuscate the ability to predict transcellular permeation that is observed when studying *in vivo* brain distribution.[6] As has been previously shown, coculturing hCMEC/D3 cells with astrocytes has led to pronounced decreases in paracellular permeability for BMECs which may mitigate this problem.[48] Moreover, the presence of the astrocytes enables a more relevant understanding of the transport across the *in vivo* neurovascular unit.

Since the discovery of the neurovascular unit, this interplay between BMECs and astrocytes at the BBB has been studied. While there are still unknowns, a lot of their interactions have been elucidated.[2,13,49,50] For BMECs, it has been shown that astrocytes play an important role in tight junction development, localization and expression of transporters, as well as upregulation of metabolic enzymes, which are currently being investigated.[32,35,50] In addition, some of these interactions may require symbiotic crosstalk leading to co-differentiation[17,51], and while some of these adaptations can be seen with an indirect coculture of BMECs with astrocytes *in vitro*; leakiness of the tight junctions is still significantly higher than *in vivo* conditions.[6] It is hypothesized that one reason for continued leakiness is an inability for astrocytes to form true direct contact with the BMECs in this model due to the presence of the Transwell® permeable support. This lack of contact may hinder cross-talk between endothelial cells and astrocytes. For this

reason, a direct contact model with hCMEC/D3 cells seeded directly onto human astrocytes was investigated.

Due to the importance of limiting paracellular permeation in *in vitro* BBB cell models, changes in permeation of five paracellular markers of various size; [^{14}C]-urea, [^{14}C]-mannitol, [^{14}C]-sucrose, [^{14}C]-PEG-4000, and [^{14}C]-inulin were measured (Table 3.1). When comparing permeation through hCMEC/D3 monolayers to the coculture, all markers trended toward a reduction in paracellular permeation for the coculture. For the largest marker, PEG-4000, results were insignificant ($p>0.05$), however, this isn't unexpected as permeation through the hCMEC/D3 monolayer was sufficiently slow it is unlikely further pore size reduction would lead to sizable changes in permeability. A similar story can be said of the smallest marker, urea. While significant reduction was seen ($p<0.05$), it is apparent that this model is still unable to prevent permeation of polar molecules in this very low molecular weight range. The most significant changes were seen for mannitol and sucrose ($p<0.01$).

Table 3.1. Comparison of molecular weight and molecular radii with apparent permeability of paracellular model compounds.

Marker	Molecular Weight	Stokes Radius (Å)	Hydrodynamic Radius (Å)	P_{app} ($x10^{-5}$ cm/s)
Urea	60	1.7	1.8	2.43 ± 0.155
Mannitol	182	3.6	4.3	1.52 ± 0.069
Sucrose	342	4.6	5.2	1.17 ± 0.008
Inulin	5000	13.9	10	0.754 ± 0.030
PEG-4000	4000	16.4	15.9	0.357 ± 0.010

To investigate the impact of direct coculture, an indirect coculture with astrocytes on the basolateral side of the Transwell was also examined. As mentioned, it is often difficult to compare models between different labs due to differences in culture protocol, media selection, passaging, and cell source.[43,44] Therefore, the indirect model was established under the same conditions and protocols as the direct contact coculture. As was hypothesized, a significant decrease in [C14]-Sucrose apparent permeability was seen when the astrocytes were in direct cell contact. Further investigation is needed to determine the underlying factors leading to this increased tightness.

To assess passive transcellular permeation the apparent permeability of [^{14}C]-propranolol was measured. Propranolol is often used as a passive transcellular marker due to its high octanol:water coefficient leading to almost exclusive transcellular permeation.[52] Due to the extra cell layer in the coculture model, it was expected that transcellular permeation would be reduced. While permeability was reduced in the

coculture, changes between mono- and coculture weren't significant ($p>0.05$). To further examine this discrepancy, [^{14}C]-propranolol permeability was also measured across human astrocyte monolayers and was found to be approximately three-fold higher than hCMEC/D3 monolayers or the direct contact coculture. This finding validates the coculture permeability data as the hCMEC/D3 cell layer appears to be the rate-limiting barrier to permeation. While astrocytes do play a role in our model, it is unknown if there is a significant contribution of paracellular flux for propranolol that may obfuscate transcellular permeation. While propranolol is unlikely to cross the tight junctions between endothelial cells, astrocyte end feet are known to be much further apart with pores 20-30 Å wide which may allow greater paracellular movement. Therefore, additional studies are required to understand differences between the apparent permeabilities for hCMEC/D3 and human astrocyte monocultures particularly to elucidate the mechanism of transport across the human astrocyte layer.

Overall, this proof-of-concept study suggests direct contact coculture of human astrocytes and hCMEC/D3s leads to some tightening of the leaky tight junctions often found in hCMEC/D3 monoculture with minimal modification to other routes of permeation. While this model is still significantly leakier than *in vivo* conditions it represents an improvement in the paracellular leakage observed in many cell culture models and an advancement in physiologically relevant screening models for determining passive diffusion properties of drugs in the BBB. It should also be noted that while *in vivo* tightness would be ideal, it may be unnecessary for drug screening. While current TEER values are much lower than found *in vivo*, it is possible that small changes in tight

junction pore radii will lead to very large increases in TEER.[41] Due to the nature of paracellular permeation, these large changes in TEER may have little effect on paracellular permeation due to the difference in the hydrodynamic size of ions being measured (sodium, potassium, calcium, chloride, magnesium, etc vs. drug molecules).[31,53] That is, NCEs targeted to the brain are often much larger and more lipophillic molecules than the ions whose movement across the cellular barrier determine TEER. In addition, the vast majority of all NCEs aren't as small or polar as urea, mannitol, or even sucrose. TEER is also dramatically influenced by several other factors like ionic strength, buffers, and temperature that can be confounding variables.

Lastly, species differences are a major cofounder in translation of preclinical screening to humans. Differences in morphology, function, and regulation are all common. Since the common goal is to expedite human translation, it may be better in theory to use a leaky human model than a tight animal model for the screening of pharmaceutical molecules, provided the human model can discriminate between compounds in series. This will reduce some issues such transport and enzyme affinities and capacities observed between species and better enable an assessment of transcellular permeation *in vivo* in humans.

3.5 Conclusion

As the occurrence of neurological diseases rise along with the number of druggable targets and compounds, a more relevant and robust *in vitro* cell culture method has

become of paramount importance for preclinical screening and lead candidate selection and optimization. The hCMEC/D3 cells have been shown to be functionally similar to primary brain endothelial cells, however, their main downfall has been the presence of leaky tight junctions. These leaky tight junctions obfuscate the delineation of transcellular routes of permeation of many compounds and potentially lead to inaccurate *in vivo* predictions. Therefore, it is believed that reducing paracellular permeation to levels closer to that found *in vivo* may lead to a more robust BBB model.

Some promise has been shown in the reduction of paracellular permeability through coculture with astrocytes. However, current models often utilize indirect contact methods in which endothelial cells and astrocytes are separated by the Transwell® permeable support. Here it is shown that direct contact coculture of human astrocytes and hCMEC/D3 cells leads a significant decrease in permeation of paracellular markers. This methodology may serve as a better model for further optimization and *in vivo* prediction. In addition, seeding of both cell types onto the apical chamber of the Transwell® is likely to be much more conducive to high-throughput screening. Though, further investigation including microscopy, transcriptomic and proteomic analysis, and drug screening must be completed to confirm *in vivo* relevancy, it is believed that this model is a step in the right direction for enhancing the ability to screen neurotherapeutic and neurotoxic agents.

3.6 References

1. Abbott NJ 2013. Blood-brain barrier structure and function and the challenges for CNS drug delivery. J Inherit Metab Dis 36(3):437-449.
2. Abbott NJ 2002. Astrocyte-endothelial interactions and blood-brain barrier permeability. J Anat 200(6):629-638.
3. Ballabh P, Braun A, Nedergaard M 2004. The blood-brain barrier: an overview: structure, regulation, and clinical implications. Neurobiol Dis 16(1):1-13.
4. Cecchelli R, Berezowski V, Lundquist S, Culot M, Renftel M, Dehouck MP, Fenart L 2007. Modelling of the blood-brain barrier in drug discovery and development. Nat Rev Drug Discov 6(8):650-661.
5. Cohen-Kashi Malina K, Cooper I, Teichberg VI 2009. Closing the gap between the in-vivo and in-vitro blood-brain barrier tightness. Brain Res 1284:12-21.
6. Hatherell K, Couraud PO, Romero IA, Weksler B, Pilkington GJ 2011. Development of a three-dimensional, all-human in vitro model of the blood-brain barrier using mono-, co-, and tri-cultivation Transwell models. J Neurosci Methods 199(2):223-229.
7. Holash JA, Noden DM, Stewart PA 1993. Re-evaluating the role of astrocytes in blood-brain barrier induction. Dev Dyn 197(1):14-25.
8. Poller B, Gutmann H, Krahenbuhl S, Weksler B, Romero I, Couraud PO, Tuffin G, Drewe J, Huwyler J 2008. The human brain endothelial cell line hCMEC/D3 as a human blood-brain barrier model for drug transport studies. J Neurochem 107(5):1358-1368.

9. Liebner S, Kniesel U, Kalbacher H, Wolburg H 2000. Correlation of tight junction morphology with the expression of tight junction proteins in blood-brain barrier endothelial cells. Eur J Cell Biol 79(10):707-717.

10. Wolburg H, Lippoldt A 2002. Tight junctions of the blood-brain barrier: development, composition and regulation. Vascul Pharmacol 38(6):323-337.

11. Schrade A, Sade H, Couraud PO, Romero IA, Weksler BB, Niewoehner J 2012. Expression and localization of claudins-3 and -12 in transformed human brain endothelium. Fluids Barriers CNS 9:6.

12. On NH, Miller DW 2014.Transporter-based delivery of anticancer drugs to the brain: improving brain penetration by minimizing drug efflux at the blood-brain barrier. Curr Pharm Des 20(10):1499-1509.

13. Abbott NJ 2005. Dynamics of CNS barriers: evolution, differentiation, and modulation. Cell Mol Neurobiol 25(1):5-23.

14. Berezowski V, Landry C, Dehouck MP, Cecchelli R, Fenart L 2004. Contribution of glial cells and pericytes to the mRNA profiles of P-glycoprotein and multidrug resistance-associated proteins in an in vitro model of the blood-brain barrier. Brain Res 1018(1):1-9.

15. Engelhardt B 2003. Development of the blood-brain barrier. Cell Tissue Res 314(1):119-129.

16. Schiera G, Bono E, Raffa MP, Gallo A, Pitarresi GL, Di Liegro I, Savettieri G 2003. Synergistic effects of neurons and astrocytes on the differentiation of brain capillary endothelial cells in culture. J Cell Mol Med 7(2):165-170.

17. Lippmann ES, Azarin SM, Kay JE, Nessler RA, Wilson HK, Al-Ahmad A, Palecek SP, Shusta EV 2012. Derivation of blood-brain barrier endothelial cells from human pluripotent stem cells. Nat Biotechnol 30(8):783-791.

18. Meyer RP, Knoth R, Schiltz E, Volk B 2001. Possible function of astrocyte cytochrome P450 in control of xenobiotic phenytoin in the brain: in vitro studies on murine astrocyte primary cultures. Exp Neurol 167(2):376-384.

19. Cohen MP, Frank RN, Khalifa AA 1980. Collagen production by cultured retinal capillary pericytes. Invest Ophthalmol Vis Sci 19(1):90-94.

20. Hirschi KK, D'Amore PA 1996. Pericytes in the microvasculature. Cardiovasc Res 32(4):687-698.

21. Mandarino LJ, Sundarraj N, Finlayson J, Hassell HR 1993. Regulation of fibronectin and laminin synthesis by retinal capillary endothelial cells and pericytes in vitro. Exp Eye Res 57(5):609-621.

22. Cecchelli R, Dehouck B, Descamps L, Fenart L, Buee-Scherrer VV, Duhem C, Lundquist S, Rentfel M, Torpier G, Dehouck MP 1999. In vitro model for evaluating drug transport across the blood-brain barrier. Adv Drug Deliv Rev 36(2-3):165-178.

23. Dehouck MP, Meresse S, Delorme P, Fruchart JC, Cecchelli R 1990. An easier, reproducible, and mass-production method to study the blood-brain barrier in vitro. J Neurochem 54(5):1798-1801.

24. Deli MA, Abraham CS, Kataoka Y, Niwa M 2005. Permeability studies on in vitro blood-brain barrier models: physiology, pathology, and pharmacology. Cell Mol Neurobiol 25(1):59-127.

25. Demeuse P, Kerkhofs A, Struys-Ponsar C, Knoops B, Remacle C, van den Bosch de Aguilar P 2002. Compartmentalized coculture of rat brain endothelial cells and astrocytes: a syngenic model to study the blood-brain barrier. J Neurosci Methods 121(1):21-31.

26. Di L, Kerns EH, Fan K, McConnell OJ, Carter GT 2003. High throughput artificial membrane permeability assay for blood-brain barrier. Eur J Med Chem 38(3):223-232.

27. Eigenmann DE, Xue G, Kim KS, Moses AV, Hamburger M, Oufir M 2013. Comparative study of four immortalized human brain capillary endothelial cell lines, hCMEC/D3, hBMEC, TY10, and BB19, and optimization of culture conditions, for an in vitro blood-brain barrier model for drug permeability studies. Fluids Barriers CNS 10(1):33.

28. Gaillard PJ, Voorwinden LH, Nielsen JL, Ivanov A, Atsumi R, Engman H, Ringbom C, de Boer AG, Breimer DD 2001. Establishment and functional characterization of an in vitro model of the blood-brain barrier, comprising a co-culture of brain capillary endothelial cells and astrocytes. Eur J Pharm Sci 12(3):215-222.

29. Jeliazkova-Mecheva VV, Bobilya DJ 2003. A porcine astrocyte/endothelial cell co-culture model of the blood-brain barrier. Brain Res Brain Res Protoc 12(2):91-98.

30. Kido Y, Tamai I, Nakanishi T, Kagami T, Hirosawa I, Sai Y, Tsuji A 2002. Evaluation of blood-brain barrier transporters by co-culture of brain capillary endothelial cells with astrocytes. Drug Metab Pharmacokinet 17(1):34-41.

31. Sorensen M, Steenberg B, Knipp GT, Wang W, Steffansen B, Frokjaer S, Borchardt RT 1997. The effect of beta-turn structure on the permeation of peptides across monolayers of bovine brain microvessel endothelial cells. Pharm Res 14(10):1341-1348.

32. Weksler B, Romero IA, Couraud PO 2013. The hCMEC/D3 cell line as a model of the human blood brain barrier. Fluids Barriers CNS 10(1):16.

33. Audus KL, Borchardt RT 1987. Bovine brain microvessel endothelial cell monolayers as a model system for the blood-brain barrier. Ann N Y Acad Sci 507:9-18.

34. Raub TJ, Kuentzel SL, Sawada GA 1992. Permeability of bovine brain microvessel endothelial cells in vitro: barrier tightening by a factor released from astroglioma cells. Exp Cell Res 199(2):330-340.

35. Weksler BB, Subileau EA, Perriere N, Charneau P, Holloway K, Leveque M, Tricoire-Leignel H, Nicotra A, Bourdoulous S, Turowski P, Male DK, Roux F, Greenwood J, Romero IA, Couraud PO 2005. Blood-brain barrier-specific properties of a human adult brain endothelial cell line. FASEB J 19(13):1872-1874.

36. Carl SM, Lindley DJ, Couraud PO, Weksler BB, Romero I, Mowery SA, Knipp GT 2010. ABC and SLC transporter expression and pot substrate characterization across the human CMEC/D3 blood-brain barrier cell line. Mol Pharm 7(4):1057-1068.

37. Vu K, Weksler B, Romero I, Couraud PO, Gelli A 2009. Immortalized human brain endothelial cell line HCMEC/D3 as a model of the blood-brain barrier facilitates in vitro studies of central nervous system infection by Cryptococcus neoformans. Eukaryot Cell 8(11):1803-1807.

38. Butt AM, Jones HC, Abbott NJ 1990. Electrical resistance across the blood-brain barrier in anaesthetized rats: a developmental study. J Physiol 429:47-62.

39. Siddharthan V, Kim YV, Liu S, Kim KS 2007. Human astrocytes/astrocyte-conditioned medium and shear stress enhance the barrier properties of human brain microvascular endothelial cells. Brain Res 1147:39-50.

40. Garcia CM, Darland DC, Massingham LJ, D'Amore PA 2004. Endothelial cell-astrocyte interactions and TGF beta are required for induction of blood-neural barrier properties. Brain Res Dev Brain Res 152(1):25-38.

41. Adson A, Raub TJ, Burton PS, Barsuhn CL, Hilgers AR, Audus KL, Ho NF 1994. Quantitative approaches to delineate paracellular diffusion in cultured epithelial cell monolayers. J Pharm Sci 83(11):1529-1536.

42. Knipp GT, Ho NF, Barsuhn CL, Borchardt RT 1997. Paracellular diffusion in Caco-2 cell monolayers: effect of perturbation on the transport of hydrophilic compounds that vary in charge and size. J Pharm Sci 86(10):1105-1110.

43. Roth WJ, Lindley DJ, Carl SM, Knipp GT 2012. The effects of intralaboratory modifications to media composition and cell source on the expression of pharmaceutically relevant transporters and metabolizing genes in the Caco-2 cell line. J Pharm Sci 101(10):3962-3978.

44. Lindley DJ, Roth WJ, Carl SM, Knipp GT 2012. The effects of media on pharmaceutically relevant transporters in the human HT-29 adenocarcinoma cell line: does culture media need to be controlled? J Pharm Sci 101(4):1616-1630.

45. Helms HC, Waagepetersen HS, Nielsen CU, Brodin B 2010. Paracellular tightness and claudin-5 expression is increased in the BCEC/astrocyte blood-brain barrier model by increasing media buffer capacity during growth. AAPS J 12(4):759-770.

46. Wolburg H, Neuhaus J, Kniesel U, Krauss B, Schmid EM, Ocalan M, Farrell C, Risau W 1994. Modulation of tight junction structure in blood-brain barrier endothelial cells. Effects of tissue culture, second messengers and cocultured astrocytes. J Cell Sci 107 (Pt 5):1347-1357.

47. Urich E, Lazic SE, Molnos J, Wells I, Freskgard PO 2012. Transcriptional profiling of human brain endothelial cells reveals key properties crucial for predictive in vitro blood-brain barrier models. PLoS One 7(5):e38149.

48. Li G, Simon MJ, Cancel LM, Shi ZD, Ji X, Tarbell JM, Morrison B, 3rd, Fu BM 2010. Permeability of endothelial and astrocyte cocultures: in vitro blood-brain barrier models for drug delivery studies. Ann Biomed Eng 38(8):2499-2511.

49. Abbott NJ, Ronnback L, Hansson E 2006. Astrocyte-endothelial interactions at the blood-brain barrier. Nat Rev Neurosci 7(1):41-53.

50. Arthur FE, Shivers RR, Bowman PD 1987. Astrocyte-mediated induction of tight junctions in brain capillary endothelium: an efficient in vitro model. Brain Res 433(1):155-159.

51. Lippmann ES, Al-Ahmad A, Palecek SP, Shusta EV 2013. Modeling the blood-brain barrier using stem cell sources. Fluids Barriers CNS 10(1):2.

52. Pade V, Stavchansky S 1997. Estimation of the relative contribution of the transcellular and paracellular pathway to the transport of passively absorbed drugs in the Caco-2 cell culture model. Pharm Res 14(9):1210-1215.

53. Knipp GT, Vander Velde DG, Siahaan TJ, Borchardt RT 1997. The effect of beta-turn structure on the passive diffusion of peptides across Caco-2 cell monolayers. Pharm Res 14(10):1332-1340.

CHAPTER 4. CYS34-PEGYLATED HUMAN SERUM ALBUMIN FOR DRUG BINDING AND DELIVERY

Adapted With Permission from From: Mehtala JG, Kulczar C, Lavan M, Knipp G, Wei A. 2015. Cys34-PEGylated Human Serum Albumin for Drug Binding and Delivery. Bioconjug Chem 26(5):941-949. Copyright 2015 American Chemical Society

4.1 Introduction

Protein function and recognition can be rationally modified by the covalent ligation of molecular structures such as optical tags[1], targeting ligands[2], carbohydrates[3], and polymers.[4,5] However, coupling methods that rely on available amines or carboxylic acids for amide bond formation typically have poor regioselectivity, and can result in intra- or intermolecular crosslinks that lead to protein denaturation, aggregation, or general loss of function.[6] Site-specific ligation methods are highly desirable for introducing additional functionality to proteins without disrupting other physicochemical properties. A useful alternative to amide bond formation involves the chemoselective addition of alkylmaleimides to exposed cysteines.[7] This method of conjugation has little to no effect on the electrostatic surface potential of proteins at physiological pH, and is thus less likely to induce unintended changes in secondary or tertiary structure. *N*- and *C*-modified proteins have the intrinsic drawback of having different net charges relative

to the native protein, which can affect their conformational behavior, dispersion stability, aggregation kinetics, biomolecular recognition, and catalytic activity.[6,8,9]

PEGylation (i.e. the ligation of one or more polyethylene glycol chains to external residues) is a widely used tactic to modify the pharmacokinetic properties of drug carriers[10,11] and protein-based biologics.[12,13] Covalently attached PEG chains can stabilize proteins by providing a surrogate hydration shell,[14] or prevent denaturation by limiting conformational freedom.[15] While much attention has been paid to antibodies and other "functional" biomolecules, passive proteins such as human serum albumin (HSA) are also important candidates because of their putative roles in drug solubilization and delivery. HSA's native role as a plasma carrier makes it an ideal candidate for transporting hydrophobic drugs that possess higher binding affinities from the bloodstream into extravascular tissue space.[16,17] HSA is thought to facilitate drug permeation by passing through endothelial layers via caveolar-mediated transcytosis.[18,19] As one of most abundant proteins in the plasma (35–50 mg/mL),[20] HSA forms aggregates reversibly and can accumulate passively in tumor tissue due to the enhanced permeability and retention (EPR) effect.[21,22] In this regard, we note that HSA-based formulations have been characterized as nanoparticles *ex vivo*, but are thought to disperse into monomeric form soon after entering the bloodstream.[23] This suggests that the pharmacokinetic properties of HSA may be tailored by judicious structural changes.

Interest in albumin-based drug delivery has been increasing due to the favorable pharmacology of HSA, its low immunogenicity, and its current availability in recombinant form. A well-known example of albumin-based formulation is HSA-bound paclitaxel (Abraxane®), currently being used for the treatment of several late-stage

cancers.[24,25,26] Paclitaxel (PTX) is a powerful antimitotic that induces apoptosis in rapidly dividing cells;[27] however, its therapeutic efficacy has been compromised by poor water solubility or by surfactants with peripheral side effects (e.g., Cremophore EL).[28,29,30] The clinical success of Abraxane® confirms the benefits of HSA as a carrier of poorly soluble drugs like PTX; nevertheless, adverse side effects such as moderate neuropathy and neutropenia persist,[26,31,32] indicating the need to further optimize drug loading and delivery.

PEGylated HSA has been prepared by conventional amide ligation, and shown to provide significant enhancements in its pharmacokinetic profile for drug delivery.[33] However, most studies have been conducted by modifying the acidic or basic residues on albumin, and the poor regioselectivity of amide-based ligations render these formulations vulnerable to unintended changes in structure or colligative properties. For example, *N*-PEGylation reduces the volume of the hydrophobic binding cavity in the second R-helix domain, despite overall retention of HSA size and shape.[34]

Both HSA and its congener bovine serum albumin (BSA) possess a free thiol residue at Cys-34, which presents the option of site-specific *S*-PEGylation using maleimide chemistry.[35,36] *S*-PEGylation of albumins can be performed with minimal perturbation to pre-existing disulfide bridges with subsequent retention of protein structure, as demonstrated in the case of PEG-(C34)BSA,[35] and can increase its circulation lifetime relative to unmodified albumins, as demonstrated in a rat model with PEG(C34)HSA.[36] These reports indicate that *S*-PEGylation at Cys-34 is an appealing alternative to amide-based ligations for developing albumin-based carriers with tailored pharmacological properties. It is worth mentioning that maleimide-based reagents have

also been developed for PEGylation across disulfide bonds,[37,38] but are not immediately relevant for proteins bearing free thiols.

In this article we characterize the carrier properties of two mono-PEGylated HSA derivatives with site-specific conjugation at Cys-34, prepared on a multigram scale using maleimide-terminated mPEG chains having molecular weights of 5 and 20 kDa. *S*-PEGylation produces minimal perturbations in conformation or solubilization of PTX, but significantly increases HSA's propensity to self-assemble into protein nanoparticles as characterized by nanoparticle tracking analysis (NTA). We also investigate the permeation of PTX through monolayers of human umbilical vascular endothelial cells (HUVEC) and brain microvascular endothelial cells (hCMEC/D3) with and without PEG(C34)HSA conjugates, and evaluate the therapeutic efficacy of PTX-loaded PEG(C34)HSA against MCF-7 breast cancer cells relative to native HSA (n-HSA). We find that C34-PEGylation has essentially no negative impact on PTX loading and subsequent permeation across cell monolayers. On the other hand, PEG(C34)HSA conjugates provide substantial increases in the transport and cytotoxicity of PTX delivered to MCF-7 cells, with negligible toxicity from PEGylated HSA alone.

4.2 Materials and Methods

Materials

Recombinant HSA was obtained from GenLantis (San Diego, CA); mPEG-maleimide was obtained from Laysan Bio (Arab, AL); hydrocortisone, Hank's balanced salt solution (HBSS), polystyrene T-75 flasks, and Transwell® permeable supports were

purchased from Sigma-Aldrich (St. Louis, MO). Paclitaxel was obtained from LC Laboratories (Woburn, MA); radiolabeled [^{14}C]paclitaxel ([^{14}C]PTX) was purchased from Moravek Biochemicals (Brea, CA). DMEM media, penicillin/streptomycin, and L-glutamine were obtained from Corning Cellgro (Manassas, VA); fetal bovine serum was obtained from Atlanta Biologicals (Atlanta, GA); MTT reagent was obtained from RPI (Mount Prospect, IL); EGM-2, EBM-2, and basic fibroblast growth factor were obtained from Lonza (Walkersville, MD). MCF-7 cells were obtained from the Purdue Center for Combinatorial Chemical Biology; HUVEC cells were obtained from the American Type Culture Collection (ATCC; Manassas, VA); hCMEC/D3 cells were provided by Dr. Pierre-Olivier Couraud at Institut Cochin (Paris, France). Phosphate buffer solution (PBS) was prepared by tenfold dilution from a concentrated stock containing 80 g NaCl, 2 g KCl, 4 g Na_2HPO_4, and 2 g KH_2PO_4. All solutions were prepared using initially deionized water using a Milli-Q ultrafiltration system from Millipore (Bedford, MA) with a measured resistivity above 18 MΩ·cm, passed through a 0.22-μm filter to remove particulate matter.

Gram and Multigram Synthesis of PEG(C34)HSA conjugates

In a typical reaction, powdered HSA (1.0 g, 15.1 μmol) was dissolved in 40 mL of sterilized PBS (adjusted to pH 6.5) in a 100-mL glass round-bottomed flask. The PBS was passed through a 0.2-μm syringe filter prior to use, and the mixture was stirred for 15 minutes. $mPEG_{5K}$ -Mal (155 mg, 31 μmol) or $mPEG_{20K}$-Mal (620 mg, 31 μmol) was dissolved in 10 mL of sterilized PBS (pH 6.5) and added in 1-mL portions over 1 minute to the stirred HSA solution. The mixture was placed in a 37 °C bath and stirred for 20

hours, then cooled to room temperature. Solutions of *S*-PEGylated HSA were transferred to dialysis membrane tubings (MWCO 12.4 kDa for PEG_{5K}-HSA; MWCO 50 kDa for PEG_{20K}-HSA) and gently agitated in 500 mL of deionized water to remove salts and excess mPEG-Mal (2 rounds, > 1 h each). Approximately 90% of each PEG(C34)HSA was set aside for cell culture studies; the remainder was subjected to additional dialysis for characterization. PEG(C34)HSA conjugates could be lyophilized and stored in the dark at 4 °C.

For PEG(C34)HSA conjugates prepared on a multigram scale, purifications were performed with an Amicon stirred ultrafiltration cell (180 mL) equipped with a cellulose membrane filter (100 kDa MWCO), both from Millipore. Reaction mixtures were concentrated to gelatinous slurries (ca. 10 mL) then redispersed in deionized water to maximum volume, and repeated for up to 6 cycles. The rate of filtration ranged from over 10 mL/min to under 1 mL/min, depending on the concentration of residual mPEG-Mal in the retentate.

Protein Characterization

Matrix-assisted laser desorption ionization mass spectra (MALDI-MS) were obtained using an Applied Biosystems Voyager DE PRO spectrometer, equipped with a nitrogen laser (337 nm) and a time-of-flight mass analyzer. Positive-ion MS were obtained in the linear mode using an accelerating voltage of 25 kV, grid voltage of 94%, and extraction delay time of 98 nsec. The *m/z* range for this study was 10–100 kDa, using 150 laser shots per spectrum and sinapinic acid as the matrix material.

Circular dichroism (CD) spectra were obtained using a Jasco J-810 spectrophotometer. Protein samples were prepared in halide-free phosphate buffer and diluted to 1 μM. The instrument was flushed with nitrogen for 1 hour prior to use; spectra were collected in triplicate from 190–260 nm at a scan rate of 7 minutes at 25 °C, with data averaging performed after background subtraction. Attenuated total reflectance infrared (ATR-IR) spectra were acquired using a Nicolet Nexus 670 FT-IR, under constant nitrogen flow. Samples were prepared by depositing 1 mL of solution onto the ATR crystal, then dried under a nitrogen stream until a thin film was obtained. The sample chamber was purged for 20 minutes prior to collecting data.

High-performance liquid chromatography (HPLC) analyses were performed on 100-μL aliquots of PEG(C34)HSA after extensive dialysis, using an Agilent 1100 Series HPLC with a Zorbax XDB-C8 column (Agilent, 4.6 mm × 15 cm). Gradient elutions were performed using 33−66% aqueous CH_3CN with 0.1% trifluoroacetic acid (TFA) at a flow rate of 0.75 mL/min; the column was equilibrated at 33% CH_3CN for at least 30 minutes prior to sample injection. Proteins were detected by absorbance at 280 nm, with yields determined by peak area integration. Levels of free mPEG-Mal were determined by HPLC at 215 nm, using a Zorbax XDB-C8 column with a gradient elution of 35–45% CH_3CN plus 0.1% TFA (5-kDa mPEG-Mal), or a Phenomenex C18 reversed-phase column (2.0 mm × 5 cm) with a gradient elution of 30–90% CH_3CN plus 0.1% TFA (20-kDa mPEG-Mal), with calibrations against a reference sample. In both cases, the amount of residual Mal-mPEG after six rounds of ultrafiltration was less than 1 wt%.

Particle Characterization

Nanoparticle tracking analysis (NTA) was performed using a Nanosight LM-10 system equipped with a blue laser (λ= 405 nm), with data analysis supported by NTA v.2.3.5.0033 (Build 16).[39] NTA was performed using PBS (pH 6.5) stored in polyethylene containers. The imaging chamber was cleaned with acetone and a microfiber cloth prior to use, then washed with particle-free water until no background signals were observed. Water was removed from the NTA chamber with a sterile plastic syringe just prior to use, and replaced with protein solution (0.1−1.0 mg/mL). Three tracking videos were collected per sample; 50 μL of fresh solution was injected in between each run to prevent protein aggregates from settling, followed by a 60-second recording at a shutter speed of 700 and a gain of 400. The number of tracks per run varied from 300 to 2000, depending on concentration. Hydrodynamic size analysis was derived from number and volume particle distributions, with population samples based on the number of tracks accumulated over several runs. Optimized parameters for video analysis (advanced mode) include a detection threshold of 10, 9 × 9 blur setting, and automated settings for track length and minimum particle size.

HSA−PTX Formulation

PTX-HSA formulations were produced from freshly prepared stock solutions of PTX in DMSO (585 μM) and PEG(C34)HSA or n-HSA in PBS adjusted to pH 6.5 (150 μM). PTX solutions were diluted serially with PBS to concentrations at 40× above the target dose. PTX and HSA stock solutions were then combined in a 1:1 v/v ratio (0.4 mL total) and allowed to stand for 4 hours at room temperature, prior to use. 10-μL aliquots

of HSA–PTX solution were added to 190 µL of cell culture media in 96-well plates containing MCF-7 cells at 10–20% confluence. DMSO concentrations were 0.1% v/v or less.

Cell Permeation Studies

HUVEC and hCMEC/D3 cells were cultured in T-75 flasks at 37 °C, 5% CO_2, and 90% humidity. HUVECs were cultured in EBM-2 supplemented with Lonza EGM-2 SingleQuots®. hCMEC/D3 cells were cultured in EBM-2 supplemented with 5% FBS, 1× penicillin–streptomycin, 1 ng /mL basic fibroblast growth factor, 1.4 µM hydrocortisone, 5 µg/mL ascorbic acid, 1% chemically defined lipid concentrate, and 10 mM HEPES buffer. After thawing, cells were passaged at least three times before transport studies with media changes every other day.

Transport studies were performed in the apical to basolateral direction in triplicate wells simultaneously. HUVECs were seeded between passages 6–10, while hCMEC/D3 cells were seeded at passages 34–42. Cells were seeded onto collagen-coated, 0.4-µm polyester Transwells®, at a density of 50,000 cells/cm^2 for HUVECs and 70,000 cells/cm^2 for hCMEC/D3 cells. HUVEC and hCMEC/D3 cells were allowed to proliferate and differentiate for 7 and 14 days respectively, with exchange of cell culture media every other day. Confluent cell monolayers were washed twice with PBS then equilibrated for 30 minutes in HBSS, just prior to permeability studies. Formulations containing [^{14}C]-PTX were added to the apical side of the Transwell® plate, which was kept on a rocker tray as aliquots were removed from the donor compartment at 15, 30, 45, 60, and 90 minute time points. Initial and remaining donor as well as cell lysate samples were also

taken for permeability and mass balance calculations. 100 μL samples were diluted in 4 mL EcoLite® scintillation fluid and counted for 5 minutes on a Beckman Coulter LS 6500 scintillation counter. Apparent permeability (P_{app}) coefficients were determined using the following equation:

$$P_{app} = \frac{dM}{dt} \cdot \frac{1}{SA \times C_0 \times 60}$$

where d*M*/d*t* (counts/min) is the steady-state rate of mass transfer, *SA* (cm^2) is the surface area of the apical membrane, and C_0 (counts) is the initial donor concentration. Studies were compared using an unpaired, two-tailed Student's *t*-test.

Cell Viability Assays

Mitochondrial oxidation assays using the tetrazolium dye MTT were performed as previously described[40] but using MCF-7 breast cancer cells, which were cultured in T-75 flasks and complete DMEM media with 10% fetal bovine serum (FBS), 1% L-glutamine, and 1% penicillin/ streptomycin prior to plating. In a typical experiment, 96-well microtiter plates (5,000 cells/well) were incubated overnight in 200 μL of media to approximately 10% confluence. Solutions in each well were replaced the following day with 190 μL of fresh media and 10 μL of PTX-HSA formulation, followed by 5 days of incubation at 37 °C under a 5% CO_2 atmosphere. The media was removed and replaced with 190 μL fresh media and 10 μL 0.5% MTT, incubated at room temperature for 14 hours, then replaced with 200 μL DMSO for homogenization. Absorbance measurements were recorded on a VersaMax microplate reader at 570 nm with background subtraction; cell viabilities were normalized to a negative control group (having reached 97%

confluence over 5 days). Experiments were run in triplicate with errors representing one standard deviation; two-tailed probability values were obtained by Student's t-test.

4.3 Results and Discussion

Synthesis and Characterization of PEGylated HSA Adducts

Following an earlier reported procedure,[36] PEG(C34)HSA adducts were prepared at 37 °C in mildly acidic PBS (pH 6.5) by combining n-HSA (25 mg/mL) with 2 or 4 equivalents of 5-kDa or 20-kDa mPEG-Mal (Scheme 1). Maintaining a pH slightly below 7 helps to keep HSA in conformations that shield its internal disulfide bonds from other solutes.[41] Analytical samples of *S*-PEGylated HSA were obtained by HPLC purification, whereas protein mixtures synthesized on a multigram scale were separated from unreacted mPEG-Mal by stirred ultrafiltration. Recombinant HSA was used instead of plasma-derived HSA, which reduces the risk of infection from unknown viruses or prions that may be present in the latter. Recombinant and plasma-derived HSA have been shown to be identical in structure.[42]

MALDI-MS and analytical HPLC were used to assess the degree of PEGylation: n-HSA produced a strong peak at *m/z* 66,553,[43] whereas PEG_{5K}- and PEG_{20K}(C34)HSA produced additional peaksets centered at 71,984 (+5,431 amu) and 87,694 (+21,141 amu), respectively (Figure 4.1a–c). HPLC analysis on dialyzed samples indicated that treatment of n-HSA (*Rt* 6.4 min) with two equivalents of 5-kDa mPEG-Mal supported a 72% conversion into PEG_{5K}(C34)HSA (Figure 4.1e), whereas treatment with two

equivalents of 20-kDa mPEG-Mal supported a 48% conversion into PEG_{20K}(C34)HSA (Figure 4.1f). The conversion efficiency was not affected by changes in reaction time, temperature or pH, but increasing the amount of 20-kDa mPEG-Mal to four equivalents increased the conversion of PEG_{20K}(C34)HSA to 77%. It should be noted that the HSA was not pretreated with reducing agents, which can further optimize maleimide addition to free cysteines;[44] therefore, the yields reported here should be viewed as a lower limit. We also note that ultrafiltration of PEG(C34)HSA from excess mPEG-Mal on a multigram scale was initially tedious due to the high viscosity of the retentate but became more efficient after several washings, with less than 1 wt% mPEG after six cycles according to HPLC. All subsequent studies using PEG(C34)HSA were performed with protein mixtures prepared from a 2:1 ratio of mPEG-Mal to n-HSA, and purified by six cycles of ultrafiltration.

Scheme 4.1. Synthesis of PEG(C34)HSA using 5- or 20-kDa mPEG-maleimide (Mal); PEG chain truncated for clarity.

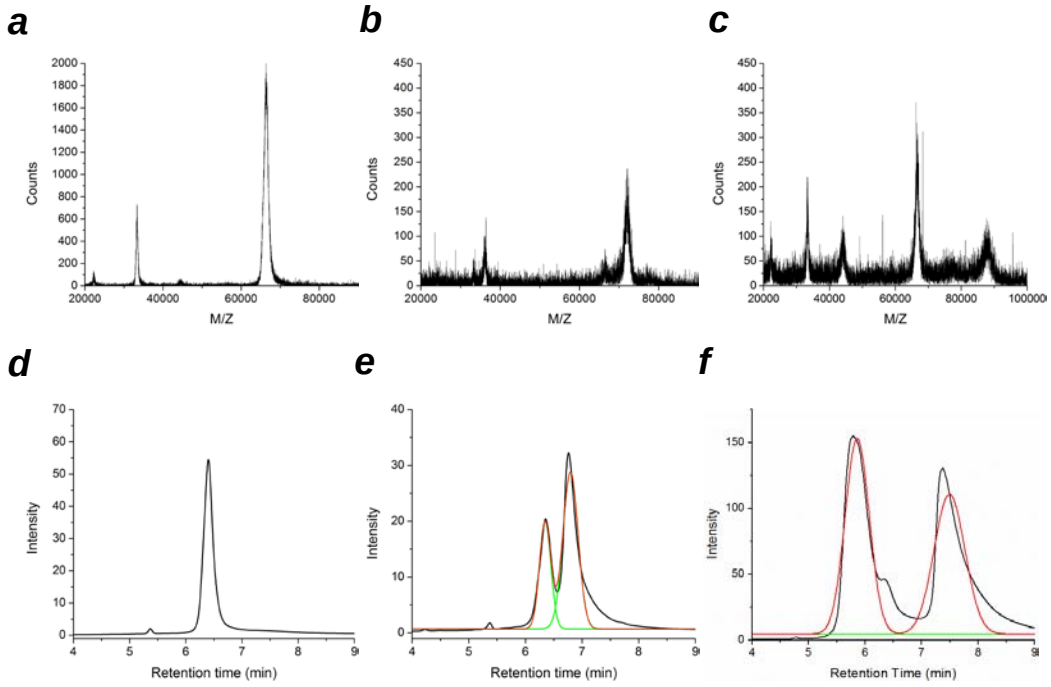

Figure 4.1. (a–c) MALDI-MS analysis of n-HSA (m/z ~66.5 kDa), PEG$_{5K}$(C34)HSA (m/z ~72.0 kDa), and PEG$_{20K}$(C34)HSA (m/z ~87.7 kDa); (d–f) HPLC traces of n-HSA (as received), HSA treated with 2 equiv mPEG$_{5K}$-Mal or 2 equiv mPEG$_{20K}$-Mal.

ATR-IR analysis confirmed retention of the PEG chain after exhaustive dialysis, with a strong peak at 1090 cm^{-1} corresponding to C–O stretching modes, and minimal differences in the amide peak region relative to n-HAS. Circular dichroism analysis of the PEG-(C34)HSA derivatives also indicated negligible changes in secondary protein structure relative to n-HSA, with very minor perturbations in 195–260 nm region (Figure 4.2). We thus presume that *S*-PEGylation at Cys-34 has minimal influence on the secondary structure of HSA.

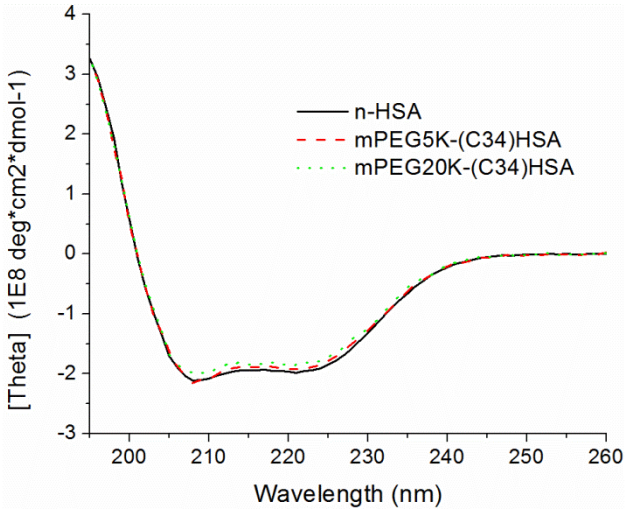

Figure 4.2. Circular dichroism spectra of n-HSA, PEG_{5K}(C34)HSA (72% conversion), and PEG_{20K}(C34)HSA (77% conversion).

Effect of PTX–HSA Formulations on Cell Viability

MCF-7 cells exposed to 10 nM PTX using a 30:1 mole ratio of PTX:n-HSA had a 1.7-fold greater therapeutic effect compared to 10 nM PTX in PBS without HSA ($p <$

0.05), whereas PTX formulated in a 10:1 mole ratio with n-HSA had 3.1-fold greater efficacy ($p < 0.005$; Figure 4.3).[45] HSA without PTX (up to 100 nM) had a negligible effect on cell viability, confirming that its primary role is to increase the solubilization of PTX. The increased drug efficacy did not vary significantly for PTX:n-HSA ratios below 10:1, implying an upper limit of 10 molecules of PTX per HSA carrier.

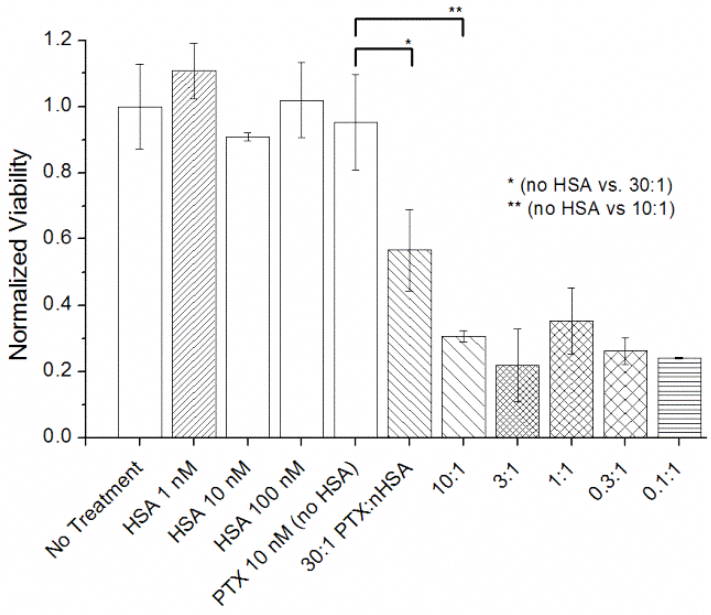

*Figure 4.3. The effect of formulating PTX (10 nM) with n-HSA on MCF-7 cell cultures, 5 days post-treatment (N=3). PTX:n-HSA mole ratios range from 30 to 0.1, with [PTX] fixed at 10 nM. Significant changes in cytotoxicity marked with * ($p < 0.05$) or ** ($p < 0.005$). Error = 1 stdev.*

MCF-7 cells exposed to 10 nM PTX in a 10:1 mole ratio of PTX and PEG_{5K}(C34)HSA or PEG_{20K}(C34)HSA experienced similar increases in toxicity relative

to PTX alone (Figure 4.4). As in the case with n-HSA, maximum efficacy was attained when PTX was formulated in a 10:1 mole ratio with PEG(C34)HSA derivatives compared to a 30:1 ratio, with no further improvements below that. These results imply that the PEG chain does not inhibit the ability of HSA to bind and release PTX. Again, control experiments indicated that PEGylated HSA derivatives have no effect on cell viability.

MCF-7 cells were exposed to a range of PTX doses (0.33 nM) formulated at 10:1 mole ratios with n-HSA, PEG_{5K}(C34)HSA, or PEG_{20K}(C34)HSA. For intermediate PTX doses (6.6 nM), we observed that formulations with PEG_{20K}(C34)HSA were at least 60% more toxic than that of PEG_{5K}(C34)HSA ($p<0.05$), and 80% more toxic than that of n-HSA ($p < 0.01$; Figure 4.5). A linear interpolation of cytotoxicity data at 3.3 and 6.6 nM yields IC_{50} values of 6.5, 5.9, and 4.7 nM when PTX is formulated respectively with 10 mol% of n-HSA, PEG_{5K}(C34)HSA, and PEG_{20K}(C34)HSA, with the latter providing a nearly 40% increase in acute cytotoxicity relative to n-HSA. While the basis for the greater potency provided by PEG_{20K}(C34)HSA has not yet been elucidated, we observe an intriguing correlation with changes in the self-association behavior of HSA induced by Cys-34 tethered mPEG chains (see below).

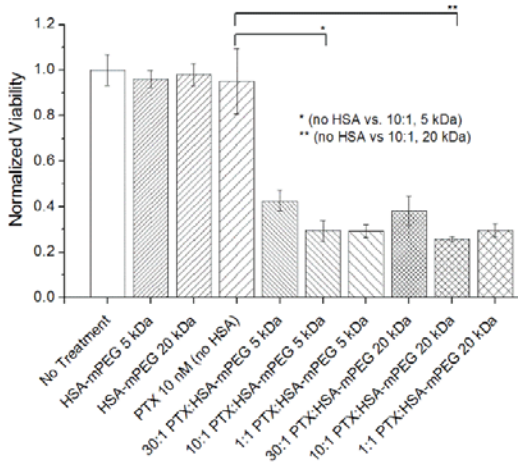

*Figure 4.4. The effects of PTX (10 nM) formulated with PEG_{5K}(C34)HSA or PEG_{20K}(C34)HSA on MCF-7 cell cultures, 5 days post-treatment, with [PTX] fixed at 10 nM (PTX:HSA = 30–0.1; N=3). Significant changes in cytotoxicity marked with * and ** ($p < 0.005$). Error = 1 stdev.*

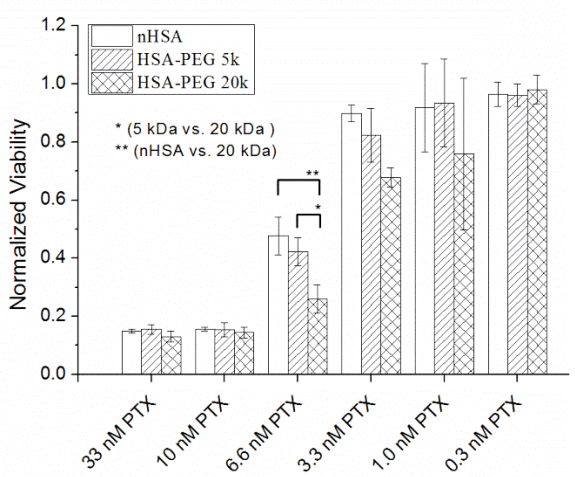

*Figure 4.5. Cytotoxicity of PTX (0.3–33 nM) formulated in a 10:1 mole ratio with n-HSA, PEG_{5K}(C34)HSA, or PEG_{20K}(C34)HSA (MCF-7 cells, 5 days post-treatment; N=3). Significant changes in cytotoxicity marked with * ($p < 0.05$) or ** ($p < 0.01$). Error = 1 stdev.*

Effects of PEGylation and PTX on Protein Nanoparticle Formation

Nanoparticle tracking analysis (NTA) was used to measure the hydrodynamic size (d_h) and concentration of submicron protein aggregates in PBS (pH 6.5). In nearly all cases, multimodal distributions were obtained with a wide variance (range of 100–400 nm); however, a comparison between datasets revealed clear differences in population sizes. At high protein concentration (1 mg/mL or 15.13 μM), mixtures containing PEG_{5K}- and PEG_{20K}(C34)HSA formed several times more nanoparticles than n-HSA (Figure 4.6a), while their d_h and volumetric mean values (d_{vol}) remained roughly the same (Table 4.1). At tenfold lower concentration (0.1 mg/mL or 1.35 μM), suspensions with PEGylated HSA again showed a higher number of nano-aggregates relative to pure n-HSA (Figure 4.6b). Although these concentrations are substantially higher than those used in the cytotoxicity assays, they show that *S*-PEGylation promotes HSA nanoparticle formation. It is worth noting that dynamic light scattering analysis of PEG_{20K}(C34)HSA at 0.01 mg/mL also indicates nanoparticle formation (d_h = 30–80 nm), whereas n-HSA at the same concentration is essentially monomeric.[36]

The effects of PEGylation on the spontaneous formation of HSA nanoparticles were also evident for excipients formulated with PTX at a 10:1 mole ratio. At low carrier concentration (0.1 mg/mL), mixtures with PEG_{5K}- and PEG_{20K}(C34)HSA formed aggregates with a narrower, bimodal distribution relative to n-HSA (Figure 4.6c).[46] It is worth noting that the number of n-HSA and PEG_{20K}(C34)HSA nanoparticles increased significantly in the presence of PTX, suggesting their formation to be driven partly by the cooperative association of hydrophobic domains. These results reveal the complex

interplay between protein concentration, PEG chain length, and the inclusion of PTX on the self-assembly of HSA nanoparticles in physiologically relevant conditions.

Table 4.1. Statistical analysis of HSA nanoparticles by NTA.

Sample	**particle count ($\times 10^6$ mL^{-1})**[a]	**hydrodynamic size (nm)**				
		mode peaks[b]	mean (d_h)	RSD (%)	d_{vol}[c]	RSD (%)
1 mg/mL (no PTX)						
n-HSA	258	100–160 (broad), 235	162	48	200	43
mPEG$_{5K}$(C34)HSA	745	100, 320	152	51	195	45
mPEG$_{20K}$(C34)HSA	671	140, 220	188	50	237	45
0.1 mg/mL (no PTX)						
n-HSA	92	120, 150, 225, 340	192	37	219	35
mPEG$_{5K}$(C34)HSA	221	125, 210, 290	166	48	206	43
mPEG$_{20K}$(C34)HSA	157	120, 180, 290	182	48	227	44
0.1 mg/mL (10:1 PTX:HSA)						
n-HSA	123	90, 140, 220	189	65	264	54
mPEG$_{5K}$(C34)HSA	161	90, 160	105	35	120	33
mPEG$_{20K}$(C34)HSA	225	105, 210	141	43	173	40
PTX, 13 μg/mL[d]	215	110, 160, 310	173	38	198	35

[a] Based on average number of tracks over three runs. [b] >100% above background. [c] Volumetric mean $d_{vol} = (\Sigma n_i d_i^3/N)^{1/3}$, where n_i is the number of particles with size d_i. [d] 15 μM PTX with 1% DMSO in PBS; no HSA present.

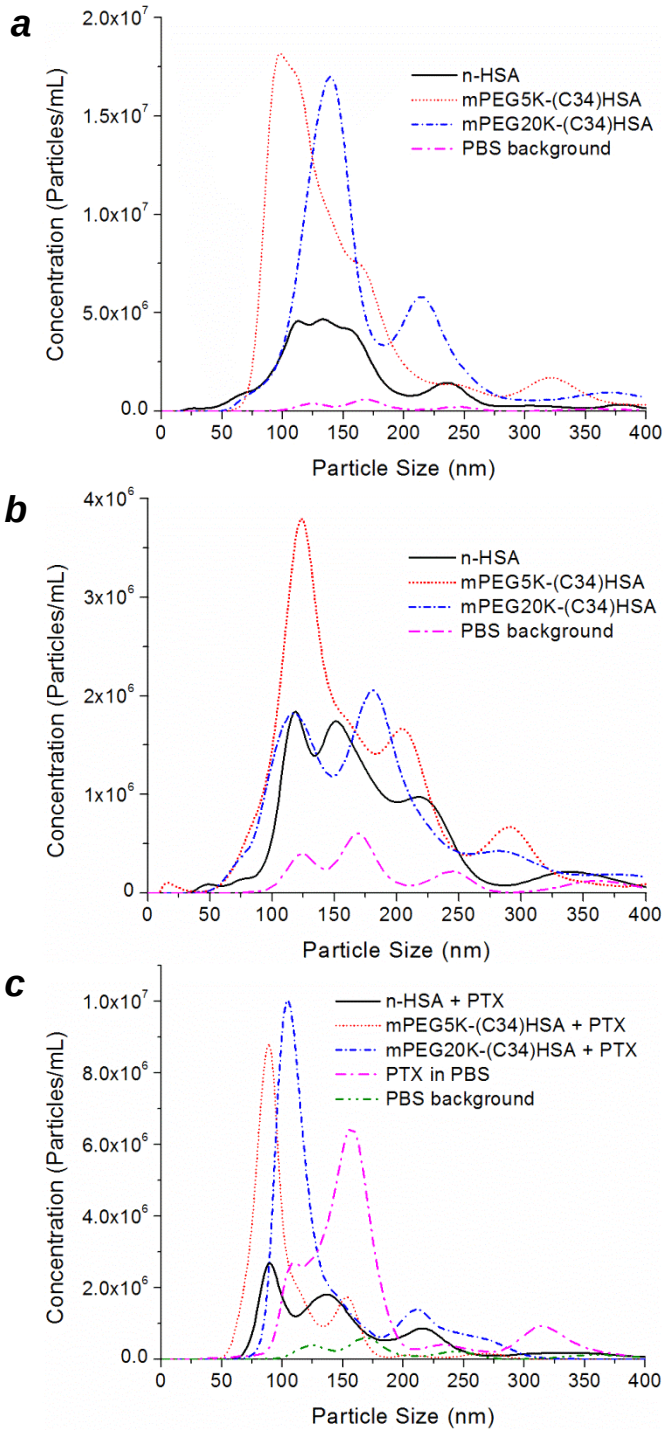

Figure 4.6. Hydrodynamic size analysis and number distribution of HSA nanoparticles by NTA, for mixtures comprised of n-HSA, PEG_{5K}(C34)HSA, and PEG_{20K}(C34)HSA in PBS. (a) 1 mg/mL (13–15 μM), (b) 0.1 mg/mL (1.3–1.5 μM), (c) 0.1 mg/mL with 10 equiv. PTX. A plot of PTX aggregates in PBS without HSA ([PTX] = 12.5 μM) is included for comparison.[44]

Effect of Formulations on PTX Permeability

Monolayers of HUVEC and hCMEC/D3 cells were initially tested to examine the effect of n-HSA and mPEG(C34)HSA on PTX permeability, using [^{14}C]-labeled drug. HUVEC monolayers are used to model the peripheral vasculature, whereas the hCMEC/D3 monolayers are representative of the blood-brain barrier.[47,48] Studies were run at 1 μM [^{14}C]-PTX alone and in 10:1 mole ratio with n-HSA or mPEG(C34)HSA, preceded by a 4-hour pre-equilibration period for the cell monolayers (Figure 4.7).[49] The HSA formulations did not produce significant differences in [^{14}C]-PTX permeation across either cell monolayer, which suggests that the binding and permeation of free PTX may be reversible. However, HUVEC monolayers exhibited significantly faster permeability rates, implying that PTX permeates more readily into the vascular periphery relative to the brain. This is expected, as hCMEC/D3 cells express high levels of efflux transporters such as P-glycoprotein that are active against PTX.[50]

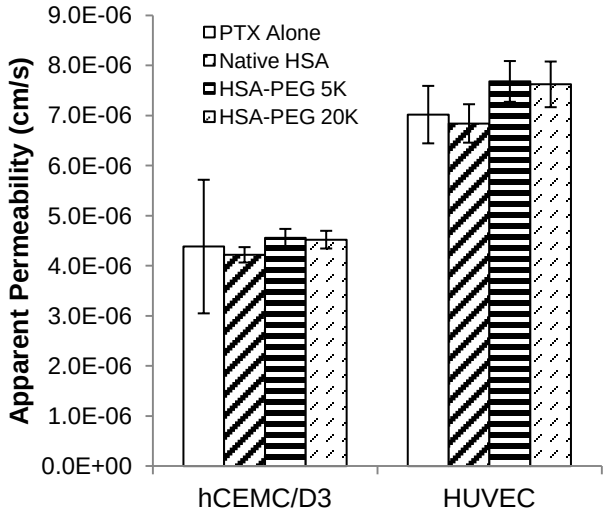

Figure 4.7. Permeability of 1 μM [^{14}C]-paclitaxel across hCMEC/D3 and HUVEC monolayers. Studies were run in triplicate simultaneously using a 10:1 mole ratio of PTX:n-HSA or PEG(C34)HSA (error = 1 stdev).

The effect of PTX concentration on HSA-mediated permeability was also investigated. P_{app} values across HUVEC monolayers were initially obtained at 0.5, 1, 10, and 25 μM PTX in a 10:1 mole ratio with n-HSA or PEG(C34)HSA, following pre-equilibration. Studies conducted at 0.5 and 1 μM PTX contained only [^{14}C]-labeled drug, whereas higher concentrations were made from unlabeled drug supplemented with 1 μM [^{14}C]PTX. At low solute concentrations, n-HSA appears to provide greater permeability then either PEG_{5K}(C34)HSA or PEG_{20K}(C34)HSA, but at higher concentrations no significant differences are observed (Figure 4.8a). The effect of drug-carrier ratio on permeability was also examined at a 5:1 ratio of PTX to n-HSA or PEG(C34)-HSA (Figure 4.8b). In this case, modest decreases in P_{app} values at higher solute concentrations

were observed for all three HSA formulations, with minor differences between carrier species.

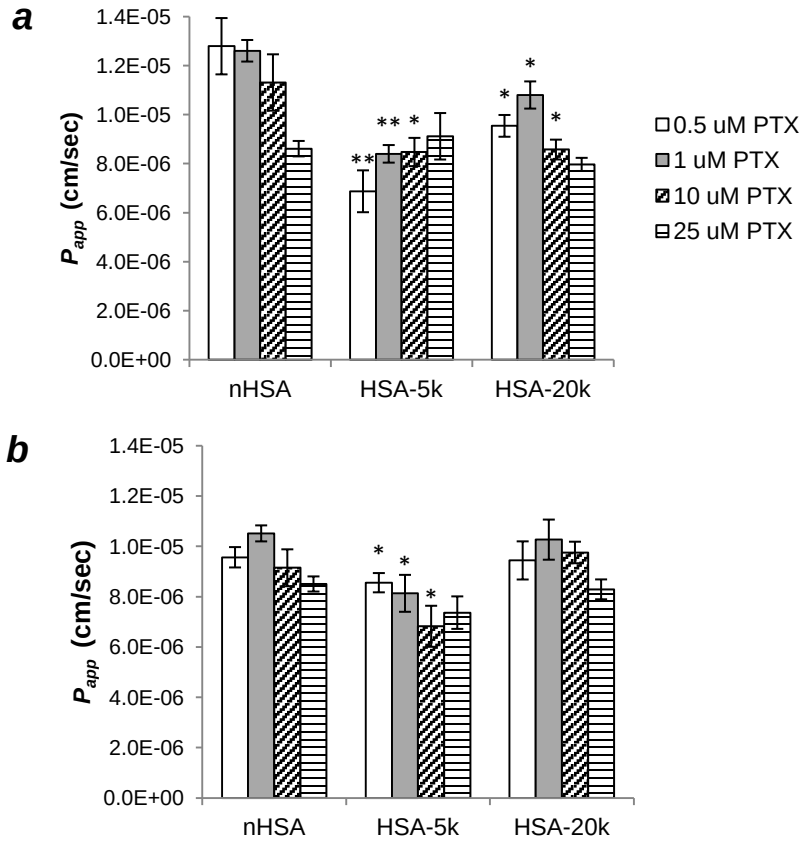

*Figure 4.8. Effect of solute concentration on HSA-mediated HUVEC permeability. (a) P_{app} of [^{14}C]-PTX using a 10:1 mole ratio of PTX to HSA carrier; (b) P_{app} of [^{14}C]-PTX using a 5:1 mole ratio of PTX to HSA carrier. Permeability studies were run in triplicate simultaneously; differences between carriers marked with * ($p < 0.05$) or ** ($p < 0.01$). Error = 1 stdev.*

While P_{app} is useful for delineating possible changes due to partitioning, diffusivity, or variations in free drug for each formulation, it only represents average marker velocities. It is perhaps more important to consider the effects of formulation on

drug flux ($P_{app} \times C_0$), which represents the actual amount of drug transferred across the endothelial barrier and is a reliable metric for estimating blood levels. Since flux is concentration-dependent, it better illustrates the effects of solubilizing formulations than the relatively small changes in P_{app}. As expected, large increases in flux are observed for both 10:1 and 5:1 mole ratios of PTX to n-HSA or its *S*-PEGylated conjugates (Figure 4.9). Again, *S*-PEGylation had little to no impact on drug transport, with minor differences attributable to the limited precision typically observed in permeation studies. This establishes that C34-PEGylated HSA can increase PTX efficacy as shown above, without compromising drug solubilization and permeability.

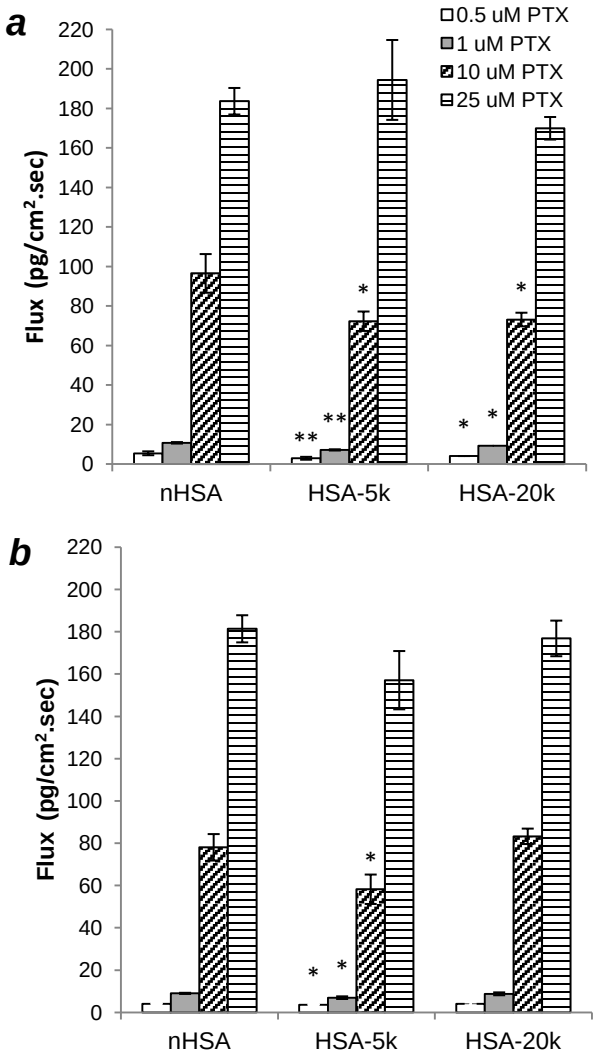

*Figure 4.9. [^{14}C]-PTX flux through HUVEC monolayers using n-HSA or PEG(C34)HSA. (a) 10:1 molar ratio of PTX to HSA carrier; (b) 5:1 molar ratio of PTX to HSA carrier. Permeability studies run in triplicate simultaneously; differences between carriers marked with * ($p < 0.05$) or ** ($p < 0.01$). Error = 1 stdev.*

The enhanced efficacy of PTX formulated with PEG_{5K}- and especially PEG_{20K}(C34)HSA is greatest near its IC_{50} value against MCF-7 breast cancer cells. We

also observe that *S*-PEGylation increases the number of HSA nanoparticles (up to 1.8-fold) relative to n-HSA, particularly in the presence of PTX. While further research is needed to establish the basis for therapeutic enhancement, we consider the following as plausible factors for the observed phenomena:

1. While the 5- and 20-kDa PEG chain attached to Cys-34 do not disrupt the tertiary structure of HSA, they may reduce its strength of association with bound PTX by increasing its conformational lability;
2. Changes in the conformational stability of *S*-PEGylated HSA may also affect the stability of their aggregates in endosomes, with greater PTX release to the cytoplasm after uptake;
3. The PEG chains may promote the nano-emulsification of HSA and PTX,[46] into forms that are favorably transported by albumin receptors.

In short, while the prescribed benefits of protein PEGylation such as extended stability and circulation times in the bloodstream are well appreciated,[12-15] there appear to be additional factors that may contribute toward favorable pharmacokinetics and drug release profiles, and await further validation.

4.4 Conclusions

We have established that formulation of PTX with PEG_{5K}(C34)HSA and especially PEG_{20K}(C34)HSA enhances its acute toxicity against MCF-7 breast cancer

cells relative to native HSA carriers, while retaining high levels of permeability across monolayers of HUVEC or hCMEC/D3 cells. The latter has important ramifications on the bioavailability of PTX administered by non-intravenous mechanisms, as well as its extravasation into diseased tissue. C34-PEGylation has a notable influence on the size distribution of HSA nanoparticles, which may be partly responsible for the increased cytotoxicity of the PTX payload.[51] Future studies are needed to generalize the therapeutic and pharmacokinetic enhancements of PEG(C34)HSA-mediated uptake for different classes of hydrophobic drugs, as well as various cancer cell lines and animal tumor models.

4.5 References

1. Kosaka N, Ogawa M, Choyke PL, Karassina N, Corona C, McDougall M, Lynch DT, Hoyt CC, Levenson RM, V Los, GV, et al 2009. In Vivo Stable Tumor-Specific Painting in Various Colors Using Dehalogenase Based Protein-Tag Fluorescent Ligands. Bioconjugate Chem 20:1367–1374.

2. Atkinson SF, Bettinger T, Seymour LW, Behr JP, and Ward CM 2001. Conjugation of Folate via Gelonin Carbohydrate Residues Retains Ribosomal-inactivating Properties of the Toxin and Permits Targeting to Folate Receptor Positive Cells. J. Biol. Chem. 276: 27930–27935.

3. Sinclair, A.M. and Elliot, S. Glycoengineering: The Effect of Glycosylation on the Properties of Therapeutic Proteins. J. Pharm Sci. 2005, 94, 1626-1635.

4. Molino, N.M., Bilotkach, K., Fraser, D.A., Ren, D., and Wang, S.W. Complement Activation and Cell Uptake Responses Toward Polymer-Functionalized Protein Nanocapsules. Biomacromolecules. 2012, 13, 974−981.

5. Monfardini, C. and Veronese, M. F. Stabilization of substances in circulation. Bioconjugate Chem. 1998, 9, 418–450.

6. López-Alonso, J. P., Diez-García, F., Font, J., Ribó, M., Vilanova, M., Scholtz, J.M., González, C., Vottariello, F., Gotte, G., Libonati, M., et al. Carbodiimide EDC Induces Cross-Links That Stabilize RNase A C-Dimer against Dissociation: EDC Adducts Can Affect Protein Net Charge, Conformation, and Activity. Bioconjugate Chem. 2009, 20, 1459–1473.

7. Chalker, J. M., Bernardes, G. J. L., Lin, Y. A., and Davis, B. G. Chemical Modification of Proteins at Cysteine: Opportunities in Chemistry and Biology. Chem. Asian J. 2009, 4, 630-640.

8. Broersen, K., Weijers, M., de Groot, J., Hamer, R.J., and de Jongh, H.H.J. Effect of Protein Charge on the Generation of Aggregation-Prone Conformers. Biomacromolecules. 2007, 8, 1648-1656.

9. Gao, J.P., Yong, Z.H., Zhang, F., Ruan, K.C., Xu, C.H., and Chen, G.Y. Positive Charges on Lysine Residues of the Extrinsic 18 kDa Protein Are Important to Its Electrostatic Interaction with Spinach Photosystem II Membranes. Acta Biochim. Biophys. Sinica 2005, 37, 737–742.

10. Harris, J. M. and Chess, R. B. Effect of pegylation on pharmaceuticals. Nat. Rev. Drug Discov. 2003, 2, 214-221.

11. Ryan, S. M., Mantovani, G., Wang, X., Haddleton, D. M., and Brayden, D. J. Advances in PEGylation of important biotech molecules: Delivery aspects. Expert Opin. Drug Deliv. 2008, 5, 371-383.

12. Duncan, R. and Gaspar, R. Nanomedicine(s) under the Microscope. Mol. Pharm. 2011, 8, 2101-2141.

13. Nischan, N. and Hackenberger, C. P. R. Site-specific PEGylation of Proteins--Recent Developments. J. Org. Chem. 2014, 79, 10727–10733.

14. Meng, W., Guo, X., Qin, M., Pan, H., Cao, Y., and Wang, W. Mechanistic Insights into the Stabilization of srcSH3 by PEGylation. Langmuir 2012, 28, 16133−16140.

15. Rodríguez-Martínez, J. A., Solá, R. J., Castillo, B., Cintrón-Colón, H. R., Rivera-Rivera, I., Barletta, G., and Griebenow, K. Stabilization of a-Chymotrypsin Upon PEGylation Correlates With Reduced Structural Dynamics. Biotechnol. Bioeng. 2008, 101, 1142-1149.

16. Ghuman, J., Zunszain, P. A., Petitpas, I., Bhattacharya, A. A., Otagiri, M., and Curry, S. Structural basis of the drug-binding specificity of human serum albumin. J. Mol. Biol. 2005, 353, 38–52.

17. Paál, K., Müller, J., and Hegedûs L. High affinity binding of paclitaxel to human serum albumin. Eur. J. Biochem. 2001, 8, 2187-2191.

18. John, T. A., Vogel, S. M., Tiruppathi, C., Malik, A. B., and Minshall, R. D. Quantitative analysis of albumin uptake and transport in the rat microvessel endothelial monolayer. Am. J. Physiol. Lung Cell. Mol. Physiol. 2003, 284, 187-196.

19. Schubert, W., Frank, P. G., Razani, B., Park, D. S., Chow, C. W., and Lisanti, M. P. Caveolae-deficient endothelial cells show defects in the uptake and transport of albumin in vivo. J. Biol. Chem. 2001, 276, 48619-48622.

20. Peters, T. All about Albumin: Biochemistry, Genetics, and Medical Applications. Academic Press, 1996, San Diego, CA.

21. Kratz, F. Albumin as a drug carrier: design of prodrugs, drug conjugates and nanoparticles. J. Control. Release 2008, 132, 171-183.

22. Elsadek, B. and Kratz, F. Impact of albumin on drug delivery — New applications on the horizon. J. Control. Release 2012, 157, 4–28.

23. Desai, N. Nab Technology: A Drug Delivery Platform Utilizing Endothelial gp60 Receptor-based Transport and Tumour-derived SPARC for Targeting. In Drug Delivery Report Winter 2007/2008 (16th ed.), pp. 37–41.

24. Desai, N. V., Trieu, Z., Yao, Z., Louie, L., Ci, S., Yang, A., Tao, C., De, T., Beals, B., Dykes, D., et al. Increased antitumor activity, intratumor paclitaxel concentrations, and endothelial cell transport of cremophor-free, albumin-bound paclitaxel, ABI-007, compared with cremophor-based paclitaxel. Clin. Cancer Res. 2006, 12, 1317–1324.

25. Green, M. R., Manikhas, G. M., Orlov, S., Afanasyev, B., Makhson, A. M., Bhar, P., and Hawkins, M. J. Abraxane®, a novel Cremophor®-free, albumin-bound particle form of paclitaxel for the treatment of advanced non-small-cell lung cancer. Ann. Oncol. 2006, 17, 1263-1268.

26. Von Hoff, D. D., Ervin, T., Arena, F. P., Chiorean, E. G., Infante, J., Moore, M., Seay, T., Tjulandin, S. A., Ma, W. W., Saleh, M. N., et al. Increased Survival in Pancreatic Cancer with nab-Paclitaxel plus Gemcitabine. New Engl. J. Med. 2013, 369, 1691-1703.

27. Kavallaris, M. Microtubules and resistance to tubulin-binding agents. Nat. Rev. Cancer 2010, 10, 194-204.

28. Gelderblom, H., Verweij, J., Nooter, K., and Sparreboom, A. Cremophor EL: The drawbacks and advantages of vehicle selection for drug formulation. Eur. J. Cancer 2001, 37, 1590-1598.

29. Anil, K. S., Alka, G., and Aggarwa49. Higher PTX concentrations were necessary, due to the limited efficiency of PTX radiolabeling and sensitivity of the scintillation detector. PTX concentrations in the basolateral compartment are estimated to be 0.1–10 nM, depending on the time point.

30. Marupudi, N. I, Han, J. E., Li, K. W., Renard, V.M., Tyler, B. M., and Brem, H. Paclitaxel: A review of adverse toxicities and novel delivery strategies. *Expert. Opin. Drug Saf.* **2007**, *5*, 609-621.

31. Aigner, J., Marme, F., Smetanay, K., Schuetz, F., Jaeger, D., and Schneeweiss, A. Nab-Paclitaxel Monotherapy as a Treatment of Patients with Metastatic Breast Cancer in Routine Clinical Practice. *Anticancer Res.* **2013**, *33*, 3407-3413.

32. Ko, Y. J., Canil, C. M., Mukherjee, S. D., Winquist, E., Elser, C., Eisen, A., Reaume, M. N., Zhang, L. Y., and Sridhar, S. S. Nanoparticle albumin-bound paclitaxel for second-line treatment of metastatic urothelial carcinoma: A single group, multicentre, phase 2 study. *Lancet Oncol.* **2013**, *14*, 769-776.

33. Dosio, F., Arpicco, S., and Brusa, P. Poly(ethylene glycol) human serum albumin–paclitaxel conjugates: preparation, characterization and pharmacokinetics. *J. Control. Release* **2001,** *76*, 107–117.

34. Meng, F., Manjula, B. N., Smith, P. K., and Acharya, S. A. PEGylation of Human Serum Albumin: Reaction of PEG-Phenyl-Isothiocyanate with Protein. *Bioconjugate Chem.* **2008,** *19*, 1352–1360.

35. Plesner, B., Fee, C. J., Westh, P., and Nielsen, A. D. Effects of PEG size on structure, function and stability of PEGylated BSA. *Eur. J. Pharm. Biopharm*. **2011,** *7*, 399–405.

36. Zhao, T., Cheng,Y. N., Tan, H. N., Liu, J. F., Xu, H. L., Pang, G. L., and Wang, F. S. Site-Specific Chemical Modification of Human Serum Albumin with Polyethylene Glycol Prolongs Half-life and Improves Intravascular Retention in Mice. *Biol. Pharm. Bull.* **2012,** *35*, 280-288.

37. Schumacher, F. F., Nobles, M., Ryan, C.P., Smith, M. E. B., Tinker, A., Caddick, S., and Baker J. R. In Situ Maleimide Bridging of Disulfides and a New Approach to Protein PEGylation. *Bioconjugate Chem.* **2011**, *22*, 132–136.

38. Smith, M. E. B., Schumacher, F. F., Ryan, C. P., Tedaldi, L. M., Papaioannou, D., Waksman, G., Caddick, S., and Baker, J. R. Protein Modification, Bioconjugation, and Disulfide Bridging Using Bromomaleimides. *J. Am. Chem. Soc.* **2010**, *132*, 1960–1965.

39. Later versions of this software have been tested, and found to produce very similar results.

40. Mehtala, J. G., Torregrosa-Allen, S., Elzey, B. D., Jeon, M., Kim, C., and Wei, A. Synergistic Effects of Cisplatin Chemotherapy and Gold Nanorod-Mediated Hyperthermia on Ovarian Cancer Cells. *Nanomedicine* **2014**, *9*, 1939-1955.

41. Katchalski, E., Benjamin, G. S., and Gross, V. The Availability of the Disulfide Bonds of Human and Bovine Serum Albumin and of Bovine γ-Globulin to Reduction by Thioglycolic Acid. *J. Am. Chem. Soc.* **1957,** *79*, 4096-4099. (b) Yang, M., Dutta, C., and Tiwari, A. Disulfide-Bond Scrambling Promotes Amorphous Aggregates in Lysozyme and Bovine Serum Albumin. *J. Phys. Chem. B* **2015,** *119*, 3969-3981.

42. Kobayashi, K., Nakamura, N., Sumi, A., Ohmura, T., and Yokoyama, K. The development of recombinant human serum albumin. *Ther. Apher.* 1998, *2*, 257-262.

43. MALDI-MS peaks at *m/z* 33,372 and 22,326 could also be observed, corresponding to doubly and triply protonated species respectively.

44. Kim, Y., Ho, S. O., Gassman, N. R., Korlann, Y., Landorf, E. V., Collart, F. R., and Weiss, S. Efficient Site-Specific Labeling of Proteins via Cysteines. *Bioconjugate Chem.* **2008,** *19*, 786-791.

45. It is worth noting that the cytotoxicity of PTX in the absence of HSA may be influenced by the amount of residual DMSO. In this study, PTX solutions were prepared by serial dilution with PBS and/or HSA in PBS from a 585 μM stock solution in DMSO (see Figure S1, Supporting Information).

46. PTX at the same concentration in PBS without HSA also formed large (>200 nm) aggregates over the same period of time.

47. Weksler, B., Romero, I. A., and Couraud, P. O. The hCMEC/D3 cell line as a model of the human blood brain barrier. *Fluids Barriers CNS* **2013**, *10*, 16 (10 pages).

48. Otani, M., Natsume, T., Watanabe, J. I., Kobayashi, M., Murakoshi, M., Mikami, T., and Nakayama, T. TZT-1027, an antimicrotubule agent, attacks tumor vasculature and induces tumor cell death. *Jpn. J. Cancer Res.* **2000**, *91*, 837-844.

49. Higher PTX concentrations were necessary, due to the limited efficiency of PTX radiolabeling and sensitivity of the scintillation detector. PTX concentrations in the basolateral compartment are estimated to be 0.1-10 nM, depending on the time point.

50. Jang, S. H., Wientjes, M. G., and Au, J.L. Kinetics of P-Glycoprotein-mediated efflux of paclitaxel. *J. Pharmacol. Exp. Ther*. **2001**, *298*, 1236-1242.

51. Surapaneni, M. S., Das, S. K., and Das, N. G. Designing Paclitaxel Drug Delivery Systems Aimed at Improved Patient Outcomes: Current Status and Challenges. *ISRN Pharmacol.* **2012**, *2012*, 623139 (15 pages).

CHAPTER 5. CHARACTERIZATION, FORMULATION, & PRECLINICAL ASSESSMENT OF AN ANTIVIRAL V-ATPASE INHIBITOR, SALIPHENYLHALAMIDE

5.1. Introduction

The 2014 Ebola outbreaks in West Africa have reinforced the concerns over high mortality and morbidity associated with pathogenic epidemics, particularly with yet unmet therapeutic viral entities.[1] This outbreak was just the most recent in a number of outbreaks worldwide caused by a number of different infectious pathogens. These outbreaks also lead to significant concerns about the potential of infectious pathogens to be weaponized and to be utilized in warfare.[2] Thus, there has been an urgent need placed on the search for therapeutic agents that may serve as countermeasures to mitigate pathogenic agents exploited for terror or warfare applications. In addition to Ebola, a number of other viral pathogens have been identified as high risk agents for weaponization and potential use in malicious manners including the encephalitic alphaviruses including the Venezuelan (VEEV), Eastern Equine (EEEV) and Western Equine (WEEV) encephalitic viruses.[2] Universal to many of these high morbidity and mortality associated viruses is that their disease inducing pathogenesis relies on the host

cell entry and intracellular trafficking via endocytosis and subsequent activation within the endolysosomal compartments.[3,4]

The combined research efforts of the investigative team have been focused on the development of an agent known to inhibit a critical protein, Vacuolar-ATPase (V-ATPase) that acidifies the endolysosomal vesicles and activates the virus. Briefly, the V-ATPase is a proton transporter which utilizes ATP to move protons against a concentration gradient into vesicles within the cell, resulting in reduction of pH within the vesicle.[3] This low pH leads to a cascade of enzymatic activity and formation of the lysosome. However, for many viruses, this low pH is necessary to trigger membrane fusion, unloading of viral RNA, and replication after endocytosis.[4] We have investigated the development of saliphenylhalamide (SaliPhe), a potent analog of salicylihalamide that is a natural product known to act as a V-ATPase inhibitor.[5,6] Therefore, salipenylhalamide may be effective at stopping replication of many viruses that utilize this mechanism to trigger unfolding. It should also be noted that V-ATPase inhibition is currently also being investigated for treatment of osteoporosis and cancer.[5-7]

While there has been some investigation into *in vitro* and *in vivo* efficacy of SaliPhe, less research has been conducted into its physicochemical properties, pharmacokinetics, and overall druggability. With a molecular weight of 459.5, SaliPhe is under the 500 MW cutoff often associated with steep drop-offs in uptake and permeation rates that increase intracellular accumulation and drug distribution.[8] In addition, it's predicted polar surface area is only 96 $Å^2$¸which is well below the cutoff of 140 $Å^2$ for

peripheral permeation and just over the cutoff for uptake into the brain 90 Å^{2}.[9] SaliPhe has an AlogP of 4.5, which, while at the high end, is within the druggable range for pharmaceutical compounds. Favorably, this high AlogP may also lead to increased distribution into the brain.[10] Current limitations with SaliPhe are predicted to be solubility related. *In vivo* efficacy studies suggest 7 mg/kg to be the efficacious intraperitoneal dose.[11] With a predicted solubility of 0.2 μg/mL at physiological pH, the drug is unlikely to reach efficacious levels without an exposure enhancing formulation.

Here we look to elucidate the relevant physicochemical properties of SaliPhe and to utilize these properties to guide formulation development. Formulations with enabling properties were screened on *in vitro* cell models to assess changes in permeability and cytotoxicity. Finally, testing was conducted on promising formulations for pharmacokinetics, biodistribution, toxicity, and efficacy in murine models. In addition, we proposed to characterize the physicochemical properties of structurally related SaliPhe analogs that were being developed to overcome several SaliPhe limitations for therapeutic utilization. SaliPhe has been previously investigated for other chronic indications, although the drug was not advanced to the market due to druggability and toxicity concerns.[11] These analogs may allow for safe and efficacious acute use of the drug, minimizing the challenges associated with chronic SaliPhe therapy.

The tasks that were conducted at Purdue included:

1. SaliPhe ADME/T Assays
2. Performance of Physicochemical and Preformulation Studies and
3. Plasma PK for 3-5 formulation/prodrugs in rats and biodistribution in mice for 2 formulations/prodrugs. *Note: Biodistribution studies were conducted in conjunction with the University of Louisville to ensure that the same mice that the efficacy studies were performed in were used to measure distribution.*

Initially we began early analysis to perform physicochemical analysis then made stable, solubility enabling formulations followed by investigation of the permeability of SaliPhe, and associated analogs, alone and in formulations across *in vitro* barriers of relevant cell models. This included human epithelial colorectal adenocarcinoma cells (Caco-2),[12-14] human umbilical vein endothelial cells (HUVEC),[15] hCMEC/D3 (human cerebral microvascular endothelial cell),[16-19] and novel direct coculture and triculture *in vitro* models of the blood brain barrier (BBB) recently developed in the Knipp laboratory.

In latter studies, two formulations of SaliPhe and one of a SaliPhe prodrug were submitted for rat PK analysis. In addition, one biodistribution study was performed at Louisville and the organs were collected and submitted for bioanalysis at the Purdue Metabolite Profiling Facility. The methodology, results and a discussion of findings is presented below.

5.2. Materials and Methods

Materials

Poloxamer 407, Poloxamer 188, Kolliphor EL, Kolliphor RH 40, Kolliphor HS 15, Kollidon 25, Kollisolv PEG E 400, propylene glycol, hydroxpropyl-β-cyclodextrin, tween 80, d-alpha tocopheryl polyethylene glycol 1000 succinate, acetonitrile, Hank's balanced salt solution (HBSS), phosphate buffered saline (PBS), Dulbecco's Modified Eagle's Medium (DMEM), fetal bovine serum, penicillin-streptomycin, non-essential amino acids, L-glutamine, hydrocortisone, type I rat tail collagen, polystyrene T-75 flasks, and Transwell® permeable supports were purchased from Sigma-Aldrich (St. Louis, MO). EGM-2, EBM-2, and basic fibroblast growth factor were obtained from Lonza (Walkersville, MD). Chemically defined lipid concentrate was purchased from LifeTechnologies (Carlsbad, CA). Human astrocytes, human pericytes, astrocyte medium, and pericytes medium was purchased from ScienCell (Carlsbad, CA). Caco-2 and HUVEC cells were obtained from the American Type Culture Collection (ATCC; Manassas, VA); hCMEC/D3 cells were provided by Dr. Pierre-Olivier Couraud at Institut Cochin (Paris, France). Labrasol and Labrafil M 1944 CS were donated by Gattefosse, (Saint-Priest, France).

Methods

HPLC Analysis

HPLC-Samples were run on an Agilent 1100 HPLC. A 1.5 mL/min 50:50 Acetonitrile:Water isocratic method was used for 10 minutes with a retention time of 6.9 minutes. An Agilent Eclipse XDB-C18, 5 μm, 4.6 x 150mm column with Security Guard-C18, 4 x3.0mm guard column was kept at 40^{o}C. UV detection was at 280 nm. Injections of SaliPhe alone were 100 μL/sample, formulated samples were 5 μL/sample.

Powder X-ray Diffraction

To assess crystallinity of the SaliPhe received, approximately 30mg was used for testing with Powder X-ray Diffraction (PXRD) on a Rigaku SmartLab XRD system. Sample was added onto a sample holder and gently crushed and flattened. Intensity was then measured from 5 to 40 degrees (2θ). Step size was 0.02 degrees at a speed of 40 θ/minute. Voltage and current used were 40mV and 44mA respectively.

Differential Scanning Calorimetry

Thermal analysis was conducted on a TA Instruments Q1000 to confirm PXRD results and establish a melting point. 2.5 mg of sample was first hermetically sealed into an aluminum pan. Changes in heat flow were measured from 25-350^{o}C at a rate of 10^{o}C/minute. N_2 was used as a purging gas and indium was used for calibration.

Octanol:Water Partition Coefficient

Approximation of LogD was conducted in 0.1N HCl, (~pH 1), 10μM Acetate Buffer pH 4.5, and pH 7.4 PBS. Prior to studies, 50mL of each aqueous solution was equilibrated with 50mL 1-octanol for 24 hours. Approximately 1mg SaliPhe was then added to 500μL of each of the pre-equilibrated 1-octanol solutions. After dissolution of the SaliPhe, 500uL of pre-equilibrated aqueous buffer was added and vortexed for 2 minutes. Samples were allowed to equilibrate overnight before samples from each phase were run according the HPLC method above with 1-octanol samples diluted 50 times in DMSO. LogD was calculated by taking:

$$\text{LogD} = \log\left(\frac{[SaliPhe_{1-octanol}]}{[SaliPhe_{Aqueous\ Buffer}]}\right)$$

Polymer Formulation Solubility Assessment

To estimate solubility in a number of polymer solutions, 10% solutions were first made up by heating reagents to 50^{o}C on a hotplate and incorporation by vortexing for up to 15 minutes. SaliPhe in 100% DMSO was then spiked into each of the polymer solutions and vortexed for 5 minutes. Following vortexing, samples were allowed to equilibrate for 90 minutes followed by a 15 minute centrifuge at 13,000 RPM. The supernatant was then removed and evaluated on the HPLC as described above.

Polymer Formulation Stability

Stability of formulations which lead to satisfactory increases in solubility were further characterized based on stability. Samples were stored at 0, 25, and 37^{o}C for one week in silanized inserts. Samples were taken multiple times on the first day followed by once each additional day Stability was estimated based on changes in AUC after triplicate injection according to the HPLC method above. Before each sample was run, silanized inserts were centrifuged at 13,000 RPM for 15 minutes and supernatant was removed. Additional stability studies were conducted for SaliPhe alone in 0.1N HCl, pH 4.5 10mM acetate buffer, and PBS.

Emulsion Formulation

An emulsion formulation was made as an alternative dosing strategy for SaliPhe. Emulsion formulations were kept simple with a single aqueous phase (PBS), oil phase (Labrafil or Capryol), and surfactant (Solutol HS 15, Cremophor EL, Lecithin, Transcutol, Labrasol, Propylene Glycol). Emulsions were made by first dissolving SaliPhe into the oil phase. The surfactant(s) were then added and vortexed for 1 minute. PBS was then added to the oil/surfactant and again vortexed for 1 minute. Vortexing was followed by microtip sonication for 1 minute. The sample was then vortexed until homogeneous. Formulations were then assessed based on translucence which was used to determine the ability of the formulation to both solubilize SaliPhe and form an emulsion. Next, the formulations were left for 5 days at room temperature to assess the

physical stability. Additional physical stability was conducted through an overnight freeze and thaw. Finally, viscosity was assessed at room temperature. It was determined through consolation with animal care that solutions more viscous than propylene glycol may be lethal to the rodents in pre-clinical studies, therefore, only those that were significantly less viscous by eye were used for further testing according to the Purdue Animal Care and Use Committee (PACUC) and the approved ACURO form that was submitted.

Cell Culture

Caco-2 cells were cultured in DMEM supplemented with 10% FBS, penicillin-streptomycin, L-glutamine, and non-essential amino acids. While culture flasks were not prepped, Transwells were coated with 65µL/well of 1mg/mL type I rat tail collagen in 60% ethanol and left to evaporate for at least 4 hours. Caco-2 cells were seeded at 75,000 cells/cm^2 and grown for 21-28 days before permeability studies were conducted.

Human Umbilical Vascular Endothelial cells (HUVEC), mimicking the peripheral vasculature for organ distribution, were cultured in EBM-2 supplemented with EGM-2 bulletkits. HUVEC flasks were precoated with 1 µg/cm^2 fibronectin. Transwells were coated with 65µL/well of 1mg/mL type I rat tail collagen in 60% ethanol and left to evaporate for at least 4 hours. HUVEC cells were seeded at 50,000 cells/cm^2 and left to proliferate/differentiate for 7 days prior to studies.

hCMEC/D3 cells were cultured in EBM-2 supplemented with 5% FBS, basic fibroblast growth factor, chemically defined lipid concentrate, HEPES buffer, ascorbic acid, penicillin streptomycin, and hydrocortisone. hCMEC/D3 flasks were precoated with 6 mL of 150μg/mL of type I rat tail collagen in water. Transwells were coated with 65μL/well of 1mg/mL type I rat tail collagen in 60% ethanol and left to evaporate for at least 4 hours. hCMEC/D3 cells were seeded at 100,000 cells/cm^2 and grown for 7 days before studies.

Human astrocytes were grown in ScienCell's complete astrocyte medium. Flasks were coated as recommended with 2 μg/cm^2 Poly-L-Lysine. Transwells were coated with 5 μg/cm^2 to promote proliferation and differentiation. Astrocytes were seeded at 40,000 cells/cm^2 and grown 2 days before culture with additional cell lines. Human Pericytes were grown in a similar fashion with the exception of utilization of ScienCell's complete pericyte medium.

For hCMEC/D3 and human astrocyte coculture studies, human astrocytes were first plated as discussed above. After two days in astrocyte medium, hCMEC/D3s were seeded directly on top of the astrocytes and grown for 7 days in hCMEC/D3 supplemented EBM-2 before studies. For triculture studies, 40,000 human astrocytes/cm^2 were seeded in astrocyte media onto Transwells® (Corning-Costar) pre-treated with 5μg/cm^2 Poly-L-Lysine and grown for 2 days. An additional 1 μg/cm^2 Poly-L-Lysine was then added to the top of the astrocytes followed by pericytes at a density of 40,000 cells/cm^2. After two additional days of growth, 15 μg/cm^2 type I rat tail collagen was added followed by 80,000 hCMEC/D3 cells/cm^2. The triculture was grown for 7

more days with hCMEC/D3 supplemented EBM-2 in the apical compartment and astrocyte medium in the basolateral compartment before permeability studies were conducted. It should be noted that the culture conditions were optimized under separate studies in our laboratory and have been disclosed via a provisional patent application.

All cells were grown in 5% CO_2, 37^{o}C, and 95% RH. Passages were conducted between 80 and 90% confluence. Cells were limited to passage 50 for Caco-2s, passage 12 for HUVECs, passage 45 for hCMEC/D3s, passage 15 for human astrocytes, and passage 12 for human pericytes.

Permeability Studies

All permeability studies were conducted statically in triplicate on 0.4μm polyethylene 12-well Transwell supports. Prior to studies, media was removed and cells were washed twice with PBS. Cells were subsequently equilibrated in HBSS for at least 20 minutes. SaliPhe solutions were then added to the donor compartment. Receiver compartments contained vehicle used in donor. Samples were taken at 30, 60, 120, and 180 minutes as well as donor C_0 and $C_{180\ minutes}$ samples. 200μL samples were taken from basolateral compartment while only 100 μL samples were taken from the apical compartment. Sample volume was replaced with blank vehicle after each time point, and the lost mass was accounted for in the permeability calculation. Samples were run on HPLC according to method above with 100 μL injections for receiver compartment

samples, 50 µL for donor compartment samples, 100 µL injections for SaliPhe alone C_0, and 5 µL for solubility enabled formulation C_0. Permeability coefficients (cm/s) were obtained through the following equation:

$$P_{apparent} = \frac{\frac{dM}{dt}}{C_0 * SA * 60}$$

where $\frac{dM}{dt}$ is the rate of SaliPhe or prodrug transfer across the cell layer, C_0 is the initial donor concentration, and SA is the surface area of the Transwell® filter support and 60 converts units in cm/min to cm/s.

In Vivo Rat PK Studies

Pre-clinical rat PK studies were conducted according to the Purdue Animal Care and Use Committee (PACUC) and the approved ACURO submitted protocols with two SaliPhe formulations (3.5mg/mL SaliPhe in 2% P407 and in the F22 emulsion) as well as OM510 in 2% P407. Studies were conducted on rats of approximately 250g and utilized the BASi Culex-S "Rat-Turn" model. Samples were analyzed by LC-MS/MS utilizing optimized protocols through the Purdue Metabolite Profiling facility, as we have utilized previously.[20-22]

Noncompartmental pharmacokinetic data analysis was performed using PK Solutions 2.0 from Summit Research Services (Montrose, CO). SaliPhe or OM510 plasma concentration time data were input into the software and the resultant profiles were curve stripped to extract the PK parameters. SaliPhe or OM510 plasma

concentrations below the limit of quantitation were set to zero for determination of PK parameters.

5.3. Results and Discussion

Powder X-Ray Diffraction (PXRD)

PXRD was run on the samples to assess crystallinity of the SaliPhe batch samples obtained. The sample appeared to be mostly amorphous as evidenced by a large amorphous halo. However, small amounts of crystallinity may be indicated by small peaks in intensity, specifically around 18 degrees. Due to concerns for material usage, replicates were not performed and confirmation of crystalinity was attempted by DSC.

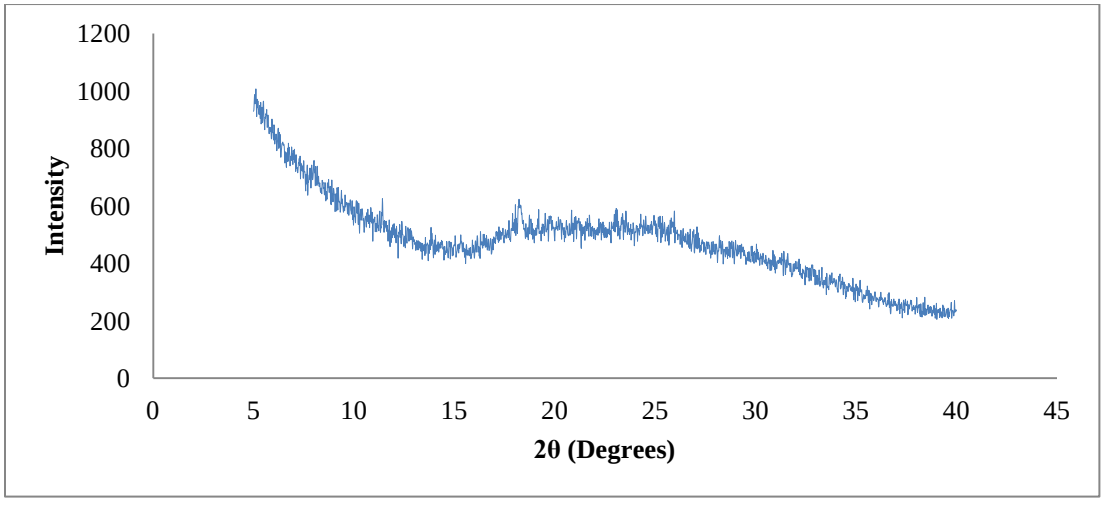

Figure 5.1. Powder x-ray diffraction of Saliphenylhalamide.

Differential Scanning Calorimetry (DSC)

The DSC shows a small endotherm at 110°C suggesting some crystallinity may be present and is melting, which could confirm the PXRD measurement. However, it is also possible that desolvation of a residual solvent may be occurring. This is followed by degradation at approximately 220°C. Additional melts between 160°C and 210°C are speculated to be either small amounts of impurities or traces of potential enantiotropicly more stable polymorphs are formed and then melting. Hot stage microscopy, thermogravimetric analysis, and potential variable temperature PXRD are recommended for future batch characterizations to decipher the nature of these transitions.

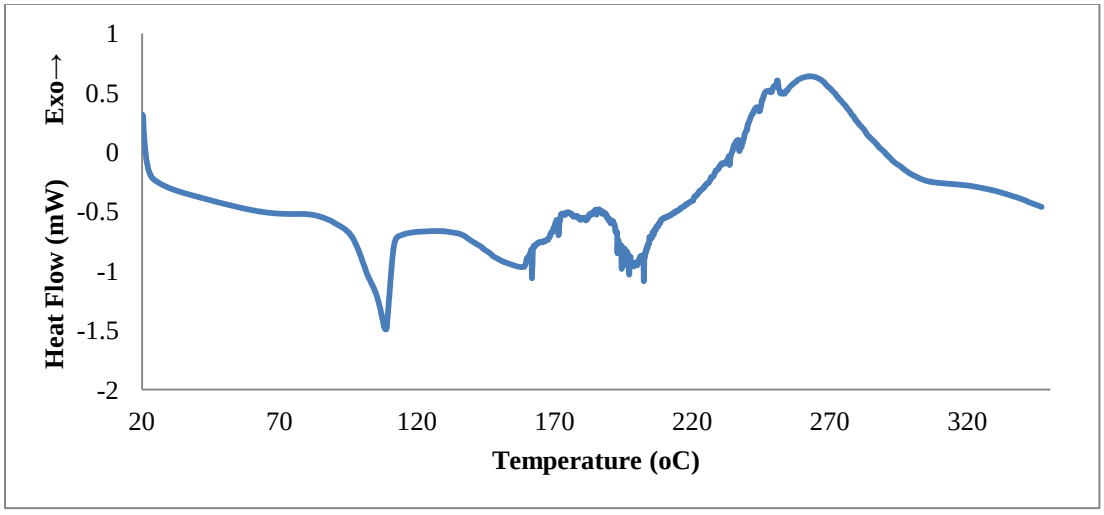

Figure 5.2. Differential scanning calorimetry of Saliphenylhalamide.

LogD

Log D values were relatively unchanged across the various aqueous conditions with a pH range spanning between ~1 and 7.4, when assessed in 0.1N HCl, pH 4.5 acetate buffer, and pH 7.4 PBS. In addition, values between 4.64 and 4.76 suggest a highly lipophillic compound at physiological pHs found in the blood and along the gastrointestinal (GI) tract. However, while high, it is in the druggable range suggested by Lipinski's "Rule of 5". Conversely, these Log D's lie outside the druggable range suggested by GSK's 4/400 rule and Pfizer's 3/75 rule which may indicate poor druggability and an increased toxicological risk respectively.[23] One benefit of the high LogD is the potential for increased uptake into the brain which may be necessary for targeting encephalitic viruses like VEEV.[9]

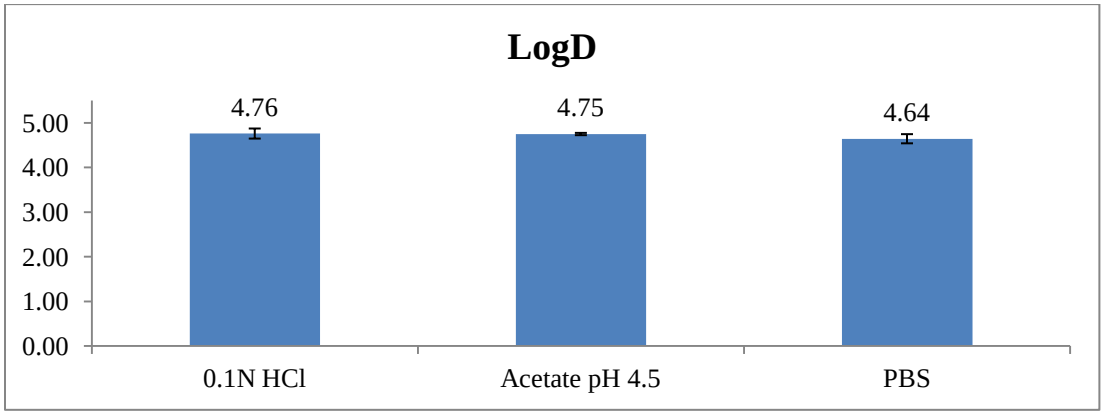

Figure 5.3. LogD values of Saliphenylhalamide. Samples performed in triplicate, error bars represent 1 standard deviation.

Polymer-Based Solubility Enhancement

As suggested above, the solubility of SaliPhe may be rate limiting in its druggability.[15,23,24] In order to potentially improve solubility through polymer complexation, a number of excipients were examined. It was determined that for exposure enabled pre-clinical formulations, a formulation solubility of at least 875 μg/mL would be necessary. Initial studies investigated solubilizing ability of 10% polymer.

Table 5.1. Solubility of Saliphenyhalamide in 10% polymer or excipient solutions.

Polymer	**Solubility in 10% w/w Polymer:HBSS (μg/mL)**
Kolliphor EL	664
Kollidon 25	194
Kolliphor RH 40	>4000
Poloxamer 407	>4000
Kolliphor HS 15	3580
Tween 80	3290
Kollisolv PEG E 400	18
Vitamin E TPGS	3780
Propylene Glycol	11
Poloxamer 188	24
Hydroxypropyl-β-Cyclodextrin	24
HBSS	5.3
50:50 ACN:Water	>4000

This study was able to eliminate several potential GRAS and Pharmaceutical R&D approved excipients from further utilization. We selected several other excipients based on their ability to generate a 4 mg/mL solution. Minimization of excipient choices enabled a reduction in polymer excipient concentration and potential confounding polymer effects. The maximum solubility at 1% of the remaining polymers was then determined.

Table 5.2. Solubility of Saliphenylhalamide in 1% polymer solutions.

Polymer	**Solubility in 1% w/w Polymer:HBSS (µg/mL)**
Kolliphor RH 40	2260
Kolliphor HS 15	200
Poloxamer 407	2270
TPGS	1060
Tween 80	910

This study suggests that SaliPhe is most soluble in Kolliphor RH 40 and Poloxamer 407. Poloxamer 407 was selected for further studies as it is much easier to handle and holds a stable solubility at 4^{o}C, which would be important for storage of stock solutions. Upon permeability testing in HUVEC cells, we did observe reduced permeability coefficients across for SaliPhe when formulated with P407 as opposed to RH40. We hypothesize that this may be due to polymer binding.

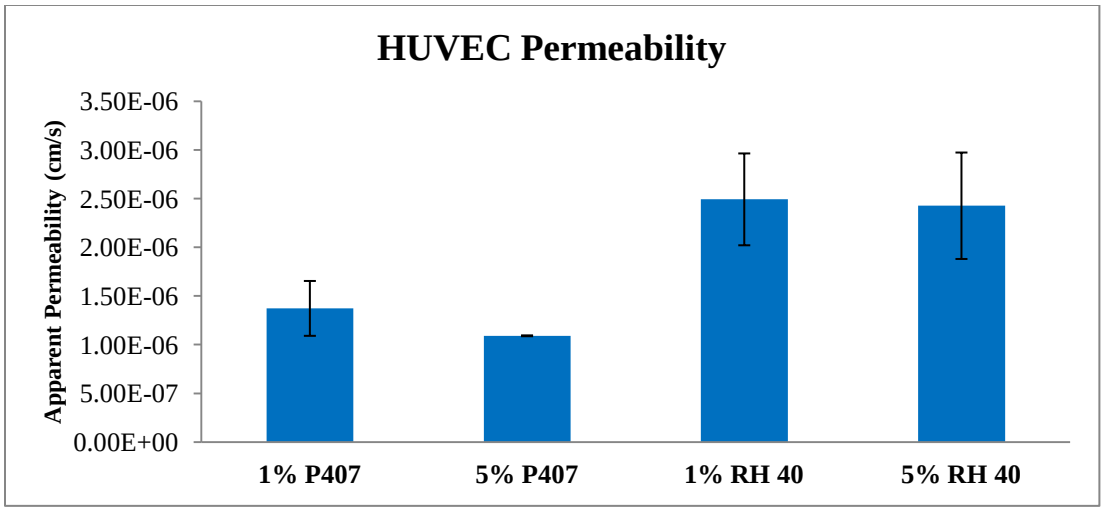

Figure 5.4. Apparent HUVEC permeability of 100ug/mL Saliphenylhalamide in 1 and 5% P407 and RH 40 formulations. Studies were run in triplicate with error bars representing 1 standard deviation.

Upon re-evaluation, we wanted to ensure that sufficient solubility of SaliPhe was maintained, thus we decided to use a 2% P407 solution for IP injection. As a 500 µL injection is the maximum allowable injection for the rats, a 7 mg/kg dose required solubility of 3.5 mg/mL. This was achievable with both 2% and 5% P407. A preliminary study conducted at the University of Louisville revealed that the 5% P407 may have potential adverse effects in rodents that were not observed with the 2% concentration. While manufacturer recommendations suggest 5% P407 formulations to be safe in rodents, we selected 2% to ensure solubilization and to minimize potential adverse outcomes.

Stability of Polymer-Based Solubility Enhancing Formulation

Similar to known stability issues of SaliPhe in acid, considerable degradation of P407 formulated SaliPhe still occurs. Approximately 40% of the drug degrades in the first hour in 0.1N HCl. It is unknown if further enzymatic degradation may occur in the stomach, however, the effect of pH alone may require co-administration with a basic buffer, or enteric coating for oral delivery. These results reinforced our focusing on the IP and IV administration routes and revealed that the peroral administration route was not feasible in these early proof-of-concept studies.

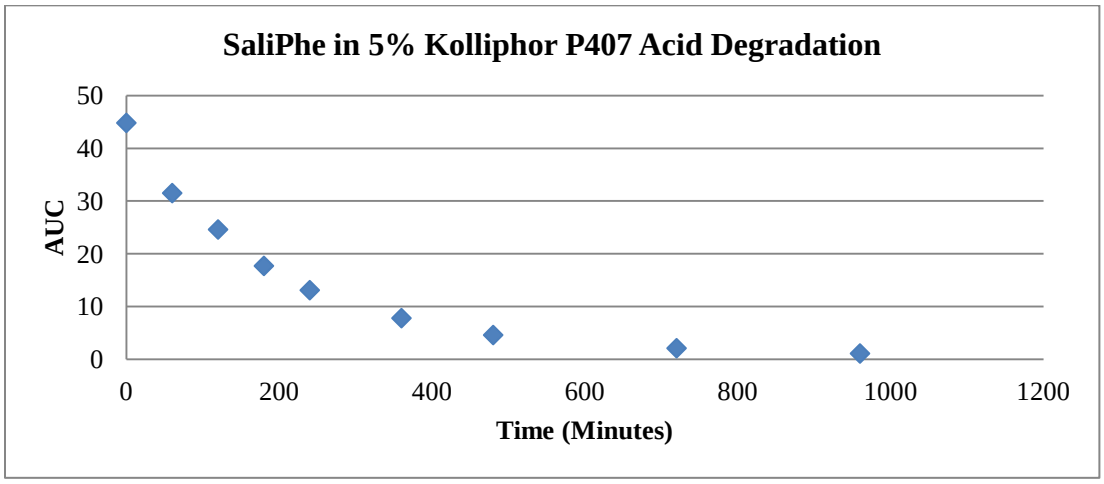

Figure 5.5. Acid degradation of Saliphenyhalamide in 2% P407 formulation.

Further investigations were conducted to determine the stability of SaliPhe in rat plasma, as the rodent Culex® units collect blood samples overnight and maintain them at 4ºC until processing and storage at -80 ºC. A 3.5 mg/mL 2% P407 formulation was

diluted 50-fold into rat plasma and allowed to equilibrate for a number of different time points. A marked drop in concentration (~50%) was seen after allowing the samples to equilibrate for 1 hour, however, it then held concentration for over 24 hours. We hypothesized that this is due to binding of SaliPhe to serum proteins in the plasma. A follow-up study revealed that an increased concentration of SaliPhe was obtained after an acetonitrile precipitation prior to analysis in the presence of plasma proteins. Other than plasma protein association, SaliPhe was determined to be stable in rat plasma. We accounted for this loss in PK studies.

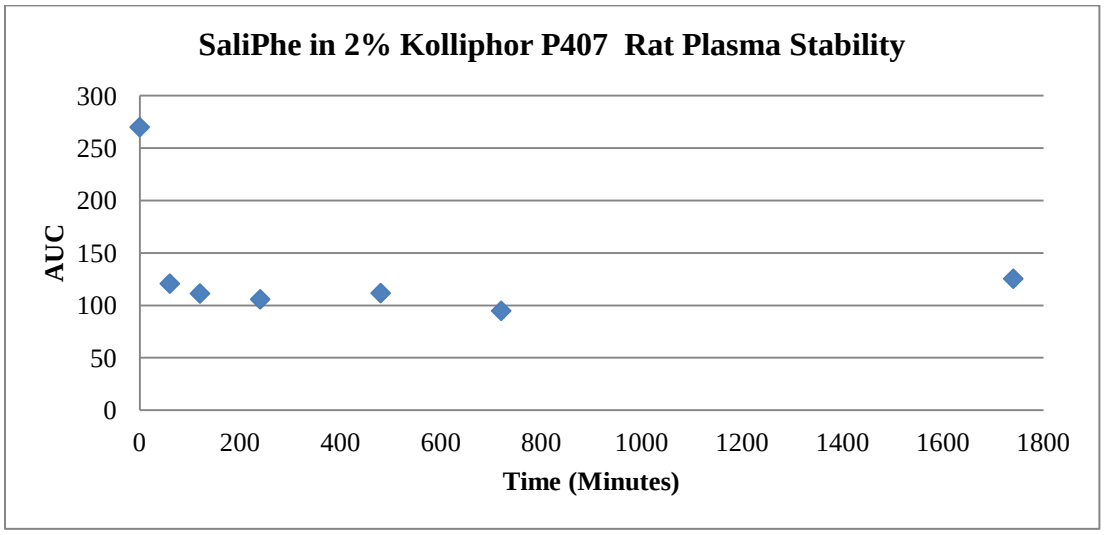

Figure 5.6. Plasma degradation of Saliphenylhalamide in 2% P407 formulation.

Kolliphor P407 Permeability Studies

Due to the combined issues of solubility enhancement, safety, and stability, a liquid formulation of 3.5 mg/mL of SaliPhe in 2% Kolliphor P407 was selected for

further preclinical investigation. Initial studies were conducted on *in vitro* cell models to elucidate potential deposition as well as changes in permeability upon dilution.

Caco-2 (human epithelial colorectal adenocarcinoma cells)

Initial permeability studies were conducted in Caco-2 cells to assess the permeability of SaliPhe across a gastrointestinal (GI) barrier. SaliPhe was added at 3, 87.5, and 175 µg/mL for solubility enhanced formulations and 3 µg/mL for SaliPhe alone. 87.5 and 175 µg/mL were selected to mimic dilution into the blood, while 3 µg/mL was run in 2% P407 and alone in HBSS to assess the effects of the formulation on permeability.

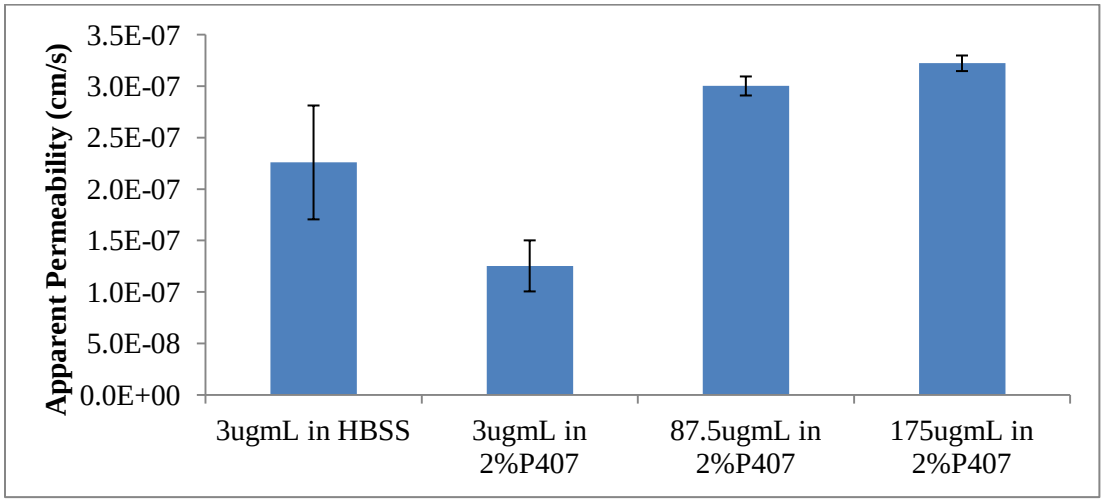

Figure 5.7. Apparent Caco-2 permeability of unformulated Saliphenylhalamide and in 2%P407 formulation. Studies were run in triplicate with error bars representing 1 standard deviation.

As can be seen in the figure above, it appears that the formulation does present a significant reduction in permeation rates, most likely due to SaliPhe binding with P407 and minimizing the concentration of free drug that can readily permeate. This phenomena has been observed in other systems, particularly with amorphous dispersions.[24] Interestingly, at higher concentration of drug in P407, this effect wasn't seen and in fact, the permeability coefficients at these higher concentrations was increased. As oral dosing of SaliPhe is currently unlikely, no further examination was done.

HUVEC (human umbilical vein endothelial cells)

As SaliPhe is most likely to be dosed IV or IP, the permeability was measured across the HUVEC cell line, which is often used as a representative cell line for the peripheral capillaries, was assessed with the same formulations utilized in the Caco-2 cell line. However, differences in permeability and permeation trends were seen. First, permeability rates for SaliPhe through the HUVEC cell line was significantly faster than Caco-2 permeability (around 10-fold). In addition, in the HUVEC cells, increased amounts of drug in the formulation didn't seem to change the permeability of SaliPhe, and if anything led to decreases. In fact the P407 formulations lead to reduced permeability across the HUVECs when compared to drug alone. We hypothesize that the kinetics of binding with P407 may minimize the free drug concentration available for permeation. We also caution that *in vitro* permeation rates are a guide and not reflective of *in vivo* conditions.

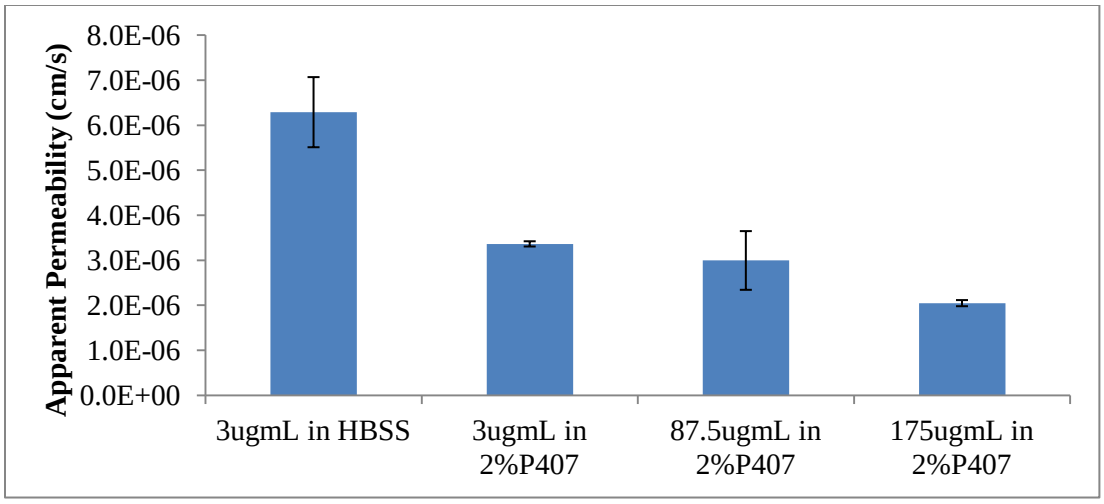

Figure 5.8. Apparent HUVEC permeability of unformulated Saliphenylhalamide and in 2%P407 formulation. Studies were run in triplicate with error bars representing 1 standard deviation.

Blood-Brain Barrier Permeability

A number of studies were conducted to determine the permeability of SaliPhe alone and in P407 formulations across BBB *in vitro* models. All models included the hCMEC/D3 cell line, with coculture studies including direct contact culture with primary human astrocytes and the triculture model grown in direct contact with both primary human astrocytes and pericytes (IP Pending). Current work in the Knipp lab suggests the co- and triculture models may serve as more physiologically relevant models for the *in vivo* BBB screening (manuscripts in preparation). Studies were conducted at 5 µg/mL SaliPhe alone and at 87.5, 175, and 437.5 µg/mL in 2% P407.

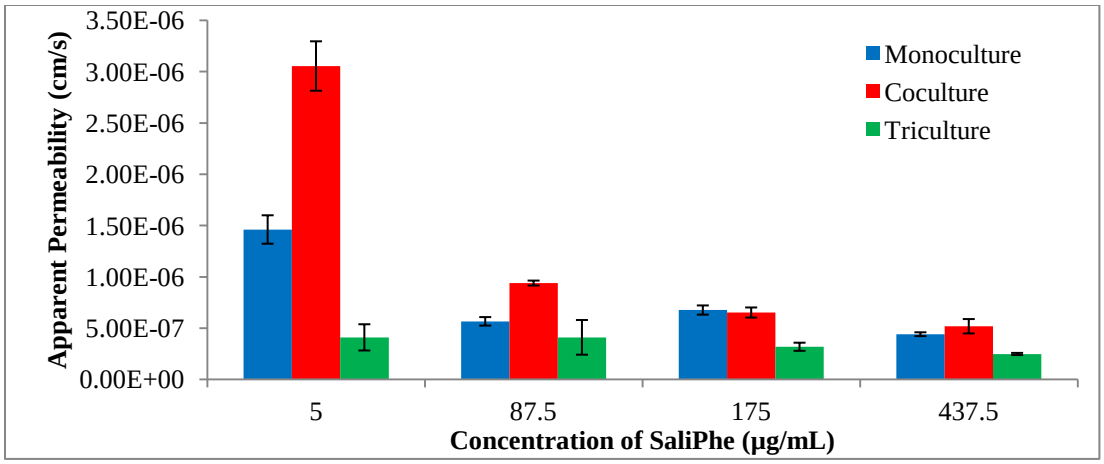

Figure 5.9. Apparent BBB permeability of unformulated Saliphenylhalamide and in 2%P407 formulation. Here, blue bars represent monoculture (hCMEC/D3 cells alone), red bars represent coculture (hCMEC/D3 cells grown on Human Astrocyte lawn), and green bars represent triculture (hCMEC/D3 cells grown on Human Astrocyte and Human Pericyte lawn). Studies were run in triplicate with error bars representing 1 standard deviation.

The study again suggests a potential decrease in permeability in P407 formulations. In addition, a non-significant decrease in permeability was seen with increased concentrations. Interestingly, permeability was highly variable between the three models for studies of SaliPhe alone. Further investigation must be conducted to determining the cause of this variability. However, with the most physiologically relevant BBB triculture model there appears to be little permeability change in relation to concentration of SaliPhe or the presence of P407. In addition, the permeability across the triculture is approximately 10-fold lower than in HUVEC cells, suggesting that

disposition into the brain may be permeability-limited under normal physiological conditions. The *in vivo* BBB is disrupted in disease states from an inflammatory response, thus the results suggest that the permeation across the normal BBB will be reduced and may alleviate any potential off target effects that might arise.

Emulsion Formulation

A number of emulsion formulations were investigated as an additional means of solubility enhancement and improving drug delivery. Formulations were selected based on transparency, stability, viscosity, and their ability to solubilize 3 mg/mL SaliPhe. Transparency was used as a criterion as it was the most rapid method to determine both solubilization and micelle formation. In addition, high viscosity can result in animal toxicity and potential death. Results of the formulation trails are shown below:

Table 5.3. Saliphenylhalamide emulsion design of experiments. Here, values represent percent of total formulation, Y implies yes formulation meets criteria, and N implies no formulation does not meet criteria. Green represents a formulation passing all criteria with red representing formulations failing one or more criteria.

Formulation #	% Total Formulation									Comments			
	PBS	Labrafil	Capryol	Solutol	Cremophor EL	Lecithin	Transcutol	Labrasol	Propylene Glycol	Stability	Clarity	Fluidity	Acceptability
1	35	30		25				10		Y	Y	N	
2	35		30	25				10		N	Y	-	
3	30		30	27					13	N	Y	-	
4	30	30		27					13	N	N	-	
5	35	30		15			10	10		Y	Y	Y/N	
6	35	30		25			10			N	N	-	
7	35	30		20			10	5		N	Y	-	
8	35	30		15			20			N	Y	-	
9	35	40		15			10			N	N	-	
10	40	35		25						N	N	-	
11	60		10		20				10	N	N	-	
12	35	30			15		10	10		N	Y	-	
13	35	30		35						N	Y	-	
14	40	20		30				10		Y	Y	N	
15	45	20		35						Y	Y	N	
16	50	20		30						Y	Y	Y	
17	60	20		20						Y	N	-	
18	55	20		25						Y	N	-	
19	60	15		25						Y	N	-	
20	60	15				25				N	N	-	
21	60	15		20		5				N	N	-	
22	55	15		30						Y	Y	Y	
23	50	15		30			5			Y	Y	Y	
24	50	15		25			10			N	N	-	

As can be seen, only formulations F16, F22, and F23 were able to meet all of the criteria. After discussion with animal care, it was determined that viscosity for F16 and F23 were high end and may cause some animal welfare concerns upon *in vivo* dosing. Therefore, the lowest viscosity formulation, F22, was selected. This emulsion consisted of 55% PBS, 15% Labrafil M 1944 CS, and 30% Solutol (Kolliphor HS15).

In addition, the F22 micelles were analyzed by a Zetasizer to determine their size and zeta-potential. As can be seen below, the micelles formed were relatively small with a diameter of only 22 nm. This was unchanged when loaded with SaliPhe at 3 mg/mL. Finally, the micelles both, blank and SaliPhe-loaded, showed a relatively neutral zeta-potential. This may lead to stability concerns, however, samples were stable for >1 week.

Table 5.4. Characterization of blank and Saliphenylhalamide F22 emulsion formulations.

	Properties	Blank	SaliPhe-loaded
F22	Size (d, nm)	22.12	23.13
	Zeta potential (mV)	-2.06	-3.97

Emulsion Formulation Permeability Studies

Based on time constraints, permeability studies of SaliPhe in the F22 emulsion were only measured across the HUVEC cell line to assess changes in the permeability coefficients with the formulation. SaliPhe was run in F22 at 75, 150, and 300 μg/mL to predict permeability at 10, 20, and 40-fold dilution into the blood and compared to 3 μg/mL SaliPhe alone. Below we see that formulation with F22 led to approximately 5-fold reduction in permeability of SaliPhe. We hypothesize that this is likely due to the inability of SaliPhe to permeate the HUVEC cells while sequestered in the emulsifying

micelles. While further work is required, it also may indicate that systemic distribution may be minimized based on the formulation *in vivo*.

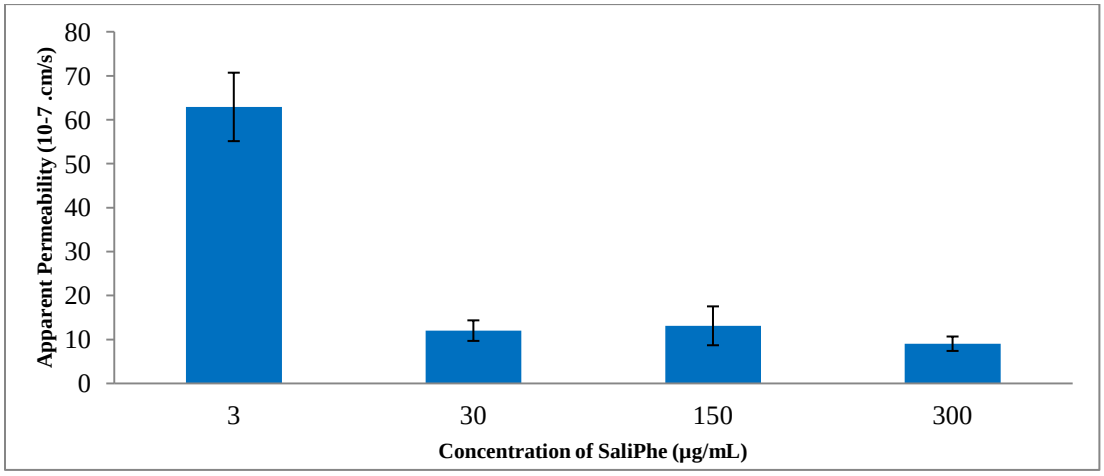

Figure 5.10. Apparent HUVEC permeability of unformulated Saliphenylhalamide and in F22 emulsion formulation. Studies were run in triplicate with error bars representing 1 standard deviation.

OM510 P407 Permeability Studies

Preliminary studies were conducted to determine the permeability of OM510 in 2% P407 across peripheral (HUVEC) and BBB (hCMEC/D3) cell models. Similar to studies above, 2 µg/mL concentration represents drug alone, while the other concentrations are representative of drug in 2% P407.

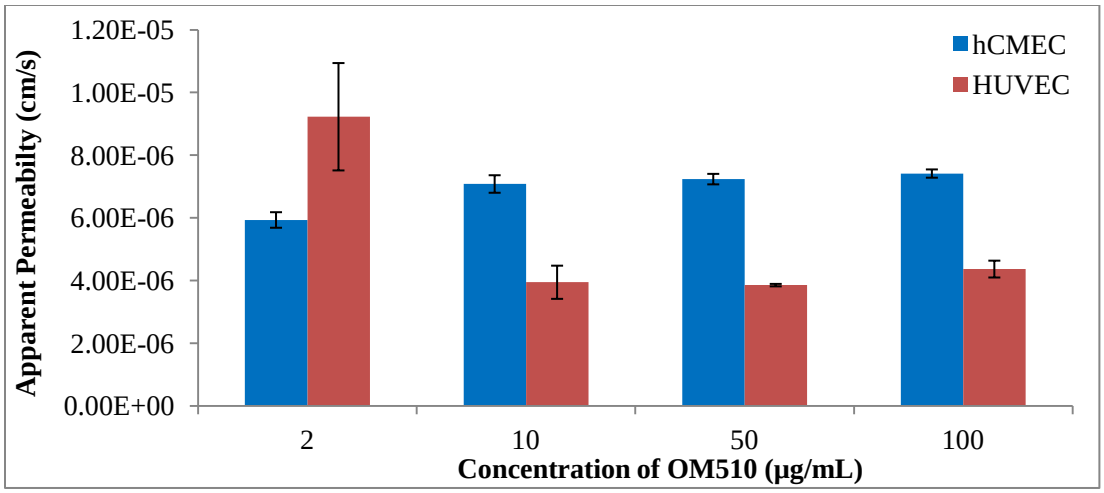

Figure 5.11. Apparent HUVEC and hCMEC/D3 monoculture permeability of unformulated Saliphenylhalamide prodrug OM510 and in 2% P407 formulation. Here, 2 µg/mL samples represent unformulated while 10, 50, and 100 µg/mL samples are formulated in 2% P407. Studies were run in triplicate with error bars representing 1 standard deviation.

These results suggest that OM510 permeability is much different than that of SaliPhe. First, permeability of OM510 appears to be approximately 10-fold faster when compared to SaliPhe. In addition, while the formulation with P407 shows similar reduced HUVEC permeability when compared to SaliPhe, no reduction is seen with the hCMEC/D3 cell line, which is similar to what was seen with the triculture model for SaliPhe.

Plasma Protein Binding

In order to determine potential protein binding, excess SaliPhe in DMSO was added to a 1% (w/w) solution of Human Serum Albumin (HSA) in PBS. Samples were allowed to equilibrate for 3 hours then centrifuged for 15 minutes at 15,000 RPM. The supernatant was then diluted 2-fold in acetonitrile to crash out plasma protein. The sample was again given 3 hours to equilibrate before being centrifuged as above. The supernatant was then analyzed by HPLC. Results suggest that SaliPhe has a solubility of approximately 100 μg/mL in a 1% HSA solution, almost 20-fold higher than that of PBS alone. This suggests SaliPhe may be highly protein bound in the plasma. We hypothesize that an HSA formulation may allow for extended delivery and increased solubility in the blood. This an area of ongoing research in our laboratory.[8]

In Vivo Rat PK Studies

Finally, in order to determine the *in vivo* effects of SaliPhe formulation, three formulations were tested in the Culex NxT "Rat Turn" Model. Studies consisted of 7 mg/kg doses of SaliPhe in 2% P407, SaliPhe in the F22 emulsion formulation, and OM510 in 2% P407.

2% P407 and F22 Emulsion SaliPhe Formulation Rat PK Studies

The pharmacokinetic (PK) studies were conducted on SaliPhe in its polymer and emulsion formulations. Samples were pulled at 0.25, 0.5, 1, 2, 4, 6, 8, 12, and 24 hours. Eight mice were dosed at 7 mg/kg with on average approximately 500 μL 3.5 mg/mL SaliPhe in P407 (4 Rats) or 550 μL 3.0 mg/mL SaliPhe in the F22 emulsion formulation (4 Rats). Both formulations showed rapid disposition with approximately 1 μg/mL remaining in the blood after 15 minutes. PK parameters are shown below:

Table 5.5. Rat pharmacokinetic parameters for 7mg/kg Saliphenylhalamide in 2% P407 and F22 emulsion formulations. C initial is initial concentration, AUC∞ is area under the curve extrapolated to infinity, Vd is volume of distribution, and CL is clearance. P-values were determined with student's T-test with n=4.

Description:		2% P407 Average	2% P407 CV	F22 Emulsion Average	F22 Emulsion CV	p-value
C initial (iv)	ng/ml	2187.0	26.2	1473.4	32.1	0.103
AUC∞ (area)	ng-hr/ml	1070.7	28.0	668.6	26.7	0.061
Vd (area)	ml	13271.5	43.0	6028.8	62.4	0.078
CL (area)	ml/hr	2430.770	27.951	3871.394	27.4	0.062
Half-life	hr	4.3	61.5	1.0	33.5	0.049

As can be seen, insignificant changes (p=0.103) in the initial blood concentration were seen between the two formulations. However, the P407 formulation appears to be

quantitatively higher, where the values are most likely not statistically significant due to high variability within the sample size. The P407 formulation did demonstrate a statistically significant higher AUC than the F22 formulation. This may be explained by the higher clearance and lower half-life of the F22 formulation. It is possible that due to the small size of the micelles that they are rapidly cleared before the drug can diffuse into the blood and eventually into the tissues. Therefore, we suggest that the 2% P407 formulation is likely to be the more likely translatable as it appears to have better solubilization through transient binding allowing disposition before clearance. Individual PK plots are shown below as well as average PK plots over the first four hours as blood levels had reduced by over 99% within this time.

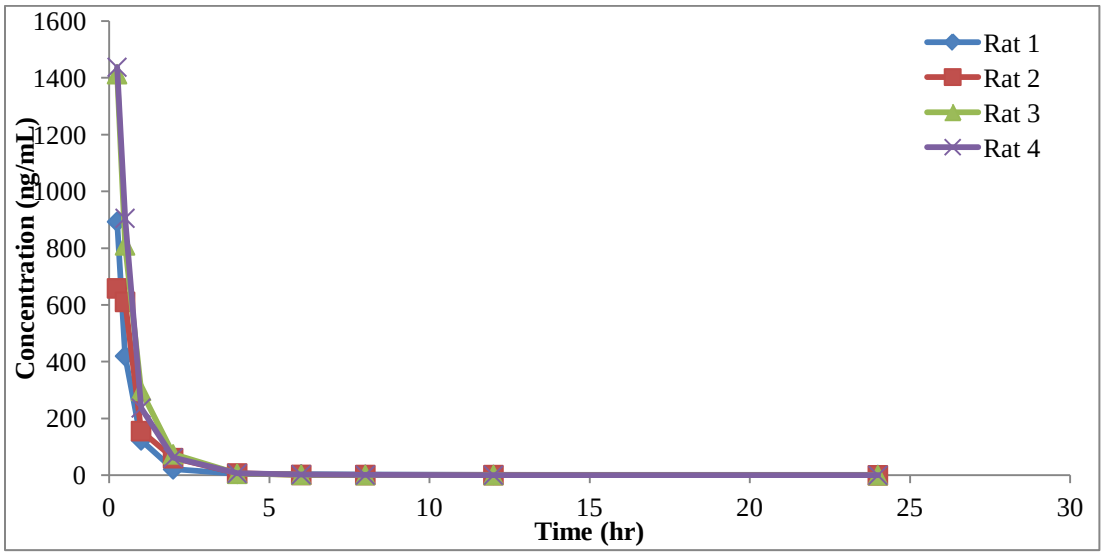

Figure 5.12. Concentration vs. time plots of 4 rats injected with 7mg/kg Saliphenylhalamide in 2% P407.

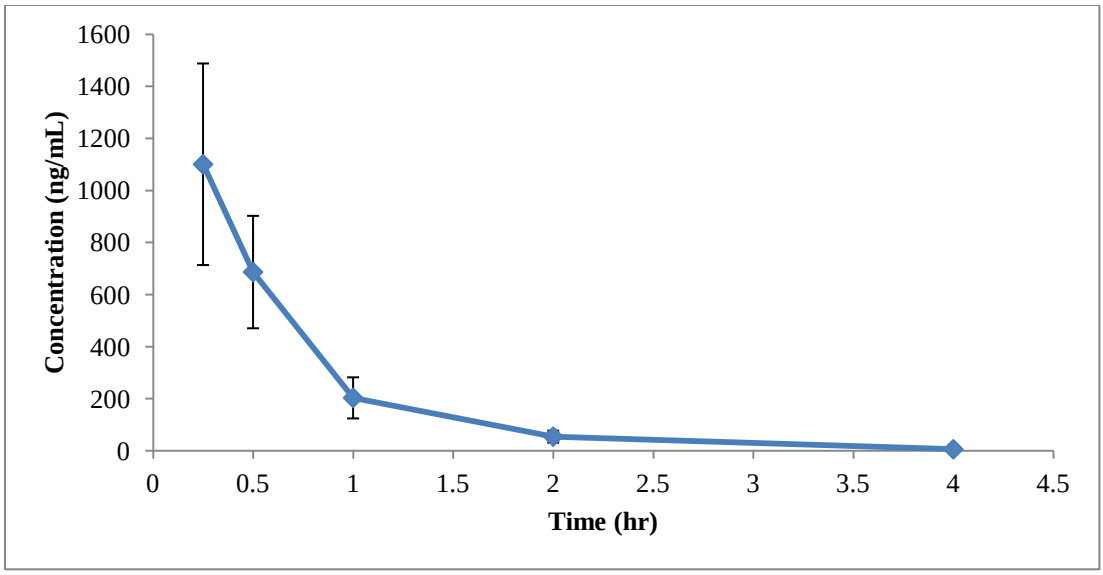

Figure 5.13. Average first four hours for concentration vs. time plots of 4 rats injected with 7mg/kg Saliphenylhalamide in 2% P407. Error bars are 1 standard deviation.

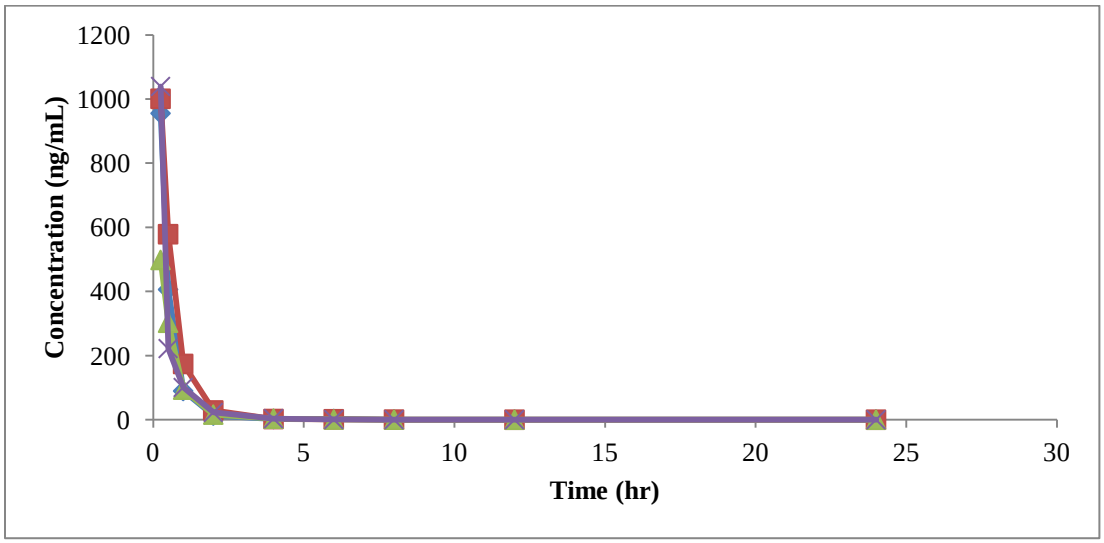

Figure 5.14. Concentration vs. time plots of 4 rats injected with 7mg/kg Saliphenylhalamide in F22 emulsion formulation.

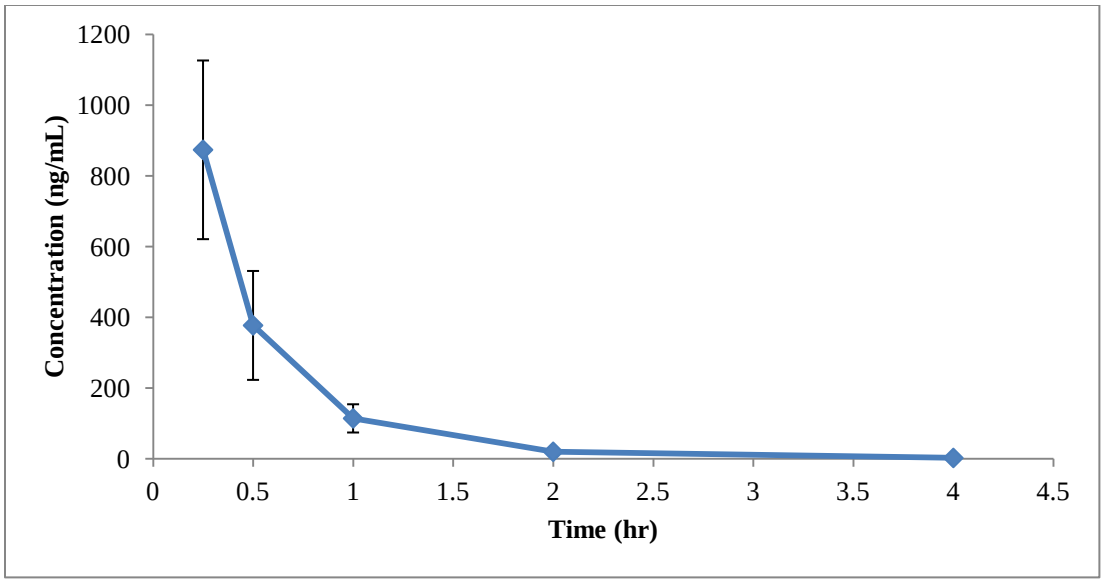

Figure 5.15. Average first four hours for concentration vs. time plots of 4 rats injected with 7mg/kg Saliphenylhalamide in F22 emulsion formulation. Error bars are 1 standard deviation.

2% P407 OM510 Formulation Rat PK Study

Due to time constraints, OM510 was tested only with the more favorable formulation of 2% P407. Again, studies were conducted in 4 mice with a 7 mg/kg SaliPhe dose (weight adjusted to account for increased molecular weight of prodrug). However, only a limited number of samples were allowed due to a restricted timeline. Therefore samples were only pulled at 0.25, 0.5, 1, and 2 hours. Unfortunately, two hours did not allow for complete PK analysis as it appears a mixture of disposition, metabolism of OMM 510 to SaliPhe, and additional clearance is still occurring in the rats.

In order to attempt to pull any useful data, the average SaliPhe PK plot was used. These PK parameters are shown below:

Table 5.6. Rat pharmacokinetic parameters for 7mg/kg OM510 in 2% P407 formulation. C initial is initial concentration, $AUC_{0\rightarrow 2hr}$ is area under the curve for 0 to 2 hour time interval, Vd is volume of distribution, and CL is clearance. Average is for n=4 rats.

Description:		2% P407 Average
C initial (iv)	ng/ml	3162.46
$AUC_{0\rightarrow 2hr}$(area)	ng-hr/ml	2453
Vd (area)	ml	19188
Half-life	hr	~1 hr

While it is difficult to assess the actual parameters for comparison, a number of testable observations can be made that will enable further interpretation. First, it appears that OM510 provides a higher initial SaliPhe concentration upon conversion of the prodrug, suggesting that it may slightly reduce disposition into the tissues. In addition, OM510 gives a much higher AUC through the first four hours than seen with SaliPhe over 24 hours. This may be due to reduced clearance, reduced disposition, or a combination of the two. Finally, the results give a half-life of approximately 1 hour, which is significantly lower than that seen with SaliPhe in 2% P407. However, it is speculated that disposition is still occurring and that the terminal phase, in which half-life

is better measured, has not yet been reached at 2 hours. Individual and average PK plots are shown below.

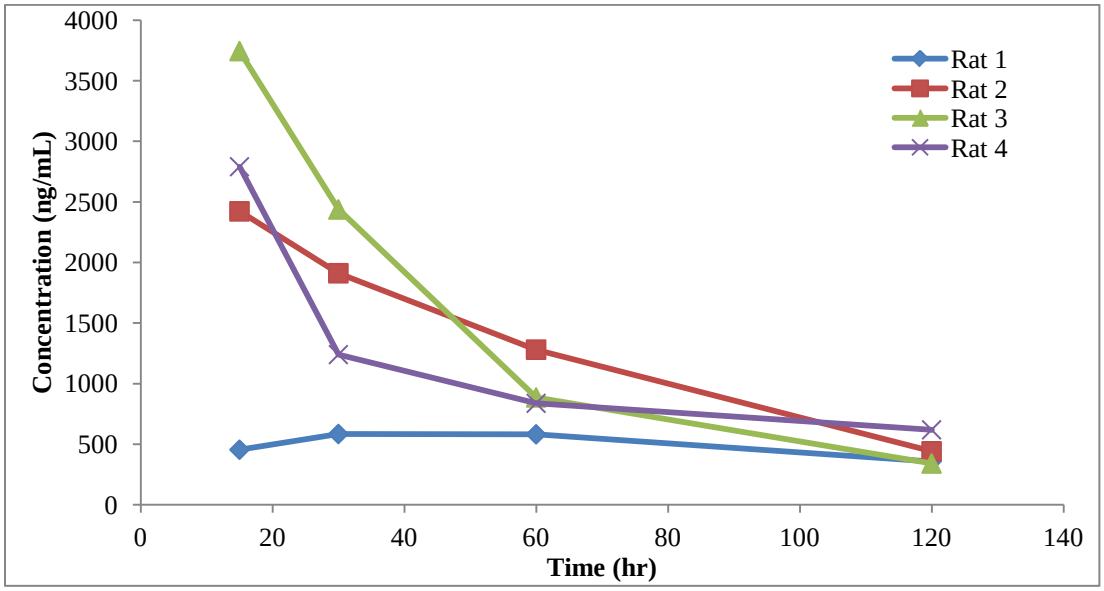

Figure 5.16. Concentration vs. time plots of 4 rats injected with 7mg/kg OM510 in 2% P407 formulation.

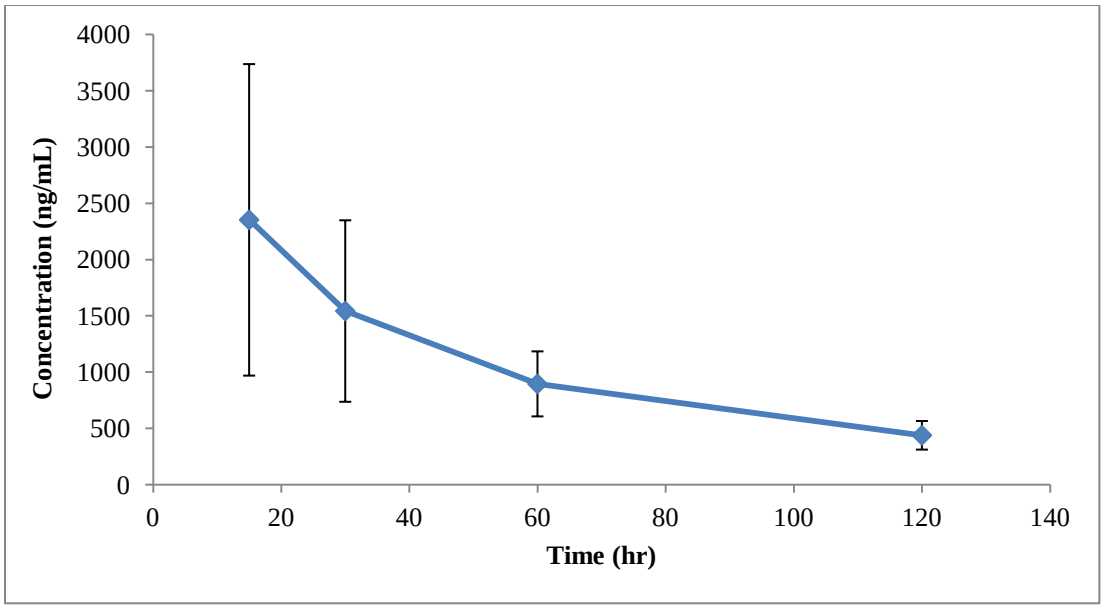

Figure 5.17. Average concentration vs. time plots of 4 rats injected with 7mg/kg OM510 in 2% P407. Error bars are 1 standard deviation.

In summary, the OMM 510 analogue may offer superior PK parameters and have an enhanced chance for translation into the clinic comparative to SaliPhe. Further research is required, but the development of additional prodrugs also may offer considerable promise for development.

In Vivo Murine Biodistribution Studies

Several attempts were made to recover and quantitate the levels of SaliPhe in the tissue samples that were provided to us for the biodistribution study. All sample preparation methods were optimized to provide the highest yield and the same

bioanalytical LC-MS/MS method used to analyze the PK samples above were utilized. However, we were unable to determine SaliPhe levels above the limit of detection in the study. Upon reflection and discussion, it was concluded that a future biodistribution study will require using a two-week dosing regimen versus the single dose study that was performed here. Based on the promising results with the OM510, we would recommend planning to perform the biodistribution study on this analogue versus SaliPhe in the future. It appears that OM510 may be superior from a PK standpoint.

5.4. Conclusions

The growing number of viral outbreaks around the globe and threat of weaponization of some of these viruses has lead to an uptick in the investigation of prospective antiviral therapeutics. Due to its utilization in viral replication, the V-ATPase represents a potential endogenous protein for antiviral drug targeting. Previous studies have shown SaliPhe to be a potent inhibitor of the V-ATPase, however, these studies were done with little knowledge of the physicochemical properties in non-pharmaceutically relevant formulations.[5-7,25-27] Therefore, here we looked to characterize SaliPhe and formulate around its potential druggability concerns.

After initial solid-state characterization, main druggability concerns focused on lack of solubility and acid liability. SaliPhe was shown to have an equilibrium aqueous solubility of less than 10 μg/mL with a predicted solubility need of 3.5 mg/mL. In addition, SaliPhe has a projected half-life in acid of less than two hours, which in combination of poor predicted GI permeation made oral dosing unviable at this time.

Therefore, solubility-enabling 2% P407 and F22 emulsion parenteral formulations were created to overcome these concerns. These formulations were then subjected to *in vitro* and *in vivo* screens to determine their effectiveness.

In vitro cell permeation screens showed poor permeability of both unformulated and formulated SaliPhe into the brain; however, HUVEC permeability suggested moderate permeation into the periphery. *In vivo* murine biodistribution studies were conducted to confirm *in vitro* predictions, but tissue concentrations were below detectable limits. Therefore, pharmacokinetic studies were conducted to determine relevant pharmacokinetic parameters. Here, the 2% P407 formulation appeared to be the more druggable formulation with higher initial concentrations, AUC, volume of distribution, and a longer half-life.

Finally, OM510, a proprietary prodrug of SaliPhe, was formulated and assessed in *in vitro* and *in vivo* screens. OM510 was synthesized to promote increased solubility and brain permeation. Due to material and time concerns, characterization was not performed. Initial *in vitro* permeability screens suggested that OM510 is much more permeable than the parent compound therefore it was moved into *in vivo* rat pharmacokinetic studies. OM510 was dosed in the 2% P407 formulation as this formulation was more successful for the parent compound. Murine pharmacokinetic studies supported *in vitro* studies suggesting that with a higher initial concentration, AUC, and volume of distribution OM510 may be a more druggable compound than the parent, Saliphenylhalamide.

5.5 References

1. Snell NJ 2003. Examining unmet needs in infectious disease. Drug Discov Today 8(1):22-30.

2. Morse MA, Hobeika AC, Osada T, Berglund P, Hubby B, Negri S, Niedzwiecki D, Devi GR, Burnett BK, Clay TM, Smith J, Lyerly HK 2010. An alphavirus vector overcomes the presence of neutralizing antibodies and elevated numbers of Tregs to induce immune responses in humans with advanced cancer. J Clin Invest 120(9):3234-3241.

3. Cosset FL, Lavillette D Cell entry of enveloped viruses. Adv Genet 73:121-183.

4. Leung JY, Ng MM, Chu JJ 2011. Replication of alphaviruses: a review on the entry process of alphaviruses into cells. Adv Virol 2011:249640.

5. Garcia-Rodriguez J, Mendiratta S, White MA, Xie XS, De Brabander JK 2015. Synthesis and structure-activity studies of the V-ATPase inhibitor saliphenylhalamide (SaliPhe) and simplified analogs. Bioorg Med Chem Lett 25(20):4393-4398.

6. Lebreton S, Jaunbergs J, Roth MG, Ferguson DA, De Brabander JK 2008. Evaluating the potential of vacuolar ATPase inhibitors as anticancer agents and multigram synthesis of the potent salicylihalamide analog saliphenylhalamide. Bioorg Med Chem Lett 18(22):5879-5883.

7. Qin A, Cheng TS, Lin Z, Cao L, Chim SM, Pavlos NJ, Xu J, Zheng MH, Dai KR 2012. Prevention of wear particle-induced osteolysis by a novel V-ATPase inhibitor saliphenylhalamide through inhibition of osteoclast bone resorption. PLoS One 7(4):e34132.

8. Lipinski CA, Lombardo F, Dominy BW, Feeney PJ 2001. Experimental and computational approaches to estimate solubility and permeability in drug discovery and development settings. Adv Drug Deliv Rev 46(1-3):3-26.

9. Hitchcock SA, Pennington LD 2006. Structure-brain exposure relationships. J Med Chem 49(26):7559-7583.

10. Pajouhesh H, Lenz GR 2005. Medicinal chemical properties of successful central nervous system drugs. NeuroRx 2(4):541-553.

11. Muller KH, Kainov DE, El Bakkouri K, Saelens X, De Brabander JK, Kittel C, Samm E, Muller CP 2011. The proton translocation domain of cellular vacuolar ATPase provides a target for the treatment of influenza A virus infections. Br J Pharmacol 164(2):344-357.

12. Knipp GT, Ho NF, Barsuhn CL, Borchardt RT 1997. Paracellular diffusion in Caco-2 cell monolayers: effect of perturbation on the transport of hydrophilic compounds that vary in charge and size. J Pharm Sci 86(10):1105-1110.

13. Knipp GT, Vander Velde DG, Siahaan TJ, Borchardt RT 1997. The effect of beta-turn structure on the passive diffusion of peptides across Caco-2 cell monolayers. Pharm Res 14(10):1332-1340.

14. Roth WJ, Lindley DJ, Carl SM, Knipp GT 2012. The effects of intralaboratory modifications to media composition and cell source on the expression of pharmaceutically relevant transporters and metabolizing genes in the Caco-2 cell line. J Pharm Sci 101(10):3962-3978.

15. Mehtala JG, Kulczar C, Lavan M, Knipp G, Wei A 2015. Cys34-PEGylated Human Serum Albumin for Drug Binding and Delivery. Bioconjug Chem 26(5):941-949.

16. Carl SM, Lindley DJ, Das D, Couraud PO, Weksler BB, Romero I, Mowery SA, Knipp GT 2010. ABC and SLC transporter expression and proton oligopeptide transporter (POT) mediated permeation across the human blood--brain barrier cell line, hCMEC/D3 [corrected]. Mol Pharm 7(4):1057-1068.

17. Poller B, Gutmann H, Krahenbuhl S, Weksler B, Romero I, Couraud PO, Tuffin G, Drewe J, Huwyler J 2008. The human brain endothelial cell line hCMEC/D3 as a human blood-brain barrier model for drug transport studies. J Neurochem 107(5):1358-1368.

18. Weksler B, Romero IA, Couraud PO 2013. The hCMEC/D3 cell line as a model of the human blood brain barrier. Fluids Barriers CNS 10(1):16.

19. Weksler BB, Subileau EA, Perriere N, Charneau P, Holloway K, Leveque M, Tricoire-Leignel H, Nicotra A, Bourdoulous S, Turowski P, Male DK, Roux F, Greenwood J, Romero IA, Couraud PO 2005. Blood-brain barrier-specific properties of a human adult brain endothelial cell line. FASEB J 19(13):1872-1874.

20. Kulkarni R, Yumibe N, Wang Z, Zhang X, Tang CC, Ruterbories K, Cox A, McCain R, Knipp GT 2012. Comparative pharmacokinetics studies of immediate- and modified-release formulations of glipizide in pigs and dogs. J Pharm Sci 101(11):4327-4336.

21. Marchant-Forde JN, Matthews DL, Poletto R, McCain RR, Mann DD, DeGraw RT, Hampsch JM, Peters S, Knipp GT, Kissinger CB 2012. Plasma cortisol and noradrenalin concentrations in pigs: automated sampling of freely moving pigs housed in the PigTurn (R) versus manually sampled and restrained pigs. Animal Welfare 21(2):197-205.

22. Roth WJ, Kissinger CB, McCain RR, Cooper BR, Marchant-Forde JN, Vreeman RC, Hannou S, Knipp GT 2013. Assessment of juvenile pigs to serve as human pediatric surrogates for preclinical formulation pharmacokinetic testing. AAPS J 15(3):763-774.

23. Doak BC, Over B, Giordanetto F, Kihlberg J 2014. Oral druggable space beyond the rule of 5: insights from drugs and clinical candidates. Chem Biol 21(9):1115-1142.

24. Newman A, Knipp G, Zografi G Assessing the performance of amorphous solid dispersions 2012. J Pharm Sci 101(4):1355-1377.

25. Soderholm S, Anastasina M, Islam MM, Tynell J, Poranen MM, Bamford DH, Stenman J, Julkunen I, Sauliene I, De Brabander JK, Matikainen S, Nyman TA, Saelens X, Kainov D 2016. Immuno-modulating properties of saliphenylhalamide, SNS-032, obatoclax, and gemcitabine. Antiviral Res 126:69-80.

26. Bimbo LM, Denisova OV, Makila E, Kaasalainen M, De Brabander JK, Hirvonen J, Salonen J, Kakkola L, Kainov D, Santos HA 2013. Inhibition of influenza A virus infection in vitro by saliphenylhalamide-loaded porous silicon nanoparticles. ACS Nano 7(8):6884-6893.

27. Denisova OV, Kakkola L, Feng L, Stenman J, Nagaraj A, Lampe J, Yadav B, Aittokallio T, Kaukinen P, Ahola T, Kuivanen S, Vapalahti O, Kantele A, Tynell J, Julkunen I, Kallio-Kokko H, Paavilainen H, Hukkanen V, Elliott RM, De Brabander JK, Saelens X, Kainov DE 2012. Obatoclax, saliphenylhalamide, and gemcitabine inhibit influenza a virus infection. J Biol Chem 287(42):35324-35332.

VITA

VITA

Christopher D. Kulczar

EDUCATION

Purdue University 2011-16

- **Ph.D.** Department of Industrial and Physical Pharmacy (IPPH)
  - College of Pharmacy, Purdue University, West Lafayette, IN
  - Advisor: Gregory T Knipp
  - GPA: 3.73

Purdue University 2007-11

- **B.S. Pharmaceutical Sciences.** MCMP Specialization
  - College of Pharmacy, Purdue University, West Lafayette, IN
  - Minors: Chemistry and Biology
  - GPA: 3.44

RESEARCH AND PROFESSIONAL EXPERIENCE

Purdue University

- Dr. Gregory T. Knipp Lab, Graduate Research Assistant 2011-16
  - Creation of Physiologically-Relevant *in vitro* Models of the Blood-Brain Barrier for Preclinical Screening
  - Synthesis, Characterization, and Efficacy Analysis of a mono-PEGylated-Human Serum Albumin for Drug Delivery
  - Characterization, Formulation, and Preclinical Assessment of Saliphenylhalamide, a Poorly Soluble V-ATPase Inhibitor
  - Investigation of the Effects of Conformation and Lipophilicity On the *in vitro* GI Permeation of Cyclic Peptides

- IPPH 525, Head Teaching Assistant 2013-15
  - Molecular Basis of Manufacturing Pharmaceuticals
  - Taught Lectures and Laboratory to Provide Practical Experience in Pharmaceutical Manufacturing

- IPPH 562, Teaching Assistant 2013
  - Introduction to Pharmaceutical Manufacturing Processes
  - Instructed Biweekly Lab in Pharmaceutical Formulation and Manufacturing

US Food and Drug Administration

- ORISE Fellow, Department of Product Quality Research 2014
  - Examined the Effects of Pharmaceutical Salts as a Pediatric Taste Masking Strategy Utilizing the Juvenile Porcine Model

Kilimanjaro School of Pharmacy, Moshi, Tanzania

- Lecturer 2013-15
  - Trained African Scientists and Regulators in Pharmaceutical Manufacturing Labs and Design of Experiments Courses

Perrigo Company

- Formulation Intern 2010
  - Utilized DOE for Scale-Up of Granular Enteric Coating Using Fluid Bed Coating
  - Formulated Chewable Tablet Around Organoleptic Challenges

TECHNICAL SKILLS

Pharmaceutical Manufacturing Unit Operations

- High and Low Shear Wet Granulation, Roller Compaction, Blending, Milling, Compression, Film Coating, Fluid Bed Drying

Characterization Testing

- Design of Experiments (DOE), Dissolution, Content Uniformity, Stability, Disintegration, Sieve Analysis, Friability, DSC, PXRD, HPLC, LC-MS

Cell Culture

- Cell Lines: hCMEC/D3, Caco-2, HT-29, HT-29 19A, HUVEC, Primary Astrocytes, Primary Pericytes, Human Stem Cell
- Substrate Permeability Studies (Transport), Uptake, General Cellular Biology Methods Including Western Blot and mRNA Profiling Arrays
- HPLC Development for Assaying Numerous Permeability Substrates

PERSONAL AFFILIATIONS

Globalization of Pharmaceutical Education Network (GPEN)
- Purdue Graduate Student Representative 2014-16

American Association of Pharmaceutical Scientists (AAPS)
- Active Member 2011-16

LEADERSHIP

American Association of Pharmaceutical Scientists (AAPS)
- Chair 2014-15
- Chair Elect 2013-14
- Vice Chair 2012-13

College of Pharmacy Grade Appeals Committee
- Student Representative 2012-14

Pharmaceutical Graduate Student Research Meeting (PGSRM)
- Purdue Representative 2012-13

Bachelor of Science in Pharmaceutical Science Club (BSPS Club)
- Treasurer 2010-11

HONORS

Invited Lecturer for IPPH Advanced Training 2013-15
- Laboratory Instructor for the Sustainable Medicines in Africa Program at the Kilimanjaro School of Pharmacy in Moshi, Tanzania

O'Malley Graduate Scholarship in Manufacturing Pharmacy 2013-15
- The O'Malley Scholarship Supports A Graduate Scholarship In Manufacturing Pharmacy In The College Of Pharmacy

Dr. Albert V. Kienly Award 2014
- The Dr. Albert V. Kienly Award is Given to An Outstanding Graduate Student Teaching Assisant

Migliaccio/Pfizer Graduate Fellowship in Pharmaceutical Sciences 2013-15
- The Migliaccio/Pfizer Graduate Fellowship in Pharmaceutical Sciences is Given to Support a Student for One Year with a Research Focus on Manufacturing Science

Purdue "5 Students Who… Move the World Forward" 2013
- Selected as One of Five Current Purdue Students Using Their Purdue Education to Help Move the World Forward

Dr. Herbert Lieberman Award 2013
- The Dr. Herbert Lieberman Award is Given For Outstanding Service as a Teaching Assistant in IPPH 562 and Many Contributions to the IPPH Department since 2011

Ronald W. Dollens Graduate Scholarship in Life Sciences 2013
- The Ronald W. Dollens Graduate Scholarship is a Merit-Based Scholarship for Graduate Students Who are Studying in the Broad Area of Cardiovascular Research

Best Poster, Pharmaceutical Graduate Student Research Meeting 2012
- Juvenile Pigs as Surrogates for Human Pediatrics During Preclinical Pharmacokinetic Testing: A Possible Means to Expedite Pediatric Drug Development?

Ross Fellowship 2011-2016
- The Ross Fellowships are for the Recruitment of Outstanding, Ph.D.-Track Students to Graduate Programs at Purdue University

MANUSCRIPTS

1. R.P. Gala, C. Popescu, G.T. Knipp, R.R. McCain, R.V. Ubale, R. Addo, T. Bhowmik, **C. Kulczar,** and M.J. D'Souza, Physicochemical and Preclinical Evaluation of a Novel Buccal Measles Vaccine. *AAPS PharmTech*

2. **C. Kulczar**, K.L. Lubin, S. Lefebvre, D.W. Miller, and G.T. Knipp. Development of a Direct Contact Astrocyte-hCMEC/D3 Blood-Brain Barrier Coculture Model. (Submitted)

3. J. Mehtala, **C. Kulczar**, M. Lavan, G.T. Knipp, and A. Wei. Cys34-PEGylated Human Serum Albumin for Drug Binding and Delivery. *Bioconjugate Chem*. 26(5):941-949 (2015).

4. D.P. Sage, **C. Kulczar**, W.J. Roth, W. Liu, G.T. Knipp. Persistent Pharmacokinetic Challenges to Pediatric Drug Development. *Frontiers in Genetics*. 5:281 (2014).

5. **C. Kulczar**, W.J. Roth, S. Carl, O.S. Gudmundsson, and G.T. Knipp. Protein and Peptide Delivery. *Drug Delivery.*, Eds. A.K. Mitra, D. Kwatra, and A.D. Vadlapudi. Jones & Bartlett Learning, LLC., Burlington, MA, pp 403-428 (2014).

6. W.J. Roth, D.P. Sage, **C. Kulczar**, W. Liu, and G.T. Knipp (Ed.). Editorial: Perspectives on Pediatric Drug Development. *Revista Mexicana De Ciencias Farmaceuticas* 43(3):5-6 (2012).

POSTERS and PRESENTATIONS

1. R.P. Gala, C. Popescu, G.T. Knipp, R.R. McCain, R.V. Ubale, R. Addo, T. Bhowmik, **C.D. Kulczar**, and M.J. D'Souza. Next Generation of Immunization: Oral Disintegrating Films Loaded with Nanoparticulate Measles Vaccine for Buccal Delivery. 10th World Meeting on Pharmaceutics, Biopharmaceutics and Pharmaceutical Technology, Glasgow, U.K. (2016).

2. **C.D. Kulczar**, S. Lefebvre, G.T. Knipp. Improvement in Blood-Brain Barrier Tightness through a Direct Contact hCMEC/D3 and Human Astrocyte Coculture Model. 2014 Globalization of Pharmaceutics Education Network (GPEN) Annual Meeting, Helsinki, Finland. (2014).

3. **C.D. Kulczar**, A. Ngendahimana, S. Lefebvre, and G.T. Knipp. Development of a Physiologically Relevant Blood-Brain Barrier Model: Direct Contact hCMEC/D3 and Human Astrocyte Coculture. 2014 AAPS Indiana/Ohio Discussion Group-Pharma Industry Challenges/Perspectives Symposium, Indianapolis, IN. (2014).

4. **C.D. Kulczar**, S. Lefebvre, G.T. Knipp. Improvement in Blood-Brain Barrier Tightness through a Direct Contact hCMEC/D3 and Human Astrocyte Coculture Model. 2013 American Association of Pharmaceutical Scientists Annual Meeting, San Antonio, TX. Abstract M1094 (2013).

5. J. Mehtala, **C.D. Kulczar**, G.T. Knipp, A. Wei. PEGylated Human Serum Albumin for Enhanced Drug Binding and Delivery of Poorly Soluble Drugs. 2013 American Association of Pharmaceutical Scientists Annual Meeting, San Antonio, TX. Abstract W5245 (2013).

6. J. Mehtala, **C.D. Kulczar**, G.T. Knipp, A. Wei. PEGylated Human Serum Albumin for Enhanced Drug Binding and Delivery of Poorly Soluble Drugs. Dane O. Kildsig Center of Pharmaceutical Processing Research Meeting, Purdue University, West Lafayette, IN. November, 2013 .
7. **C.D. Kulczar**, Sylvia Lefebvre, G.T. Knipp. Improvement in Blood-Brain Barrier Tightness through a Direct Contact hCMEC/D3 and Human Astrocyte Coculture Model. 2013 Pharmaceutical Graduate Student Research Meeting. Iowa City, IA. June, 2013.
8. **C.D. Kulczar**, W.J. Roth, C.B. Kissinger, R. Vreeman, S. Hannou, B.R. Cooper, R.R. McCain, and G.T. Knipp. Juvenile Pigs as Surrogates for Human Pediatrics During Preclinical Pharmacokinetic Testing: A Possible Means to Expedite Pediatric Drug Development? 2012 Pharmaceutical Graduate Student Research Meeting, Omaha, NE. July, 2012.
9. **C.D. Kulczar**, W.J. Roth, C.B. Kissinger, R. Vreeman, S. Hannou, B.R. Cooper, R.R. McCain, and G.T. Knipp. Juvenile Pigs as Surrogates for Human Pediatrics During Preclinical Pharmacokinetic Testing: A Possible Means to Expedite Pediatric Drug Development? 2012 Garnet E. Peck Symposium in Industrial Pharmacy, West Lafayette, IN. October, 2012.

PUBLICATIONS

PUBLICATIONS

1. R.P. Gala, C. Popescu, G.T. Knipp*, R.R. McCain, R.V. Ubale, R. Addo, T. Bhowmik, **C. Kulczar**, and M.J. D'Souza*, Physicochemical and Preclinical Evaluation of a Novel Buccal Measles Vaccine. AAPS PharmTech (2016).

2. D.P. Sage, **C. Kulczar**, W.J. Roth, W. Liu, G.T. Knipp. Persistent Pharmacokinetic Challenges to Pediatric Drug Development. Frontiers in Genetics. 5:281 (2014).

3. **C. Kulczar**, W.J. Roth, S. Carl, O.S. Gudmundsson, and G.T. Knipp. Protein and Peptide Delivery. Drug Delivery., Eds. A.K. Mitra, D. Kwatra, and A.D. Vadlapudi. Jones & Bartlett Learning, LLC., Burlington, MA, pp 403-428 (2014).

4. W.J. Roth, D.P. Sage, **C. Kulczar**, W. Liu, and G.T. Knipp (Ed.). Editorial: Perspectives on Pediatric Drug Development. Revista Mexicana De Ciencias Farmaceuticas 43(3):5-6 (2012).